UNIVERSITE CATHOLIQUE DE LOUVAIN
Faculté de Sciences Appliquées
Département de Mécanique
Unité de Thermodynamique et Turbomachines (TERM)

Friction Relaxation Model for Fast Transient Flows

Beata Kucieńska

Thèse présentée pour l'obtention du grade de
Docteur en Sciences Appliquées

July 2004

'If I have the gift of prophecy,
and know all mysteries and all knowledge;
and if I have all faith, so as to remove mountains,
but don't have love, I am nothing'.

1 Corinthians 13.2, The Bible

Acknowledgments

I think I shall need to write another book to thank all the persons without whom I would not be able to finish this thesis. I will mention just some of you.

Professor Giot, it would be very difficult to find a better supervisor than you: so patient, indulgent, competent, experienced, comprehensive. You gave me a lot of attention and help, and you had a time to talk to me when I needed it. You made me feel that my work is important to you even if you had hundreds other very important things to do. Thank you from all my heart for your help, guidance, time and your kindness during these 3.5 years. I would wish to have similar bosses as you in my future carreer.

Doctor Jean-Marie Seynhaeve, I know that I have not been very skilful in expressing my gratitude for all these hours that you spent with me on explaining and teaching me so many things. But believe me, that I have always deeply appreciated your help. Many thanks for everything: the time you devoted to me, for all the explanations, all books and all softwares, for your sense of humour, and above all for all the discussions. Especially at the beginning when I found myself alone in a new world your sense of humour and kindness were the real blessings for me. Thank you for always repeating me that we are just a little dust in this world, I will try to remember this. I had a real chance to have you as my second superior - I learnt so many things from you.

I am also very grateful to my Polish professor - Zbigniew Bilicki, who unfortunately passed away during my first year of thesis. Without him this thesis would not have been written. His suggestions during our last meeting at the UCL were the basic inspiration for the development of the Friction Relaxation Model presented in this work. He was not only a great scientist but also a man with a great heart.

Professor Georgy Lebon, I am also deeply grateful to you for your presence at the seminar about the Extended Irreversible Thermodynamics and for your book about the EIT that was the source of indispensable information. Your knowledge about the EIT was extremely helpful during my work.

Doctor Hervé Lemonnier, I would like to express my gratitude for all your remarks, comments, suggestions, for the very detailed review of my thesis, for your respectful and kind attitude, for all the meetings during the WAHA project, where you shared with us your knowledge and experience, significantly participating in the development of my thesis.

Doctor Iztok Tisejl, thank you so much for your work on the WAHA code, which I used to make the calculations, for all your e-mails, suggestions and discussions during these 3.5 years, for your hospitality during my stay in Ljubljana, for your patience and knowledge. I truly appreciate your help.

Professor Grégoire Winckelmans, thank you very much for all discussions and very important comments on my work, especially for the remarks considering the coefficients of the Friction Relaxation Model. I am conscious that all your suggestions increased the quality of my thesis and I am grateful for your help.

I also wish to express my gratitude to Professor J. C. Samin for his acting as the chairman of the jury.

Bernard François and Frank Hesbois, I hope that you will not forget your 'Miss PC' and I also hope than there will be no more girls at the unit TERM, having such a destructive influence on the computers. Thank you for all the efforts you made trying to bring my computers to life and what is more, doing it with much kindness. You were a real help for me.

Edmond Mulemangabo, you were also obliged to spend many hours in my office because of the 'deaths' and 'resurrections' of my PC. Thank you very much for all your work, which was indispensable, for your kindness, for the music you gave me and for the stories about snakes in Kenia.

Mme Antoinette Dupont, thank you very much for your help, especially at the beginning of my stay in Belgium. Thank you for the shopping we did together and for the guitar you helped me to buy, which often brightened my days when they were becoming grey.

I would like to thank to all my colleagues who worked with me in the same office: Goéric, thank you for your help and for your IT knowledge that you always, so kindly, shared with me. Alina, thank you for your help, your support and all the discussions we had. Bamdad, thank you very much for your kindness, all your advices and suggestions in the last period of my thesis.

Cosmina, I cannot even imagine what my life would be if I did not meet you. You stayed close to me during the darkest days, you gave me the force and the inspiration to continue when I felt weak, thank you very much my dear friend - I will never forget you.

Michel Bokungu, you were a friend and a brother to me, thank you so much for your good and gentle heart. Your love and your friendship are incredibly important to me. Wherever I go you will go with me because you entered into my heart, and one day I will visit you in your country.

Annette Broome, it was an honour to meet you on my way, you gave me the most beautiful gift of love and wisdom, thank you for your enormous heart, I will never forget these precious moments spent with you.

Agata, my dearest sister, thank you very much for everything; your support, encouragement and all the conversations. It's a real grace and honour to have you as a sister.

My deep gratitude goes to my whole family, especially to my Mother. Thank you Mom for your encouragement and affection, you always believed in me. Your love is my force to live.

I would like to thank my Polish friends who always stayed close to me in spite of the distance. Thank you very much Ada Olejniczak, Ewa Tocha, Ela Sadowska, Ewa Sikora, you were always ready to listen to me and to help me, your presence is a wonderful treasure, thank you for your love and faithfulness, you know what the real friendship is and I love you all.

I deeply thank also to my Polish friends in Louvain-la-Neuve: Agnieszka Romanowicz and Beata Dunaj for all the wonderful moments that we spent together, for all the suppers, conversations and encouragements, which made my life brighter. I was a lucky person to have you close to me.

Many other persons that I did not mention here gave me the encouragement, the strength and the motivation to continue and finish this thesis. I am grateful for every advise, every suggestion and every smile. I thank to every person, who helped me during this 3 and a half years in Belgium, I thank also to the members of my church and all my 'kokoteurs' and many other persons whom I met in Belgium. I thank you for your time, your presence, and your kindness. You are all precious to me.

Finally I would like to thank God, whom I love with all my heart. Without his grace nothing would be possible.

SUMMARY

The thesis deals with the problem of friction during rapid transient 1-D flows in a pipe caused by water hammers. The evolution of the wall shear stress is interpreted in terms of two steps. The first step is the dramatic change of the wall shear stress during the passage of the pressure wave; the corresponding new value of the shear stress is much greater than the value predicted in steady-state. The second step, which begins after the passage of the pressure wave, is a relaxation process; here the shear stress decreases, tending to the new steady-state value corresponding to the new average velocity. The Extended Irreversible Thermodynamics theory is proposed as a tool to model the wall shear stress during the relaxation process.

The Friction Relaxation Model presented in this thesis describes both steps of the evolution of the wall shear stress during water hammers, and therefore it enables to take into account the information about the velocity gradient at the wall, which is otherwise not available in 1D modelling.

Contents

1 Introduction **9**

2 State of the art of transient friction research **15**

3 Derivation of the Friction Relaxation Model **25**

3.1 Introduction 25

3.2 Interpretation of the shear stress evolution in terms of two steps 26

3.3 Modelling of the first step of the transient wall shear stress evolution 27

3.3.1 Sudden deceleration 27

3.3.2 Sudden acceleration 28

3.3.3 Relation between pressure wave amplitude and sudden change of wall shear stress 29

3.4 Modelling of the second step of the transient wall shear stress evolution 31

3.4.1 Basic assumptions of Extended Irreversible Thermodynamics 31

3.4.2 EIT as a tool to fast transient modelling 33

3.4.3 Derivation of the relaxation equation for wall shear stress from Extended Irreversible Thermodynamics . . 34

3.5 Friction Relaxation Model 37

3.6 Modelling of the relaxation time 41

3.7 Modelling of the k_T coefficient 42

3.8 Results for a liquid flow 42
3.9 Sensitivity analysis 46
3.10 Conclusions 47

4 Approximation of the Friction Relaxation Model by algebraic laws 51
4.1 Introduction 51
4.2 Approximated wall shear stress model based on wave detection 53
4.3 Approximated wall shear stress model based on last time step 57
4.4 Conclusions 63

5 Comparison between the Friction Relaxation Model and other transient friction models 65

6 The Friction Relaxation Model for Two-Phase Flows 71
6.1 Introduction 71
6.2 Homogenous Equilibrium Model 72
6.3 Homogeneous Relaxation Model 79
6.4 Two-Fluid Model 87
6.4.1 Basic Equations 87
6.4.2 Wall friction 91
6.4.3 Results 95
6.5 Conclusions 113

7 Conclusions 119

A Description of the codes and numerical schemes used to perform the computations 125
A.1 Basic equations 126
A.2 Numerical scheme 127

B Analytical solution of the friction relaxation equation for short times 135

C Velocity profiles during wave passage calculated with FLUENT 137

D The comparison between original and approximated Friction Relaxation Model for refined grid 143

Nomenclature

A	pipe cross-section (m^2)
a	pressure wave velocity (m/s)
C_i	interfacial friction coefficient
CVM	virtual mass term (N/m^3)
D	diameter of a pipe (m)
d	wall thickness (m)
E	elasticity modulus (N/m^2)
e	specific total energy (J/kg)
F_{wall}	wall friction forces per unit of volume(N/m^3)
f	steady friction (Darcy) coefficient
g	gravitational acceleration (m/s^2)
h	specific entalphy (J/kg)
k_T	transient friction coefficient ($kg/m/s^3$)
p	pressure (Pa)
p_i	interfacial pressure(Pa)
Q_{if}, Q_{ig}	interface-liquid and interface-gas heat transfer rates (W/m^3)
R	radius of a pipe (m)
Re	Reynolds number
s	entropy (J/kg/K)
T	temperature (K)
t	time (s)
u	specific internal energy (J/kg)

V	volume (m^3)
W_f	weighting function
w	velocity (m/s)
w_i	velocity of the interfacial area(m/s)
w_p	pipe velocity in the flow direction (m/s)
w_r	relative velocity (m/s)
X	quality (mass fraction of a gas phase)
x	axial coordinate (m)

Greek letters

α	void fraction
Δt	time step
Δx	length of numerical cell
Γ_g	vapor generation rate ($kg/m^3/s$)
ϵ	roughness of a pipe (m)
μ	dynamic viscosity (kg/m/s)
θ	relaxation time (s)
ν	kinematic viscosity (m^2/s)
ρ	density (kg/m^3)
σ	entropy production rate ($kg/m/K/s^3$)
τ	transient wall shear stress ($kg/m/s^2$)
τ_s	steady wall shear stress

Subscripts

f	liquid phase
g	gas phase
j	numerical cell index
m	mixture

Superscripts

n	time level

Chapter 1

Introduction

This work deals with the modelling of dissipative effects in transient single- and two-phase flows associated with water hammers.
A water hammer is a pressure shock wave induced in a flow by a sudden change of the boundary conditions. It is a destructive force that can damage residential or industrial plumbing systems. Shock forces due to water hammers can rupture copper supply lines or cause leaking at joints. Pumps, valves, faucets, toilets, and fast solenoid-activated valves (such as commonly found in washing machines and dishwashers) are all examples of devices that can induce water hammers within a piping system. Water hammers can result in noisy, banging sounds as pipes rattle and expand to absorb the pressure wave. Shock waves in typical water pipes travel at up to 1500 m/s and can exert tremendous, instantaneous pressures, sometimes reaching to over 70 bars. If left uncontrolled, a water hammer can damage pipes, valves and eventually weaken joints.
If the water is flowing in a pipe and a valve placed downstream is suddenly closed, the momentum flux of the flowing water reverses direction and must be dissipated during the transition to a new steady state. This momentum flux is initially reflected back through the piping system in a direction opposite to the original flow, creating an oscillating shock wave. Depending on the extent of the shock wave, a loud banging or rattling sound can be heard

as pipes expand and move as the shock wave dissipates. If there were no friction losses, the shock wave would continue infinitely. The Friction Relaxation Model proposed in this thesis enables to predict friction losses and resulting dissipation of pressure waves during a water hammer event.

This thesis is related to a research performed in the frame of the WAHALoads (Two-phase Water Hammer Transients and Induced Loads on Materials and Structures of Nuclear Power Plants) project of the European Commission. The global objective of the project is to achieve an accurate prediction of the loads on equipment and support structures caused by water hammer (Giot et al. [18]).
In Nuclear Power Plants water hammer phenomena can occur during abnormal operation due to the condensation following an inflow of sub-cooled water into pipes or other equipment filled with steam or steam-water mixtures. They may also happen due to valve closing and opening or pipe ruptures. During normal operation, water hammers may be caused by standard actions such as start-up or shut-down of systems and components. During plant transients, water hammers may occur as a consequence of the activation of emergency core cooling systems (ECCS) or auxiliary feed water systems. Water hammers induce dynamic stresses in the wall of the pressure-retaining equipment and support structures and can cause serious damages. They can also cause flashing i.e. liquid vaporization due to sudden pressure drop. The proper prediction of pressure and void fraction during fast transients is important for the design of pipe components and supports in order to ensure that there will be no damage to the equipment.
Such an accident happened for example on June 17, 1998 in the United States. A severe water hammer event occurred in the Washington Nuclear Project Unit 2 (WNP-2) Fire Protection System. The water hammer was caused by the draining of a 12"riser and its subsequent refilling due to the simultaneous start up of the fire water pumps. As a result of this event, an isolation valve in the line was ruptured that allowed the flooding of several areas including the Reactor Heat Removal (RHR) and Emergency Core Cool-

ing System (ECCS) rooms, and this caused severe damage to the equipment in these rooms. Due to this event, the U.S. Nuclear Regulatory Commission (NRC) issued the Information Notice 98-31[1] requiring the utilities to review their Fire Protection Systems to determine if they are vulnerable to similar events, and, if so, they required that appropriate actions be taken.
In the framework of the WAHALoads project a new code based on new physical modelling and appropriate numerical scheme has been developed. In particular the research was concentrated on new closure laws better suited for single and two-phase fast transient flows.

The objective of this thesis is the development of a closure law for transient shear stress in single and two-phase flows. Such closure law introduced in the set of equations describing the flow has a great impact on the prediction of the pressure and void fraction versus time and space. This is known from many studies devoted to this subject in the past and reviewed in chapter 2.
In chapter 3, which is the heart of the thesis, the derivation of the Friction Relaxation Model is presented. The evolution of the shear stress during fast transient flows is interpreted in terms of two steps.
The first step is a sudden rise of the shear stress. This shear stress peak being caused directly by the passage of the pressure wave, its amplitude is assumed to be proportional to the amplitude of the pressure wave.
The second step is the relaxation of the transient shear stress. During this relaxation phase, the shear stress tends exponentially from the value caused by the pressure wave to the value corresponding to the new steady state (determined by the Darcy equation). That would be achieved if the flow conditions remained unchanged after the passage of the pressure wave which had caused the shear stress peak. The relaxation phase is modelled by a relaxation equation derived from Extended Irreversible Thermodynamics theory. This theory is useful to describe phenomena for which the hypothesis of local

[1] http://www.nrc.gov/reading-rm/doc-collections/gen-comm/info-notices/1998/in98031.html

equilibrium is questionable. This is the case for fast transient flows where we deal with strong gradients and fast changes in the system.
The Friction Relaxation Model includes both steps of the shear stress evolution. The numerical results for 1D transient shear stress in air flow are compared with the results obtained with a 2D code (FLUENT), including $k - \epsilon$ model of turbulence. On the basis of shear stress results obtained with FLUENT, transient friction coefficients for air flow are evaluated. The coefficients for water are evaluated on the basis of a comparison with some experimental results. The effect of a transient shear stress is more important for a liquid than for a gas, the difference between steady and transient shear stress in water (experiment of Holmboe and Rouleau, 1967) reaches two orders of magnitude.
The Friction Relaxation Model is a differential equation. Therefore, the introduction of this equation into the codes computing transient flows may be complicated and time-consuming. In chapter 4, two approximations of the model by algebraic laws are proposed. Because of their simplicity the approximated equations may have practical importance for the programmers who would decide to put the transient friction model in their code. Finally, the approximated Friction Relaxation Model based on the shear stress value from the last time step is included into the WAHA code described above.
In chapter 5, the exact Friction Relaxation Model and the approximated one are compared with several transient friction models found by other researchers. The similarities and differences between the models are analyzed.
Finally, in chapter 6, the Friction Relaxation Model is put into the set of equations for two-phase flows. It is introduced into three two-phase models: Homogenous Equilibrium Model, Homogenous Relaxation Model and Two-Fluid Model. For the analyzed case of the two-phase transient flow caused by a fast closure of a downstream valve, the transient friction equation produces more damping for pressure and velocity, smaller amount of vapour and a phase shift in comparison with steady friction results.
The code selected for the use of the transient friction equation in the Two-

Fluid Model is the code written in the frame of WAHA project. The numerical results obtained with this code are compared with experimental results for Simpson experiment and UMSICHT PPP experiment. The transient friction equation has a negligible impact on the results for the PPP experiment but it improves the results for the Simpson experiment.

Chapter 2

State of the art of transient friction research

The comparisons between the numerical and experimental results show that the calculations for fast transients made with a steady friction formula do not give good results. This was demonstrated by Zielke [46], Eichinger and Lein [16], Pezzinga [27], Brunone et al. [9], Axworthy et al. [2] and others. There is still a need for physically-based transient models of the dissipative effects, that would give better predictions of the evolution of the state variables. One can find quite many transient friction models in the literature and several transient friction formulas seem quite promising.

In 1968, Zielke [46] found a frequency dependent model for laminar transient flows. He applied the Laplace transform to the momentum equation for parallel axisymmetric flow of an incompressible fluid and derived the equation which relates the wall shear stress to the instantaneous mean velocity and to the weighted past velocity changes:

$$\tau(t) = \frac{4\rho\nu}{R}w(t) + \frac{2\rho\nu}{R}\int_0^t \frac{\partial w}{\partial t}(u)W_f(t-u)du \tag{2.1}$$

where τ represents the wall shear stress, ν the kinematic viscosity, w the velocity and W_f a weighting function which is a function of the dimensionless time:

$$t_0 = \frac{\nu t}{R^2}$$

For $t_0 > 0.02$ the proposed correlation for weighting function is:

$$W_f(t_0) = e^{-26.3744 t_0} + e^{-70.8493 t_0} + e^{-135.0198 t_0} + e^{-218.9216 t_0} + e^{-322.5544 t_0}$$

For $t_0 < 0.02$:

$$\begin{aligned} W_f(t_0) =& 0.282095 t_0^{-0.5} - 1.250000 + 1.057855 t_0^{0.5} + 0.937500 t_0 + \\ & 0.396696 t_0^{0.75} - 0.351563 t_0^2 \end{aligned}$$

The numerical results obtained with this equation were compared with the experimental results of Holmboe and Rouleau [20] for a laminar flow of oil, having a viscosity almost fifty times greater than the viscosity of water. The water hammer phenomenon was induced by the fast closure of a downstream valve. The results obtained with Zielke's equation were in very good agreement with the experimental results (Fig. 2.1) but the use of his model in a numerical code requires much computation time and large memory capacity.

Trikha [38] derived an approximate expression for the frequency-dependent friction in laminar flow based on Zielke's solution. The use of this approximate expression requires much less computation time than the use of the exact expression. The results obtained by Trikha using this approximated model were very close to those obtained by Zielke [46] using the exact expression. They were also in good agreement with the experimental results for an oil flow obtained by Holmboe and Rouleau [20].

A similar approach to Zielke's one was adopted by Achard and Lespinard in 1981 [1]. They have started with the 2D, time-dependent, local balance equations for a cylindrical, laminar flow and worked out the conditions for

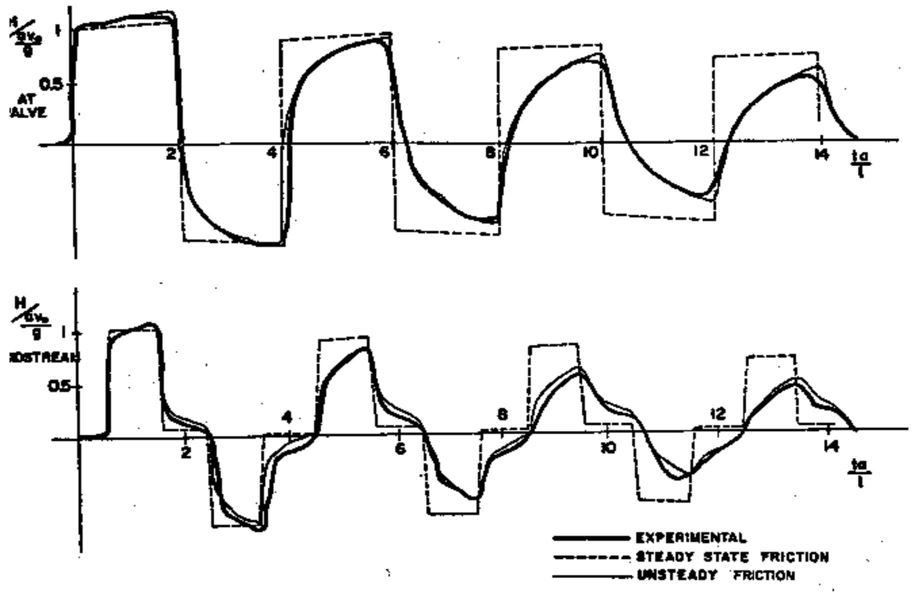

Figure 2.1: Comparison of experimental results Holmboe and Rouleau for a laminar flow of oil (continous thick line) with calculated results using steady-state friction (dashed line) and Zielke model (continuous thin line). Upper curve: head at the valve, lower curve: head at the midpoint.

which 1D cross-section averaged equations give the same results. They noticed that for the low-frequency cases the solution obtained by Zielke can be approximated by an ordinary, constant-coefficient, differential equation. The higher order the equation is, the better the approximation obtained is supposed to be. However, the study of accuracy shows that the simple first order differential equation (Eq. 2.2) gives excellent results up to the frequency given by $f_{max} \approx 20\nu/2\pi R^2$.
This model is a relaxation equation. Its non-dimensional form is:

$$\frac{d\tau}{dt} = \frac{4w - \tau}{\theta} + 6\frac{dw}{dt} \tag{2.2}$$

where θ is a relaxation coefficient. Moreover this kind of approximation remains physically consistent even for large frequencies, since they allow the

system to have a purely inertial behaviour when $f \to \infty$.
Achard and Lespinard postulated that the structure of their equation could be extended to turbulent cases. However for turbulent transient flows there is no analytical solution for unsteady wall shear stress and the problem of 1D transient friction modelling becomes much more complicated. The two-dimensional or quasi two-dimensional models proposed in the literature (Vardy and Hwang [39], Eichinger and Lein [16], Silva-Araya and Chaudhry [32], Pezzinga [27]) give results, which are quite close to experimental data.

One can also find some 1D turbulent models which seem attractive because of their simplicity. For example in 1959 Carstens and Roller [12] derived an expression for the unsteady shear stress assuming that the turbulent velocity profiles for steady and unsteady flows are similar. A term proportional to the instantaneous local acceleration is added to the classical steady-state term. The wall shear stress has the following form:

$$\tau = \frac{f \rho w^2}{2} + \frac{k}{4} \rho D \frac{\partial w}{\partial t} \tag{2.3}$$

where f is the steady-state coefficient, ρ is the density, D is the pipe diameter, w the velocity, t the time and k is the unsteady friction factor. The numerical value of k proposed by the authors is 0.2245. Their experimental results were not sufficiently accurate to either confirm or deny the reliability of this equation.
This kind of approach to shear stress modelling seemed attractive for other researchers, who also developped and investigated simple, unsteady shear stress formulae involving the derivatives of the velocity (e.g. Safwat and Polder [29], Brunone et al. [6, 7], Axworthy et al. [2], Vitkovsky et al. [43], Bughazem and Anderson [10]). These models are easy to apply in numerical codes and give promising results but they require more theoretical justification.

In 1973, Safwat and Polder [29] conducted an experiment in a U-tube that confirmed the dependence of the friction in oscillatory flows on the frequency of oscillations. They proposed a shear stress model similar to the Carstens and Roller model:

$$\tau(t) = \alpha w(t) + \beta \frac{\partial w}{\partial t} \tag{2.4}$$

The values of coefficients α and β were found to be dependent on the frequency of oscillations. Good agreement with the experiment was obtained.

The model proposed by Brunone et al. [6, 7] has become especially popular recently. On the basis of their own experimental tests they proposed an empirical formula based on the instantaneous acceleration:

$$\tau = \frac{f\rho w^2}{2} + \frac{k}{4}\rho D\delta\frac{\partial w}{\partial t} \tag{2.5}$$

where k is an unsteady friction coefficient empirically deduced and δ represents an operator that is equal to one when the product $w\frac{\partial w}{\partial t}$ is positive, and zero otherwise. Later they improved their model, making it a continous one (Brunone et al. (1991)):

$$\tau = \frac{f\rho w^2}{2} + \frac{k}{4}\rho D(\frac{\partial w}{\partial t} - a\frac{\partial w}{\partial x}) \tag{2.6}$$

where x is the axial coordinate and a is the pressure wave velocity. The results obtained with this equation were in good agreement with experiments performed by the authors for fast transient flows caused by fast closure of the valve located at the downstream end of a 100 m long pipe.

Vardy et al. [40] proposed a weighting function model of turbulent, transient friction at moderate Reynolds numbers developed in a similar manner as Zielke's model for laminar flows. Their model was based on a representation of a velocity distribution in a turbulent flow as a laminar annulus surrounding a uniform core. They solved a Laplace transformation of the boundary region equation with $w = 0$ at the wall and $w = w_{core}$ at the interface between the core and the annulus. The result was combined with a Laplace transformation of the core region equation, enabling a solution to be obtained for the complete cross-section. An inverse Laplace transformation yielded the weighting function for the transient wall shear stress equation. The wall shear stress history calculated with this model was very close to the wall shear stress history predicted using a five-region eddy viscosity model (Fig. 2.2).

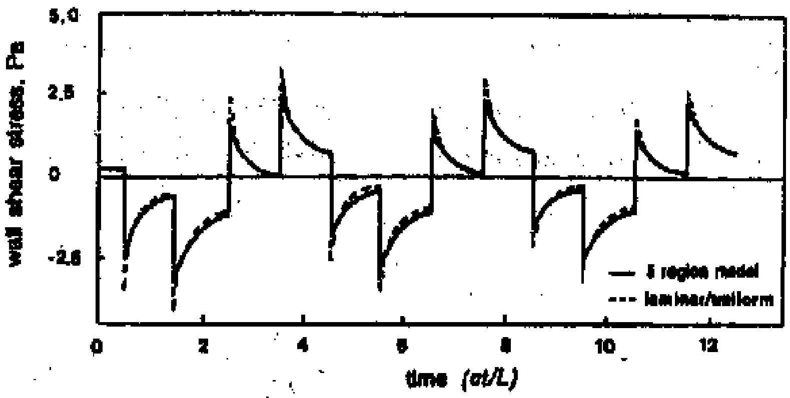

Figure 2.2: Wall shear stress at mid length of pipe predicted with a five-region eddy viscosity model (continuous line) and Vardy et al. model for turbulent flows at moderate Reynolds numbers (dashed line).

Vardy et al. developped a family of weighting functions similar to Zielke's weighting functions for transient laminar flows [46]. Zielke curve was found to be an upper bound asymptote valid for low Reynolds numbers. Vardy et al. argued that, at moderately large Reynolds numbers, the weighting functions curves may be truncated earlier than at low Reynolds numbers, thus reducing the amount of information that must be retained in computer memory. The pressure history obtained with their model was in a good agreement with the experimental results of Holmboe and Rouleau for turbulent flows (Fig. 2.3).
They also followed the approach of Trikha and suggested the approximation of weighting functions by exponential relationships.

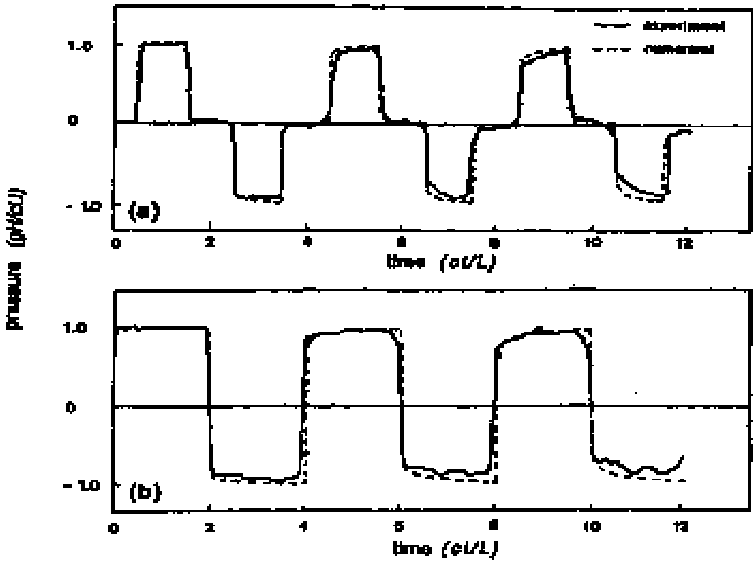

Figure 2.3: Pressure history in Holmboe and Rouleau apparatus at the mid-length of the pipe (a) and at the valve (b). Continuous line - experimental results, dashed line - numerical results obtained with Vardy model.

Vardy and Brown [41] extended their model to transient flows at high Reynolds numbers by assuming the turbulent viscosity to vary linearly within a thick shear layer surrounding a core of uniform viscosity. In case of low Reynolds number turbulent flows and short time intervals their model is identical to an earlier model developed by Vardy et al. [40]. In the case of laminar flows, it gives results equivalent to those of Zielke [46]. Like in Zielke's model, the wall shear stress is the sum of a steady part and an unsteady contribution, which is expressed by an integral:

$$\tau_{un}(t) = \frac{2\mu}{R}\int_0^T W_t(t^*)\frac{\partial w}{\partial t}dt^* \tag{2.7}$$

where μ is a laminar dynamic coefficient of viscosity, W_t is a weighting function for turbulent flows and R denotes the pipe radius. The time t^* is measured backwards from the current instant $t = T$.

The predicted value of the weighting function is dependent upon the non-dimensional time and the product fRe (f being steady friction coefficient). It decreases with increasing time and increasing fRe.
The weighting function can be approximated satisfactorily by a simple expression:

$$W_t = \frac{Ae^{-Bt}}{\sqrt{\pi t}} = \frac{A^* e^{-B^*\Psi}}{\sqrt{\Psi}} \tag{2.8}$$

where Ψ is the non-dimensional time and A^* and B^* are dimensionless forms of coefficients A and B. Coefficient A^* is constant and B^* is an inertial shear coefficient, being a unique function of the Reynolds number.
On the basis of the weighting function model, Vardy and Brown [42] proposed a theoretical justification of transient friction models based on instantaneous acceleration. If the term $\frac{\partial w}{\partial t}$ in Eq. 2.7 is assumed to be constant, it can be taken outside the integral and a model similar to Brunone's model [6, 7] is obtained. The acceptance of assumption of constant acceleration in the case of fast transient flows is questionable, but Vardy and Brown [42] proposed the range of applicability for which this assumption is valid. They derived an analytical expression for the unsteady coefficient of the Brunone et al. model as:

$$k = 2\sqrt{C} \tag{2.9}$$

where C is a shear decay coefficient related to the Reynolds number:

$$C = \frac{7.41}{Re^{\kappa}} \tag{2.10}$$

where $\kappa = \log_{10}(\frac{14.3}{Re^{0.05}})$.

A significant step forwards was also made with the use of the Extended Irreversible Thermodynamics (EIT) by Axworthy et al. [2] in an attempt to provide a physical basis to models based on acceleration. They derived the following equation for the unsteady wall shear stress:

$$\tau = \frac{f\rho w^2}{2} + \frac{\rho D}{4} k_A (\frac{\partial w}{\partial t} + w\frac{\partial w}{\partial x}) \tag{2.11}$$

where k_A is a phenomenological coefficient representing the frequency and is a function of time and space. As it is shown in Fig. 2.4 the results obtained with this model are in a good agreement with water hammer experiments of Pezzinga and Scandura [26]. Water hammer in Pezzinga experiment was caused by the fast closure of an upstream valve. However the derivation of the

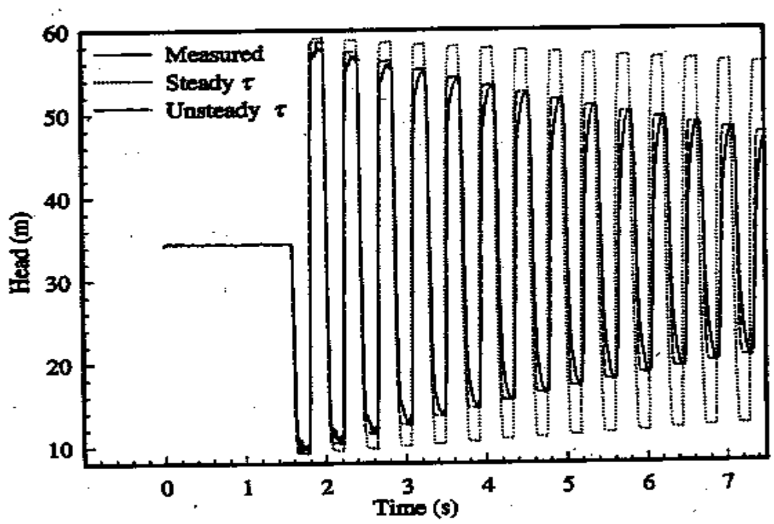

Figure 2.4: Pressure history at the valve in Pezzinga experiment. Continuous line - experimental results, dotted line - steady friction results, dashed line - unsteady friction results obtained with Axworthy model.

transient shear stress equation is somehow questionable. The introduction of the velocity into the thermodynamic space does not seem to be in agreement with the basis of EIT (Jou et al. [21]), as the velocity cannot be considered as a dissipative flux. Despite this remark, it is intended to show in this thesis that EIT, when correctly applied, can be indeed a solid theoretical basis to derive closure laws for fast transient flows, for which the assumption of local equilibrium is questionable.

Chapter 3

Derivation of the Friction Relaxation Model

3.1 Introduction

In this chapter the Friction Relaxation Model is derived. It is shown that the evolution of a transient shear stress involves two phases (or two steps). Each step is modelled separately. The model of the first phase is empirical. The use of Extended Irreversible Thermodynamics theory is proposed to model the second (relaxation) phase. The evolution equation for the transient shear stress during relaxation is obtained by introducing the transient shear stress into the thermodynamic space. We suppose that further enlargement of the thermodynamic space would lead to the equation containing both steps of the shear stress evolution but until now only the second step has been successfully modelled by EIT.

Some predictions of the wall shear stress and pressure in air flow obtained with the Friction Relaxation Model are compared with the results obtained with a CFD code (FLUENT) and are found to be in good agreement with them. This confirms that the transient wall shear stress equation proposed by us allows to model two-dimensional effects related to the velocity profile distortion induced by a pressure wave passage. The numerical calculations for water flow performed with the Friction Relaxation Model are compared with experimental results of Holmboe and Rouleau [20]. The transient friction coefficients present in the Friction Relaxation Model are evaluated on the basis of experimental results.

3.2 Interpretation of the shear stress evolution in terms of two steps

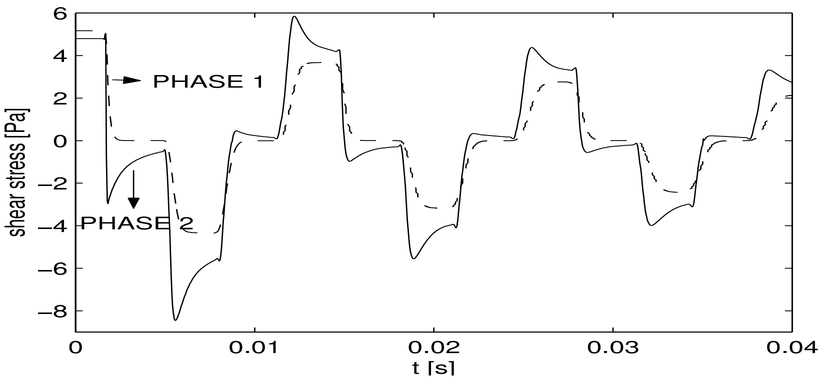

Figure 3.1: Air flow. Wall shear stress in the middle of the pipe versus time. Solid line - axisymmetric calculations made with FLUENT; dashed line - 1D steady state shear stress model.

2D axisymmetric water hammer simulations have been performed with FLUENT in order to better understand what happens with the wall shear stress when a pressure wave passes through the tube. The two-layer model of turbulence was chosen to do the calculations (FLUENT 5 user's guide, volume 2). In the two-layer model, the whole domain is subdivided into a viscosity-affected region and a fully-turbulent region. In the fully turbulent region, the $k-\epsilon$ model is employed. In the viscosity-affected near-wall region, the one-equation model of Wolfstein [44] is employed. The grid at the wall is refined ($y^+ < 5$).

Calculations were made for the fast closure of a valve in a tube having a length of 1.13 m and an internal diameter of 32 mm. The fluid was air. The initial, steady-state mass flow rate of the air is equal to 0.042 kg/s, the temperature is 293 K, and the pressure is 1 bar. For the same conditions, a calculation was run with a 1D model using a steady-state expression for the wall shear-stress.

It can be observed in Fig. 3.1 that the steady-state wall shear stress equation is not sufficient to predict well the transient shear stress evolution calculated with FLUENT. It appears that the evolution of the transient shear stress presents two steps. At each passage of a pressure wave, the first step, which is very short, is a dramatic change of the wall shear stress. The second step, much longer, is the exponential tendency to reach a new steady-state value of the wall shear stress. Calculations of shear stress history performed with FLUENT confirm the results obtained by other researchers, e.g. Vardy and Hwang [39], Brunone et al. [8], Silva-Arraya and Chaudry [32]. In the following sections, it is shown how to derive a transient wall shear stress model which includes the information about both steps.

3.3 Modelling of the first step of the transient wall shear stress evolution

It is shown in Fig. 3.1 that during both deceleration and acceleration the steady-state friction model predicts much smaller values of the wall shear stress than those obtained with CFD simulations performed with FLUENT. It is important to understand the source of this discrepancy.

3.3.1 Sudden deceleration

The velocity profiles obtained by FLUENT simulations in 2D in the vicinity of a wall before and immediately after a sudden deceleration are shown in Fig. 3.2. The velocity is shown as a function of a non-dimensional variable

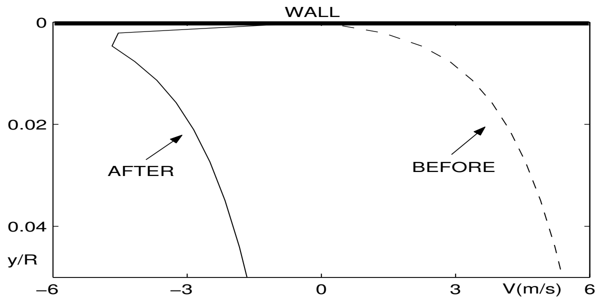

Figure 3.2: Velocity profile during deceleration before and after the passage of a pressure wave.

which is the distance from the wall divided by the radius of the pipe. For clarity, only the part of the profile very close to the wall is shown. In case of a sudden deceleration, immediately after the passage of the wave, the average velocity is close to zero even though the velocity gradient at the wall is very large. Therefore the steady wall shear stress corresponding to and calculated by means of the average velocity is also close to zero, while the real shear stress is very significant. The velocity and the shear stress at the wall have the signs opposite to the velocity in the core flow (the velocity in the core flow is not shown in the figure). This phenomenon is called 'annular effect' and was firstly described by Richardson and Tyler [28].
More information about the behaviour of the velocity profiles during deceleration can be found in Appendix C.

3.3.2 Sudden acceleration

The velocity profiles obtained by FLUENT simulations in 2D in the close vicinity of a wall before and immediately after sudden acceleration are shown in Fig. 3.3. During sudden acceleration the average velocity changes from zero (in the Fig. 3.3 the velocity profile at the wall is still in non-equilibrium caused by the previous passage of a pressure wave, but the cross-section averaged velocity is equal to zero) to some finite value. However, after the

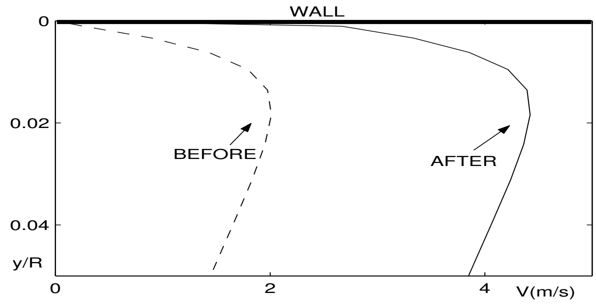

Figure 3.3: Velocity profile during acceleration before and after a passage of a pressure wave. The velocity profile before the passage of the wave had been disturbed and had not yet reached its steady-state form.

passage of a pressure wave the velocity gradient at the wall is larger than the one predicted by the steady-state (Darcy) equation. The velocity and the shear stress at the wall have the same signs as the velocity in the core flow (the velocity in the core flow is not shown in the figure).
More information about the behaviour of the velocity profiles during aceleration can be found in Appendix C.

3.3.3 Relation between pressure wave amplitude and sudden change of wall shear stress

The abrupt change of the wall shear stress during a water hammer is caused by the pressure wave. When the pressure wave is passing, it is not causing significant changes in the velocity profile shape except in the immediate neighborhood of the wall. Similar observations can be made on the basis of velocity profiles presented in the papers by Vardy and Hwang [39], Pezzinga [27]. In fact we deal with a kind of translation of the velocity profile about a certain vector. This translation being caused by the pressure wave, the length of the translation vector is supposed proportional to the amplitude of pressure wave. The amplitude of this wave is estimated by Joukowski equation:

$$\Delta p = \rho a \Delta w \tag{3.1}$$

where a is the wave velocity and Δw is the difference between the velocities before and after the passage of the wave. For the fast closure of a valve, this difference is equal to the initial velocity. If we assume that the sudden change of the wall shear stress, being caused by the pressure wave, is proportional to the amplitude of the pressure wave, we have:

$$\Delta \tau = k_w \rho a \Delta w \tag{3.2}$$

where k_w is a coefficient of proportionality, which has to be adjusted against experiments.

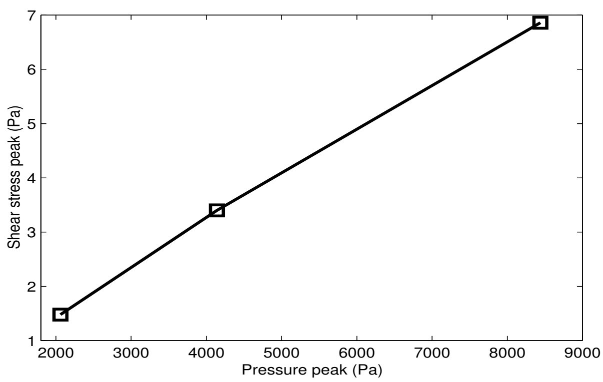

Figure 3.4: Proportionality of the shear stress peak to the pressure peak

Several 2D axisymmetric calculations with FLUENT have been performed for air flow in order to confirm the hypothesis presented in Eq. 3.2. In table 3.1 the results of three tests for different initial velocities are shown. The shear stress peaks and the pressure peaks were calculated at the midpoint during sudden decelerations after the closure of the valve. One can notice that the shear stress peak is proportional to both: the pressure peak and the initial velocity. The proportionality of the shear stress peak to the pressure

Table 3.1: Proportionality of the shear stress peak to the pressure peak

Initial velocity (m/s)	Δp (Pa)	$\Delta \tau$ (Pa)	k_w
5	2060	1.48	0.00072
10	4140	3.40	0.00082
20	8440	6.86	0.00081

peak is also presented in the Fig. 3.4.
Table 3.1 confirms the validity of the hypothesis 3.2.
As the shear stress peak caused by the passage of a pressure wave is proportional to the change of velocity, it is supposed to be greater for turbulent flows than for laminar flows.

3.4 Modelling of the second step of the transient wall shear stress evolution

Contrary to the first step, during the second (relaxation) phase the shape of the velocity profile changes, tending to the steady-state profile. As the velocity profile is tending to reach the steady-state shape, the value of shear stress evolves to the steady-state value. An equation describing the second step of the wall shear stress evolution can be derived from Extended Irreversible Thermodynamics.

3.4.1 Basic assumptions of Extended Irreversible Thermodynamics

Although Classical Irreversible Thermodynamics has been able to describe well many non-equilibrium phenomena, the observations have been made that, in certain cases, it is not sufficient. The example of such phenomenon is the experiment with marbles made by Reynolds in 1885 (Jou et al. [21]).

He observed that when a leather bag is filled with marbles, topped up with water and then twisted, the marble density decreases, when the rate of shear is increased, at constant temperature and pressure. This means that the density is not a function of only pressure and temperature. In the case of the experiment with the marbles, density is also a function of shearing rate. This example shows that, in certain situations, it may be necessary to enlarge the thermodynamic space to describe the observations. The classical thermodynamic variables become functions of some additional variables. Therefore it was suggested to extend the thermodynamic space by these additional variables. This is the basic concept of Extended Irreversible Thermodynamics. The additional variables are called dissipative fluxes.

EIT does not make the assumption of local equilibrium, while Classical Irreversible Thermodynamics (CIT) is based on the local equilibrium hypothesis (Jou et al. [21], Bilicki et al. [5]). In CIT, all thermodynamic variables are defined in the state of equilibrium. It is assumed that the relationships between state variables defined in equilibrium remain valid also outside equilibrium. EIT postulates the extension of the thermodynamic space by the variables that reflect the non-equilibrium of the system, such as the dissipative fluxes. This extension results in a different state equation for non-equilibrium than for equilibrium. The generalized entropy depends both on the classical variables and on the dissipative fluxes. Taking this dependance into account, new closure laws for the dissipative fluxes can be derived. The dissipative fluxes (like the fluxes of mass due to diffusion, momentum due to friction, and energy due to heat conduction) have the status of independent variables at the same level as the classical variables (e.g. pressure, temperature).

In this thesis, it is suggested that this extension of the thermodynamic space enables to model the information about the non-equilibrium which is lost in the systems described with the 1D cross-section averaged equations. This means that the choice of the thermodynamic space depends also on the number of dimensions taken into account in the modelling. The classical thermodynamics may be sufficient in 3D or 2D, whereas new variables may need to be introduced in 1D to account for non-equilibrium profile effects. This is the case in the fast transient flows. Therefore, in order to evaluate the dissipation effects during non-equilibrium events, we propose to extend the thermodynamic system described with the variables averaged in the cross-section by the wall shear stress considered as a 1D momentum flux. This extension enables to model the 2D information about the velocity profile lost in 1D modelling.

3.4.2 EIT as a tool to fast transient modelling

EIT can be especially useful for the class of phenomena where the thermodynamic variables are significantly influenced by non-equilibrium, so that the local equilibrium hypothesis is no longer valid. Such situations occur during fast transient events such as water hammers as shown in Fig. 3.2 and 3.3. The steady-state closure law for the wall shear stress is not satisfactory in fast transients, so that there is a need to find a new equation which would include the information about non-equilibrium.

The local equilibrium hypothesis assumes that we can divide a system into many cells treated as macroscopic thermodynamic subsystems with uniform thermodynamic quantities inside each cell. This hypothesis is obviously not valid for fast transient phenomena where strong gradients in space and strong derivatives with respect to time are observed. In the vicinity of a pressure wave, large differences occur between the flow variables upstream and downstream of the wave. Just after the passage of the wave, the wall shear stress starts to relax until it reaches the steady-state value. The time constant is called relaxation time. As shown by Jou et al. [21] (see the derivation of the Cattaneo equation for heat flux), the evolution equations for dissipative fluxes in EIT may have the form of relaxation equations.

In fast transient flows described by 1D cross-section averaged equations, the information about non-equilibrium resulting from a passage of a pressure wave is lost. After the passage of the wave, even if the averaged velocity is constant, the velocity profile, especially in a close neighborhood of a wall, is evolving. The EIT applied into 1D description of the system enables to model this evolution.

3.4.3 Derivation of the relaxation equation for wall shear stress from Extended Irreversible Thermodynamics

In this section, EIT is used to derive a relaxation equation which describes the second step of the transient wall shear stress evolution.

The basic set of one-dimensional balance equations of mass, momentum and energy averaged in the cross-section for an adiabatic flow in a horizontal cylindrical pipe is:

$$\frac{\partial \rho}{\partial t} + \frac{\partial \rho w}{\partial x} = 0 \tag{3.3}$$

$$\rho \frac{\partial w}{\partial t} + \rho w \frac{\partial w}{\partial x} + \frac{\partial p}{\partial x} = -\frac{4}{D}\tau \tag{3.4}$$

$$\rho \frac{\partial u}{\partial t} + \rho w \frac{\partial u}{\partial x} + p \frac{\partial w}{\partial x} = \frac{4w}{D}\tau \tag{3.5}$$

where all dependent variables are cross-section area averaged, w denotes the cross-section averaged velocity, u the internal energy per unit mass, and p the pressure. τ is the shear stress exerted by the fluid on the wall. For steady flow τ is expressed by:

$$\tau_s = \frac{f \rho w |w|}{2} \tag{3.6}$$

We need a closure equation for the wall shear stress in transient flow and EIT seems to be a way to determine this law as was suggested by Axworthy et al. [2]. These authors introduced the velocity in the entropy state equation as the variable which would reflect the local non-equilibrium of the thermodynamic system. We suggest another extension of the thermodynamic space, which leads to a relaxation equation for the wall shear stress. According to EIT theory (Jou et al. [21]), we introduce the shear stress as a one-dimensional dissipative flux to the state equation:

$$s = s(u, \rho, \tau^2) \tag{3.7}$$

The square of the shear stress is chosen in order to ensure its positive value. Indeed, the shear stress exerted by the fluid on the wall has the same sign as the velocity and can be either positive or negative during a water hammer event. Then the total differential of the entropy has the form:

$$ds = \left(\frac{\partial s}{\partial u}\right)_{\rho,\tau} du + \left(\frac{\partial s}{\partial \rho}\right)_{u,\tau} d\rho + \left(\frac{\partial s}{\partial \tau^2}\right)_{\rho,u} d\tau^2 \tag{3.8}$$

The total derivative of the entropy is:

$$\frac{ds}{dt} = \left(\frac{\partial s}{\partial u}\right)_{\rho,\tau} \frac{du}{dt} + \left(\frac{\partial s}{\partial \rho}\right)_{u,\tau} \frac{d\rho}{dt} + \left(\frac{\partial s}{\partial \tau^2}\right)_{\rho,u} 2\tau \cdot \frac{d\tau}{dt} \tag{3.9}$$

We define the non-equilibrium temperature:

$$\left(\frac{\partial s}{\partial u}\right)_{\rho,\tau} \triangleq \frac{1}{T} \tag{3.10}$$

and the non-equilibrium pressure:

$$\left(\frac{\partial s}{\partial \rho}\right)_{u,\tau} \triangleq -\frac{p}{T\rho^2} \tag{3.11}$$

Note that these definitions are consistent with CIT definitions for temperature and pressure and 1D assumptions. The one-dimensional mass (Eq. 3.3) and energy (Eq. 3.5) balance equations for adiabatic flow are used to calculate the total derivatives of internal energy and density. Then we obtain:

$$\frac{ds}{dt} = \frac{1}{T}\left(-\frac{p}{\rho}\frac{\partial w}{\partial x} + \frac{4w}{D\rho}\tau\right) - \frac{p}{T\rho^2}\left(-\rho\frac{\partial w}{\partial x}\right) + 2\left(\frac{\partial s}{\partial \tau^2}\right)_{\rho,u} \tau\frac{d\tau}{dt} \tag{3.12}$$

Finally Eq. 3.9 can be written:

$$\frac{ds}{dt} = \frac{4w}{D\rho T}\,\tau + 2\left(\frac{\partial s}{\partial \tau^2}\right)_{\rho,u} \tau\frac{d\tau}{dt} \tag{3.13}$$

In the case of a unit mass of fluid undergoing an adiabatic transformation of state, either in steady state or in the transient conditions created by the passage of a pressure wave (second step of the model), the entropy balance equation is given by:

$$\frac{ds}{dt} = \frac{\sigma}{\rho} \tag{3.14}$$

where σ is the positive entropy production rate. By comparing Eq. 3.13 and Eq. 3.14, we obtain an expression for σ:

$$\boxed{\sigma = \tau \left(\frac{4w}{DT} + 2\rho \left(\frac{\partial s}{\partial \tau^2} \right)_{\rho,u} \frac{d\tau}{dt} \right)} \tag{3.15}$$

Here the wall shear stress can be identified as the generalized flux and the term in the brackets as the generalized force. To guarantee the positiveness of the rate of entropy production, we assume that there exists a linear relation between force and flux:

$$\tau = L \left(\frac{4w}{DT} + 2\rho \left(\frac{\partial s}{\partial \tau^2} \right)_{\rho,u} \frac{d\tau}{dt} \right) \tag{3.16}$$

where L is a positive proportionality coefficient which can be calculated from CIT. Indeed in steady state conditions Eq. 3.16 reduces to:

$$\tau = L \frac{4w}{DT} \tag{3.17}$$

Moreover, using the wall shear stress for steady flows ($\frac{d\tau}{dt} = 0$) given by Fanning's formula:

$$\tau = \frac{f \rho w |w|}{2} \tag{3.18}$$

and identifying Eq. 3.17 and Eq. 3.18, we conclude that the proportionality coefficient L between the force and the flux is:

$$L = \frac{f \rho |w| DT}{8} \tag{3.19}$$

Using Eq. 3.19, the transient shear stress 3.16 is finally expressed as:

$$\tau = \frac{f \rho w |w|}{2} + \frac{f \rho^2 |w| DT}{4} \left(\frac{\partial s}{\partial \tau^2} \right)_{\rho,u} \frac{d\tau}{dt} = \tau_s - \theta \frac{d\tau}{dt} \tag{3.20}$$

where τ_s stands for steady shear stress and

$$\theta \triangleq -\frac{f\rho^2|w|DT}{4}\left(\frac{\partial s}{\partial \tau^2}\right)_{\rho,u} \tag{3.21}$$

is interpreted as a relaxation time. By comparison with FLUENT simulations in 2D, we found that the order of magnitude of this relaxation time is 0.001s. Collecting the above results, we obtain the relaxation equation for the transient shear stress in the simplified form:

$$\boxed{\frac{d\tau}{dt} = \frac{\tau_S - \tau}{\theta}} \tag{3.22}$$

This equation describes the second step of a transient shear stress evolution. If θ is constant it can be interpreted as follows. When the transient wall shear stress is greater than the steady shear stress, the shear stress derivative is negative, which means that the transient shear stress decreases exponentially, tending to the steady state value. In the case of a transient wall shear stress smaller than the steady one, the derivative has a positive sign, so the transient shear stress increases to reach the steady state. For the case of fast transient flows, the unsteady shear stress is always greater than the steady shear stress, so it decreases exponentially, having the steady-state value as an asymptote.

3.5 Friction Relaxation Model

Collecting the above information about the two steps of the shear stress evolution, the new transient shear stress model can be proposed. The model contains:

- The sudden shear stress peak during the passage of a pressure wave evaluated as:

$$\Delta\tau = k_w \rho a \Delta w \tag{3.23}$$

- The subsequent relaxation to the steady-state value of the shear stress according to the equation:

$$\frac{d\tau}{dt} = \frac{\tau_s - \tau}{\theta} \tag{3.24}$$

Looking at Fig. 3.1, we can notice that the wall shear stress peak predicted by Eq. 3.2 is the initial condition for the relaxation phase. This shear stress peak occurs only in the region where the wave is actually passing, *i.e.* in the flow region where the derivative $\frac{\partial w}{\partial t}$ is significant. In other regions (steady-state regions), this derivative is negligible. Therefore, the introduction of the instantaneous acceleration instead of the velocity into the term responsible for the wall shear stress peak (Eq. 3.2) will make this term significant only in the region were the wave 'exists' at a given time.

The temporal derivative of the velocity is used because the local variation of the velocity ($\frac{\partial w}{\partial t}$) generates the non-equilibrium which will then progressively vanish according to the relaxation equation. Therefore, the term responsible for the first step of the shear stress evolution has to be considered as a local source term.

Thus the full equation including both steps describing the shear stress evolution becomes:

$$\boxed{\frac{d\tau}{dt} = \frac{\tau_s - \tau}{\theta} + k_T \rho |a| \frac{\partial w}{\partial t}} \tag{3.25}$$

where $|a|$ is the absolute value of the pressure wave velocity and k_T is the

transient friction coefficient. The relaxation time θ has the order of milliseconds.
There is also a possibility to use the spatial derivative of the velocity to detect the wave (Brunone et al. [6] used the combination of both derivatives in their model), but the use of the temporal derivative of the velocity allows the sign of the transient shear stress at the wall to be changed during deceleration and to remain unchanged during acceleration. Moreover, the temporal derivative after integration in time during the wave passage will give the difference Δw between the velocities after and before the passage of the wave, which is present in Eq. 3.23.
We will refer to equation (3.25) as to the Friction Relaxation Model.

In the codes the derivative $\frac{\partial w}{\partial t}$, which serves as a wave detector, can be replaced by the backward finite difference $\frac{\Delta w}{\Delta t}$ (Δt is a time step and Δw is a difference between the values of the velocity from two last time steps). Then the Friction Relaxation Model can be written as:

$$\frac{d\tau}{dt} = \frac{\tau_s - \tau}{\theta} + k_T \rho |a| \frac{\Delta w}{\Delta t} \tag{3.26}$$

This replacement makes the form of the Friction Relaxation Model conservative.

The results of the calculations performed with a 1D code including the Friction Relaxation Model (see appendix for the information about the code) were compared with 2D simulations performed with FLUENT. Let us look at the comparison between the shear stress predicted by the Friction Relaxation Model and the 2D simulations shown in Fig. 3.5.
We can notice that the two steps of the shear stress evolution (the sudden shear stress peak and the subsequent relaxation) are correctly predicted by the Friction Relaxation Model. The relaxation time θ and the coefficient k_T were fitted against FLUENT simulations. The values of the coefficient k_T were found to differ for acceleration and deceleration; on the basis of calculations for air flows, we found that the value of k_T for deceleration is about 75% of the value for acceleration. The corresponding pressure evolutions are

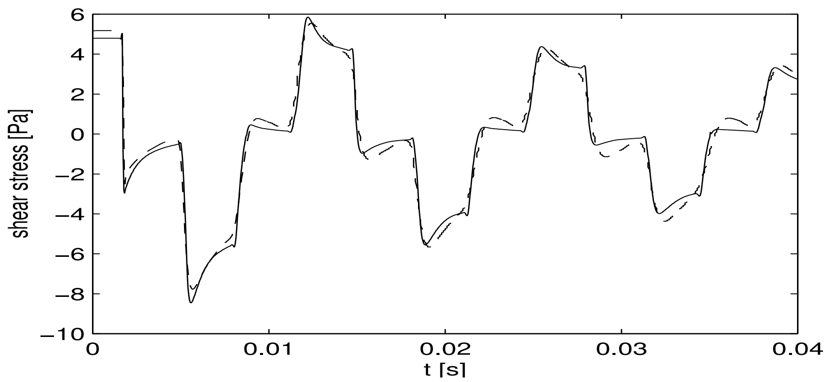

Figure 3.5: Air flow. Wall shear stress in the middle of the pipe versus time. Comparison between the proposed Friction Relaxation Model (dashed line) and 2D calculations made with FLUENT (solid line). Relaxation time $\theta = 0.0014s$, k_T for acceleration $= 5.3 \cdot 10^{-4}$, k_T for deceleration $4.1 \cdot 10^{-4}$.

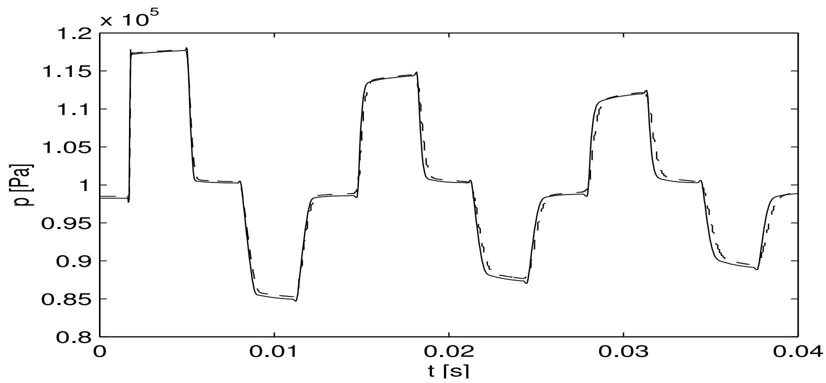

Figure 3.6: Air flow. Pressure in the middle of the pipe versus time. Comparison between the proposed Friction Relaxation Model (dashed line) and 2D calculations made with Fluent (solid line). Relaxation time $\theta = 0.0014s$, k_T for acceleration $= 5.3 \cdot 10^{-4}$, k_T for deceleration $4.1 \cdot 10^{-4}$.

shown in Fig. 3.6. The amplitude of the wall shear stress peak in the first step of the wall shear stress evolution is proportional to the coefficient k_T.

The Friction Relaxation Model in the form presented by Eq. 3.25 is proposed for single-phase transient flows caused by fast manoeuvres in simple pipes.

3.6 Modelling of the relaxation time

The relaxation time has the order of milliseconds and is proportional to the diameter of the pipe (see Eq. 3.21). In pipes with large diamaters it takes more time for the velocity profile to reach its steady - state shape than in pipes with small diameters.
It also appears that θ is larger for laminar flows than for turbulent flows *i.e.* the turbulence increases the speed of the transfer of information from the core to the boundary layer.
Thus we define a non-dimensional relaxation time as:

$$\theta_0 \triangleq \theta \frac{w}{D} \tag{3.27}$$

θ_0 is supposed to be proportional to the Reynolds number for laminar flows in pipes with a smooth wall and to be constant for turbulent flows:

- For laminar flows:

  $$\theta_0 = C_0 Re \tag{3.28}$$

  where C_0 is a non-dimensional parameter. Consequently, from Eq. 3.27:

  $$\theta = C_0 \frac{D^2}{\nu} \tag{3.29}$$

  where ν stands for kinematic viscosity.

- For turbulent flows:

  $$\theta_0 = C_1 \tag{3.30}$$

  where C_1 is a constant. Consequently, from Eq. 3.27:

  $$\theta = C_1 \frac{D}{w} \tag{3.31}$$

The velocity w is a characteristic velocity of the fast transient flow; it is suggested to interpret it as the initial velocity or the difference Δw between the velocities before and after the passage of a pressure wave. The suggestions about the expressions for θ presented here can serve as the basis for further modelling which should be verified against an adequate number of dedicated experiments. In this thesis most of the calculations have been done with θ evaluated on the basis of the shear stress history obtained with FLUENT.

One should take care about the value of the time step Δt with respect to θ during the calculations. In order to obtain correct results the condition:

$$\Delta t < \frac{\theta}{20} \tag{3.32}$$

has to be satisfied.

3.7 Modelling of the k_T coefficient

The creation of a wide experimental database is necessary in order to propose an exact model of the coefficient k_T. This research is outside of the scope of this thesis. It appears that this coefficient is dependent on the material properties and is constant for a given fluid at high Reynolds numbers. In this thesis most of the calculations have been done with k_T evaluated on the basis of the Holmboe and Rouleau experiment [20]; however the flow in this experiment is slightly turbulent and more experimental data are needed for the appropriate modelling of k_T.

3.8 Results for a liquid flow

The above numerical tests were done for air flows. Although both the amplitude and shape of shear stress are completely different in transient conditions than in steady state, the difference of a few Pascals in shear stress doesn't have a great impact on the value of pressure, which is of the order of a few bars. The impact on the propagation velocity in air flow is also negligible. Therefore it is acceptable to use the steady state equation to predict the shear stress in air flow during fast transients.

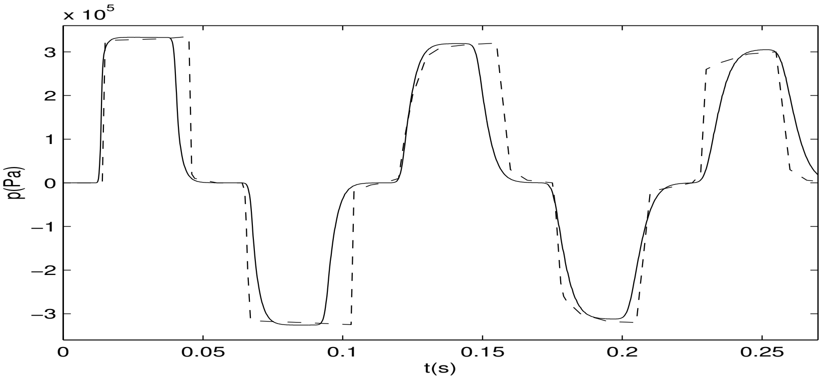

Figure 3.7: Water flow. Pressure in the middle of the pipe versus time. Comparison between the Friction Relaxation Model (solid line) and the experimental results of Holmboe and Rouleau (dashed line). Relaxation time $\theta = 0.0014s$, k_T for acceleration $= 2. \cdot 10^{-4}$, k_T for deceleration $1. \cdot 10^{-4}$.

On the contrary, in water flows, the difference between the steady and the transient shear stresses is very large. In order to evaluate the shear stress jump during the passage of a pressure wave, a comparison with experimental results has been done. The experiment of Holmboe and Rouleau [20] was used as a test case. The water hammer was caused by the fast closure of a downstream valve in a pipe of a diameter 0.0254 m and length 36.1 m. The initial velocity was 0.244 m/s. The calculations with the Friction Relaxation Model were done using the WAHA3 code described shortly in section 6.4 and in details in the WAHA3 manual (Tiselj et al. [37]). The effect of the pipe elasticity, which decreases the velocity of a pressure wave, was taken into account in the calculations ($E = 2 \cdot 10^{11}$, $d = 1.5$ mm).

The coefficients k_T were chosen in order to obtain the same pressure attenuation as in the experiment (Fig. 3.7). Here (water flow) k_T for deceleration

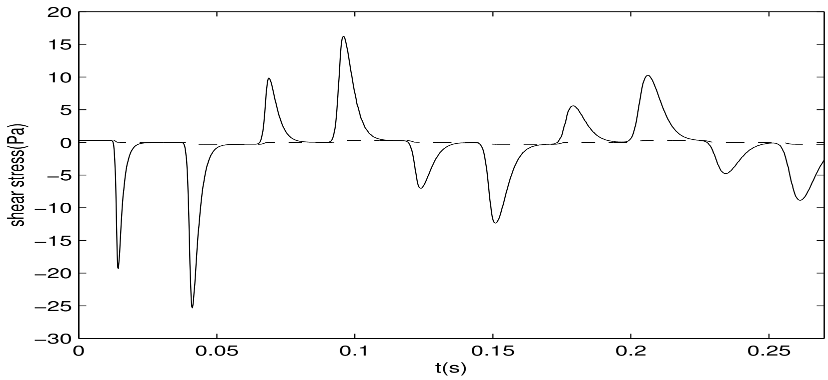

Figure 3.8: Water flow. Transient wall shear stress in the middle of the pipe versus time (solid line). Relaxation time $\theta = 0.0014$s, k_T for acceleration $= 2 \cdot 10^{-4}$, k_T for deceleration $1 \cdot 10^{-4}$. Dashed line - steady wall shear stress.

is 50% of k_T for acceleration. The relaxation time is kept equal to 1.4 ms, as for the air flow calculations.

It is observed that the difference between steady and transient shear stresses is about two orders of magnitude, especially at the beginning of the relaxation step (see Fig. 3.8). During the first passage of the wave, the steady state shear stress is equal to 0.3 Pa while the transient shear stress jumps to −20 Pa. After this jump, the steady shear stress is equal to zero while the transient shear stress remains significant (order 10^2 and 10^1) during the largest part of the period. One can also notice that, as time evolves, the first step is more and more dissipated. It is no longer a straight line, as at the very beginning. This dissipation is due to the derivative of velocity with respect to time.

The transient shear stress, although significantly different from the steady shear stress, has a rather small influence on the pressure amplitude for this experiment (Fig. 3.7). At the beginning of a fast transient, the steady-state equation is sufficient to predict the pressure peaks correctly (Fig. 3.9), but, after two wave periods, we can observe that the pressure amplitude predicted by the steady-state equation is greater than the one measured in the experi-

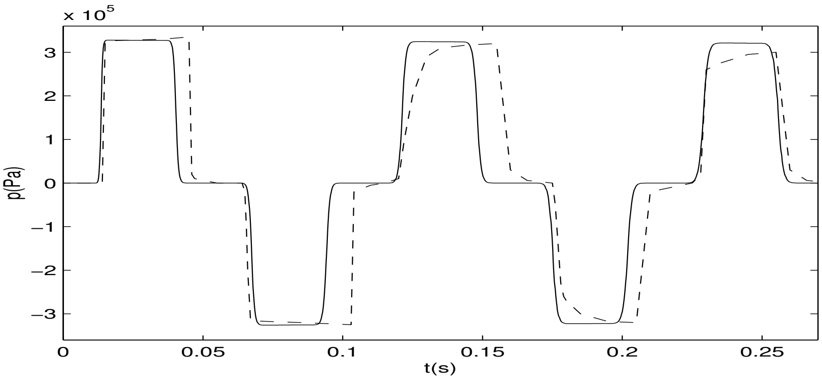

Figure 3.9: Water flow. Pressure in the middle of the pipe versus time. Comparison between results obtained with steady-state shear stress (solid line) and experimental results of Holmboe and Rouleau (dashed line).

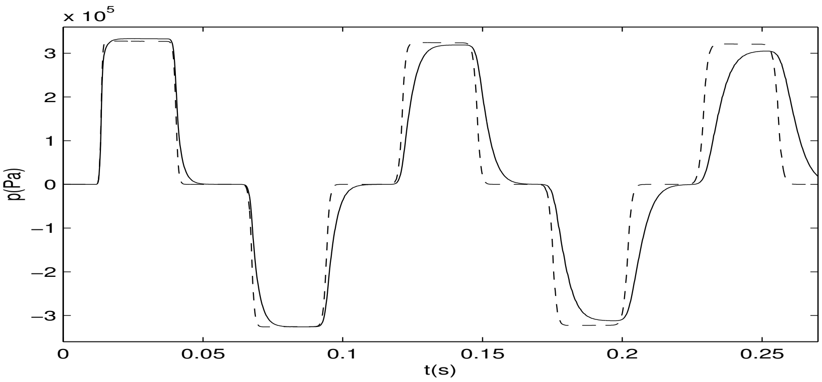

Figure 3.10: Water flow. Pressure in the middle of the pipe versus time. Comparison between results obtained with steady-state wall shear stress (dashed line) and transient wall shear stress (solid line).

ment. By comparing the results obtained with transient friction with results obtained with steady friction in Fig. 3.10, we can also observe some positive phase shift predicted by the Friction Relaxation Model.

3.9 Sensitivity analysis

The sensitivity of the Friction Relaxation Model to changes of the parameters θ and k_T was analyzed for the case of the experiment of Holmboe and Rouleau [20].

The influence of the relaxation time on the transient shear stress can be seen in Fig. 3.11. The calculations were done for relaxation times 1.4 ms and 2.8 ms. A larger relaxation time results in a larger energy dissipation and a larger wave period (Fig. 3.12).

The influence of coefficients k_T on the transient shear stress can be seen in the Fig. 3.13. The calculation were done for the coefficients k_T twice larger than those adjusted against experimental data of Holmboe and Rouleau both for acceleration and deceleration. Larger coefficients k_T also result in larger energy dissipations and larger wave periods (Fig. 3.14). The change of θ seems to have more impact on the pressure history than the change of k_T.

Of course larger coefficients θ and k_T give pressure histories which are not in a poor agreement with experimental results of Holmboe and Rouleau (Fig. 3.12 and 3.14).

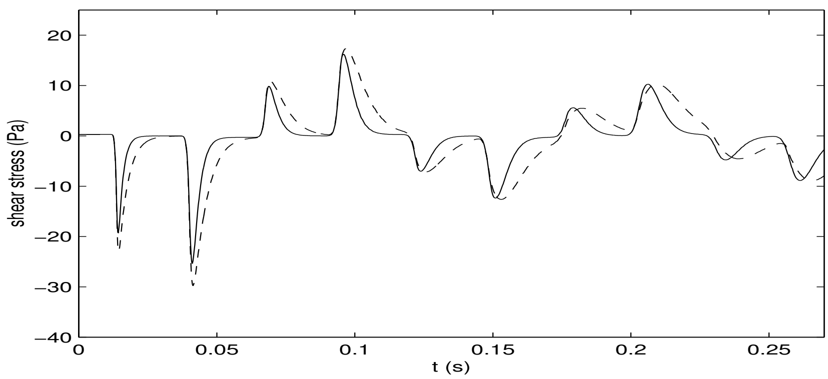

Figure 3.11: Water flow. Wall shear stress in the middle of the pipe versus time for different relaxation times: $\theta = 0.0014s$ (solid line), $\theta = 0.0028s$ (dashed line); k_T for acceleration $= 2 \cdot 10^{-4}$, k_T for deceleration $1 \cdot 10^{-4}$.

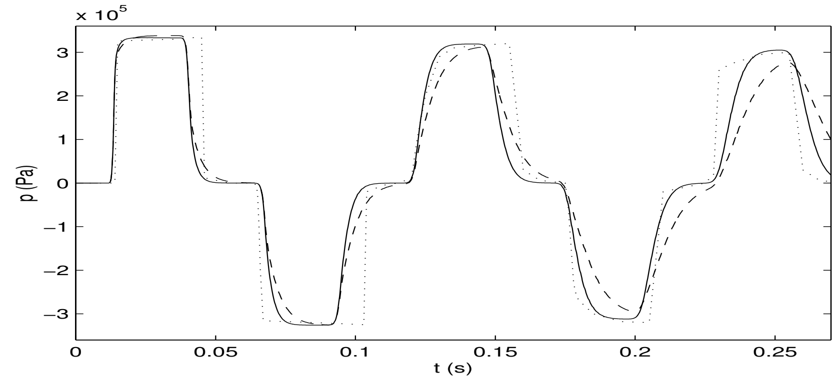

Figure 3.12: Water flow. Pressure in the middle of the pipe versus time for different relaxation times: $\theta = 0.0014s$ (solid line), $\theta = 0.0028s$ (dashed line); k_T for acceleration $= 2 \cdot 10^{-4}$, k_T for deceleration $1 \cdot 10^{-4}$. Pointed line - experimental results.

3.10 Conclusions

The evolution of the shear stress during fast transient flows is interpreted in terms of two steps. The first step is a sudden rise of the shear stress during the wave passage. The amplitude of this shear stress peak caused directly by the passage of a pressure wave is assumed to be proportional to the amplitude of this pressure wave.

The second step is the relaxation of the transient shear stress after the wave passage. During this relaxation phase, the shear stress tends exponentially from the value caused by the pressure wave to the value corresponding to the new steady state. The relaxation phase is modelled by a relaxation equation derived from the Extended Irreversible Thermodynamics theory.

The Friction Relaxation Model includes both steps of the shear stress evolution. It contains two coefficients that are needed to be evaluated on the basis of experimental data. One is the transient friction coefficient k_T responsible for the first step of the shear stress evolution, the other is the relaxation time θ responsible for the second step.

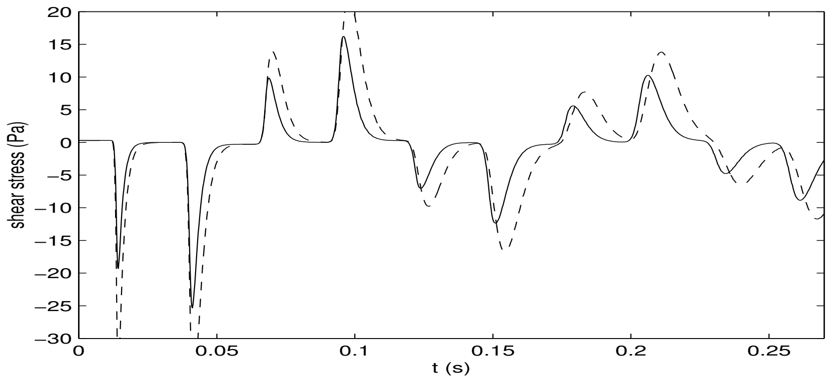

Figure 3.13: Water flow. Wall shear stress in the middle of the pipe versus time for different coefficients k_T: $k_T = 2 \cdot 10^{-4}$ acceleration, $1 \cdot 10^{-4}$ deceleration (solid line), $k_T = 4 \cdot 10^{-4}$ acceleration, $2 \cdot 10^{-4}$ deceleration (dashed line); $\theta = 0.0014s$

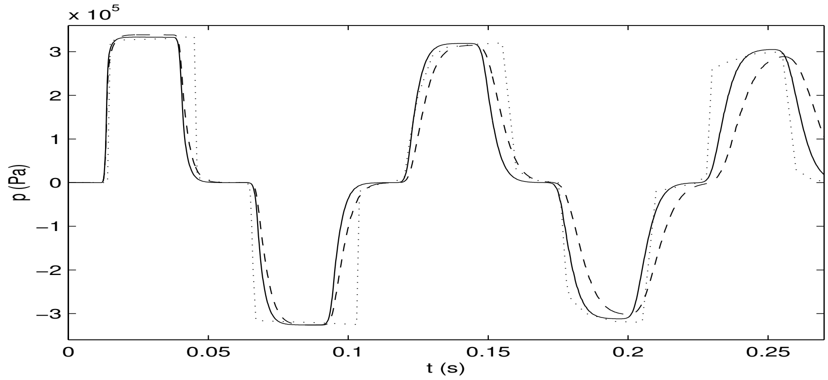

Figure 3.14: Water flow. Pressure in the middle of the pipe versus time for different coefficients k_T: $k_T = 2 \cdot 10^{-4}$ acceleration, $1 \cdot 10^{-4}$ deceleration (solid line); $k_T = 4 \cdot 10^{-4}$ acceleration, $2 \cdot 10^{-4}$ deceleration (dashed line); $\theta = 0.0014s$. Pointed line - experimental results.

By the comparison of the transient shear stress results obtained with a 1D code including Friction Relaxation Model with the results obtained with

FLUENT for air flow, k_T was found to be different for acceleration and deceleration. The value for deceleration is about 75% of the value for acceleration for the flow of air.
The value of k_T for water transient flows was evaluated on the basis of experimental data of Holmboe and Rouleau [20], here the value of k_T for deceleration was about 50% of the value for acceleration. **The order of magnitude of k_T for water flow is the same as for air flow**.
The value of relaxation time θ was retained the same for water flow as for air flow and the results were satisfactory. It seems that the relaxation time has always the order of milliseconds. Globally, the effect of the transient shear stress is much more important for a liquid flow than for a gas flow.
The sensitivity of the model to the change of the parameters θ and k_T was analyzed. The larger values of both parameters result in more dissipation and positive phase shift for the case of a transient flow caused by a fast closure of a downstream valve.

Chapter 4

Approximation of the Friction Relaxation Model by algebraic laws

4.1 Introduction

In this chapter, two approximations of the Friction Relaxation Model are proposed. The approximated equations are explicit, do not contain differential terms and are supposed to have practical significance for programmers who look for a simple transient friction model that can be put in a code without significant and time-consuming modifications of the code.
Both approximated equations are based on the information from the past. The first equation is based on the information recorded at the moment of a wave passage through a given point, the second one is based on the information from the last time step.

The Friction Relaxation Model is a partial differential equation, which cannot be solved analytically and introduced into the momentum equation. Therefore the full model of single-phase transient flow contains four evolution equations: mass, momentum, energy and shear stress:

$$\frac{\partial \rho}{\partial t} + \frac{\partial \rho w}{\partial x} = 0 \tag{4.1}$$

$$\rho \frac{\partial w}{\partial t} + \rho w \frac{\partial w}{\partial x} + \frac{\partial p}{\partial x} = -\frac{4}{D}\tau \tag{4.2}$$

$$\rho \frac{\partial u}{\partial t} + \rho w \frac{\partial u}{\partial x} + p \frac{\partial w}{\partial x} = \frac{4w}{D}\tau \tag{4.3}$$

$$\frac{\partial \tau}{\partial t} + w \frac{\partial \tau}{\partial x} = \frac{\tau_s - \tau}{\theta} + k_T \rho \left| a \right| \frac{\partial w}{\partial t} \tag{4.4}$$

The programmers looking for a simple model of dissipative effects for fast transient flows may find it too laborious and time-consuming to introduce one more partial differential equation into existing codes.
However, it is possible to use a simplified, approximated form of the Friction Relaxation Model that describes the same phenomenon of transient shear stress evolution *i.e.* the shear stress peak and the relaxation. The model has to satisfy the conditions:

1. Immediately after the passage of the wave, the value of the shear stress has to be the sum of the value of shear stress before the passage of the wave and the shear stress jump $\Delta\tau$.

2. Between two passages of the wave through the given point, the shear stress has to decrease exponentially with the rate of decrease determined by the relaxation time θ.

3. For times tending to infinity, the shear stress has to tend to the steady-state value:

$$\lim_{t \to \infty} \tau = \tau_s$$

.

Both approximations of the Friction Relaxation Model proposed in this thesis satisfy these three conditions.
The results obtained with approximated models were verified against the

results obtained with the original model for the case of a water hammer caused by a fast closure of a downstream valve in a pipe having a length of 50 m and a diameter of 20 mm. The initial velocity is 5m/s and the temperature is 293 K. The upstream tank has a constant pressure: 8 MPa. The chosen case was similar to the benchmark performed in the frame of WAHA project; only the diameter was smaller in order to produce more dissipative effects.
The codes used to make the calculations were developed by the author of this thesis and are described in appendix. The Godunov method was used (the grid had 400 nodes, Courant-Friedrichs-Lewy number = 0.5), which is stable if the condition: $CFL \leq 0.5$ is satisfied, [35].

4.2 Approximated wall shear stress model based on wave detection

Equation 4.5, an algebraic equivalent of the Friction Relaxation Model, was suggested based on the properties 1-3.

$$\tau(t) = \tau_s(t) + (\tau(t_0^-) - \tau_s(t) + k_a \Delta p(t_0)\mathrm{sgn}(\tau(t_0)))e^{\frac{-(t-t_0)}{\theta_a}} \qquad (4.5)$$

where τ_s is the steady shear stress, t_0 is the time of the wave passage through a given point, $\tau(t_0^-)$ is a shear stress before passage of the wave through a given point, k_a is a transient friction coefficient, $\Delta p(t_0)$ is the amplitude of a pressure wave for a given point, $\mathrm{sgn}(\tau(t_0))$ is the sign of the shear stress before passage of the wave, and finally θ_a is the relaxation time. At every time step, the values t_0, $\tau(t_0^-)$ and $\Delta p(t_0)$ need to be kept in memory for the node through which the wave passes. These values are kept in memory until the next wave comes to this node, so they are constant between two passages of the pressure wave through a given point. Obviously, the wave is dissipated into several nodes; the values of t_0, $\tau(t_0^-)$ and $\Delta p(t_0)$ are assigned to the node which is supposed to be 'the center' of the wave.

The expression $k_a \Delta p(t_0)$ represents the jump of the transient shear stress during the wave passage. The jump is proportional to the amplitude $\Delta p(t_0)$ of the pressure wave and its decrease in time follows the decrease of pressure wave. The shear stress immediately after the jump is equal to: $\tau(t_0) = \tau(t_0^-) + k_a \Delta p(t_0) \mathrm{sgn}(\tau(t_0))$.
The value $\tau(t_0)$ is thus the initial condition for the relaxation phase. The coefficient k_a is negative for deceleration and positive for acceleration. This convention, together with the expression $\mathrm{sgn}(\tau(t_0))$, allows the transient shear stress to change the sign during deceleration and to leave it equal to the sign before wave passage during acceleration.
It appears that similarly as in the exact FRM, the value of k_a for deceleration is about 50% of the value for acceleration for water flow. The coefficients k_a are different than k_T, because of the absence of the derivative $\frac{\partial w}{\partial t}$ and the punctual interpretation of the shear stress peak which is assigned to only one node in this approximated model. The relaxation time θ_a has a similar meaning as θ in the exact FRM *i.e.* determines the rate of the evolution of the transient shear stress during relaxation. It has also the order of milliseconds but its value is different than θ in the original Friction Relaxation Model due to the absence of the derivative $\frac{\partial w}{\partial t}$.
After the passage of the wave, the transient shear stress decreases exponentially and, if the wave doesn't come back, it becomes equal to the steady shear stress at infinity.

The algebraic equation 4.5 allows the introduction of the transient shear stress model containing two steps into existing codes without changing the number of governing equations. However, the process of shear stress evolution described by this equation is a kind of idealization of the reality. The wave is assigned to only one node. Therefore the numerical dissipation of the wave is avoided, but at the same time the physical dissipation is not taken into account. Because the CFL condition has to be satisfied, the wave normally stays during several time steps at a given node. A programmer has to be prudent to avoid the interpretation of this phenomenon by the code as the

passage of another wave.
Another problem is the determination of the node, which is supposed to be the center of the wave. It is here proposed to choose the node where the derivative $\frac{\partial p}{\partial x}$ is maximum.

The results of this approximated model are shown in Fig. 4.1 and 4.2. The relaxation time and coefficients k_a have been adjusted against the pressure results obtained with the original Friction Relaxation Model in order to obtain the same amplitudes (Fig. 4.2). In Fig. 4.1, we observe that the effect of the dissipation of the shear stress peak, which is present in the exact Friction Relaxation Model, is cancelled in the approximated model.

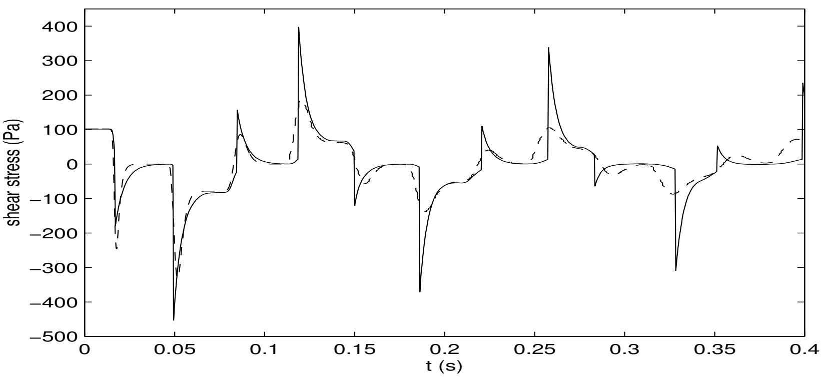

Figure 4.1: Water flow. Solid line: wall shear stress calculated with the approximated model in the middle of the pipe versus time; $\theta_a = 5$ms, k_a for acceleration $= 6 \cdot 10^{-5}$, k_a for deceleration $=-3 \cdot 10^{-5}$. Dashed line: wall shear stress calculated with the exact model, $\theta = 1.4$ms, $k_T = 2 \cdot 10^{-4}$ for acceleration, $k_T = 1 \cdot 10^{-4}$ for deceleration.

The major difference between the approximated equation 4.5 and the original Friction Relaxation Model is that, in the approximated equation 4.5, the shear stress jump is immediate (takes place during one time step) while, in the original model, the jump, although very short in comparison with

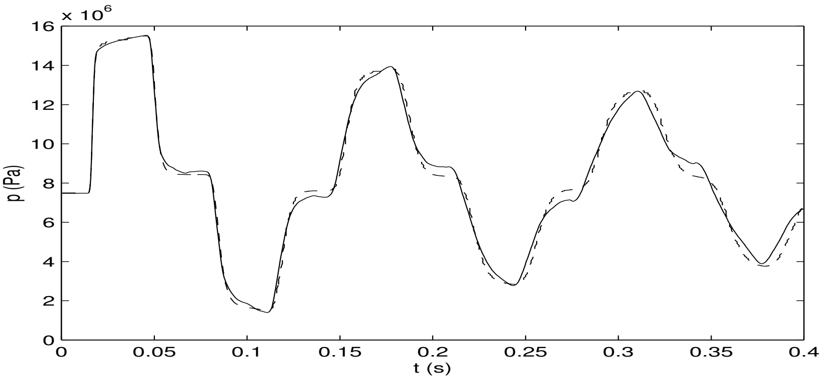

Figure 4.2: Water flow. Pressure in the middle of the pipe versus time. Comparison between the approximated model (solid line) and the exact model (dashed line)

the relaxation step, is not immediate. In the original model, the relaxation phenomenon, described by an exponential decrease is not excluded during the first phase but is dramatically dominated by the the jump of the wall shear stress.

As already said, the proposed model is simple and can appear useful for the programmers who look for an algebraic transient friction model that does not require big modifications of their code. However, the detection of the place where the wave is present at a given moment may be problematic. The method proposed here, based on the maximal pressure derivative, may sometimes lead to wrong results. For example, if some numerical instabilities occur, the wave may be detected at a wrong place. Sometimes it can also happen that the maximum of the derivative $\frac{\partial p}{\partial x}$ jumps over a few nodes and, for these nodes, the information about the additional energy dissipation due to the wave passage is lost. Therefore the model based on the wave detection is not recommended. It is rather suggested to use another approximation of the Friction Relaxation Model, described in section 4.3.

4.3 Approximated wall shear stress model based on last time step

In this section, an approximated shear stress model, which is a combination of analytical and numerical solution of the Friction Relaxation Model, is proposed. This approximated equation is supposed to have the same properties as the original model:

$$\frac{d\tau}{dt} = \frac{\tau_s - \tau}{\theta} + k_T \rho \left| a \right| \frac{\partial w}{\partial t}$$

The analytical solution of an ordinary differential equation of the type:

$$\frac{d\tau}{dt} = \frac{\tau_s - \tau}{\theta} \tag{4.6}$$

where τ_s is a constant, is an exponential function:

$$\tau = Ce^{\frac{-t}{\theta}} + \tau_s \tag{4.7}$$

where C is a constant determined by the initial conditions.
This exponential function describes the relaxation step of the transient shear stress evolution. During this phase, the actual shear stress value is dependent on the previous shear stress value. The relation between the values of the shear stress at two subsequent time steps is determined by the relaxation time. Therefore, one cannot find a transient shear stress model containing a relaxation step which would be only based on instantaneous conditions. The 'instantaneous' equations proposed in the literature contain the information about the first step - shear stress jump, but do not describe relaxation. Zielke [46] showed that the transient shear stress in laminar flows depends on the shear stress history. Vardy et al. [40] proposed a model similar to Zielke's model for turbulent flow and also confirmed this dependence.

We would like to propose an approximated model, which is a combination of an analytical (for the second step of shear stress evolution, see Eq. 4.7) and numerical (for the first step) solution of the exact Friction Relaxation

Model and is based on the shear stress value calculated at the previous time step:

$$\tau(t) = \tau_s(t) + \tau_{un}(t) \tag{4.8}$$

$$\tau_{un}(t) = \tau_{un}(t - \Delta t)e^{\frac{-\Delta t}{\theta}} + k_T \rho \left|a\right| \Delta_t w \tag{4.9}$$

where Δt is a time step and $\Delta_t w$ is a difference between velocity values at two last time steps. Initially: $\tau_{un}(0) = 0$.

The transient shear stress is the sum of the steady shear stress τ_s and an unsteady contribution τ_{un}. The unsteady contribution contains an exponential decrease responsible for the relaxation and the difference between the velocity values at the last two time steps, which allows to detect the presence of the wave and determine the shear stress jump during the first phase. This difference is the equivalent of the time derivative of the velocity in the original Friction Relaxation Model .

The convective derivative $w\frac{\partial \tau}{\partial x}$, which is present in the original Friction Relaxation Model (Eq. 3.25), in the approximated model is neglected. The results of the approximated Friction Relaxation Model presented below confirm that this derivative has a very little importance.

The derivative $\frac{\partial w}{\partial t}$ in the original Friction Relaxation Model (Eq. 3.25) can be interpreted as a Dirac distribution. For short times, equations 4.8 and 4.9 resemble to the solution of the linear equation of the same form as Friction Relaxation Model :

$$\frac{dy}{dt} = \frac{y_s - y}{\theta} + A\delta(t) \tag{4.10}$$

where y_s and A are constant. The solution of this equation is presented in the Appendix B.

Equations 4.8 and 4.9 satisfy the conditions 1-3 from section 4.1. During the passage of the wave, the absolute value of the wall shear stress increases drastically about the value $\Delta\tau = k_T \rho \left|a\right| \Delta_t w$; between two passages of the wave, it decreases exponentially, and if the wave doesn't come back, it becomes equal to steady-state value at infinity. The coefficients θ and k_T have exactly the same meaning as in the original Friction Relaxation Model.

The results of the approximated Friction Relaxation Model based on the last time step are compared with those of the original Friction Relaxation Model in Fig. 4.3 and 4.4 for the case of a fast closure of a valve described in the introduction to this chapter ($Re = 10^5$). The coefficients θ and k_T are the same in both models. Both shear stress and pressure histories obtained from the approximated model are almost identical to those obtained from the original one.

In Appendix D more calculations were done in order to prove that the results of the approximated Friction Relaxation Model based on last time step are in agreement with the original model, independently of the number of nodes.

In order to evaluate the range of application of the approximated Friction Relaxation Model based on the last time step, the calculations for more extreme conditions (very high and very low Reynolds numbers) were done.
The shear stress and the pressure histories for $Re = 3 \cdot 10^6$ are shown in Fig. 4.5 and 4.6. The diameter of the pipe was 600 mm, therefore the relaxation time for this case was assumed to be much larger than for the previous one. The shear stress peak for deceleration in Fig. 4.5 is visible only at the beginning of the flow, afterwards only the peaks during acceleration can be clearly observed. This is due to the long relaxation time, but it is also possible that for such a strongly turbulent flows, the coefficients k_T should be larger.
The pressure and wall shear stress histories presented in Fig. 4.5 and 4.6 prove that the approximated model can be applied for very strongly turbulent flows and the results are very close to the results of the original model.

The shear stress and the pressure histories for low Reynolds number ($Re = 4000$) are shown in Fig. 4.7 and 4.8. The velocity was 0.2 m/s, θ and k_T coefficients were assumed to be the same as in the Holmboe and Rouleau experiment (section 3.8).
The pressure and wall shear stress histories presented in the Fig. 4.7 and 4.8,

calculated with the approximated model, are also very close to the results of the original model, the difference is almost invisible.
These calculations prove that, if needed for practical reasons, the approximated equation can be introduced into numerical codes instead of the exact Friction Relaxation Model expressed by a partial differential equation.

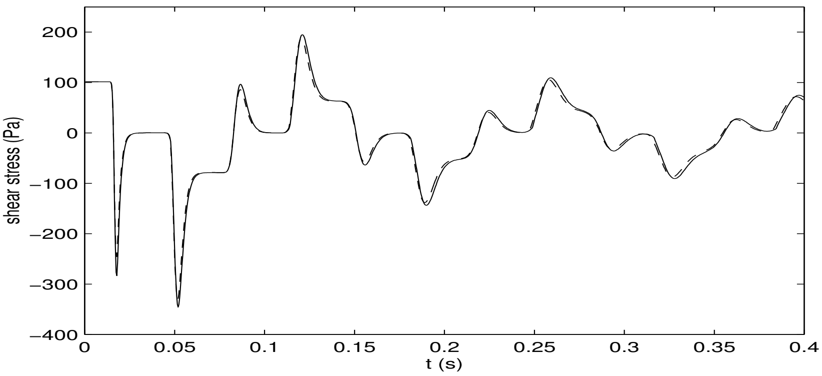

Figure 4.3: Water flow, $Re = 10^5$. Wall shear stress in the middle of the pipe versus time. Comparison between the exact Friction Relaxation Model (dashed line) and the approximated Friction Relaxation Model based on last time step (solid line). Relaxation time: $\theta = 1.4$ms, k_T for acceleration $2 \cdot 10^{-4}$, k_T for deceleration $1 \cdot 10^{-4}$.

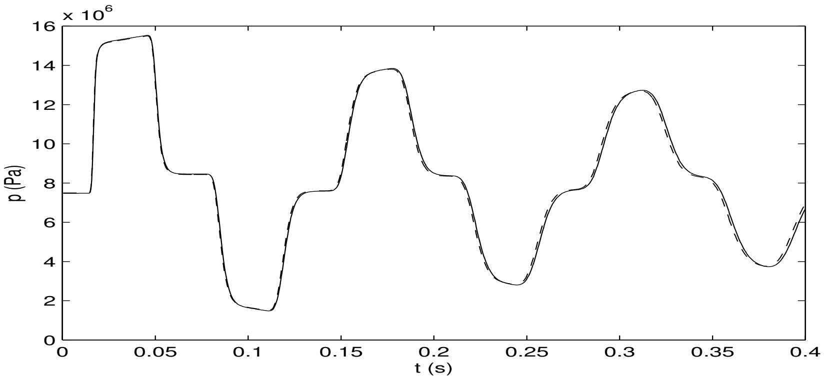

Figure 4.4: Water flow, $Re = 10^5$. Pressure in the middle of the pipe versus time. Comparison between the exact Friction Relaxation Model (dashed line) and the approximated Friction Relaxation Model based on last time step (solid line). Relaxation time $\theta = 1.4$ms, k_T for acceleration $2 \cdot 10^{-4}$, k_T for deceleration $1 \cdot 10^{-4}$.

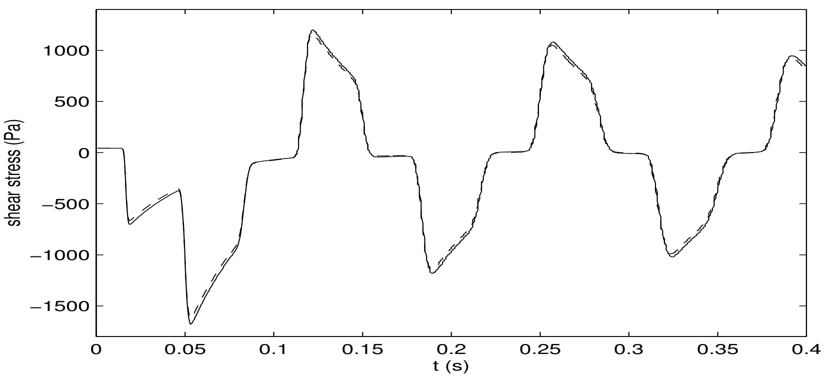

Figure 4.5: Water flow, $Re = 3 \cdot 10^6$. Wall shear stress in the middle of the pipe versus time. Comparison between the exact Friction Relaxation Model (dashed line) and the approximated Friction Relaxation Model based on last time step (solid line). Relaxation time: $\theta = 42$ms, k_T for acceleration $2 \cdot 10^{-4}$, k_T for deceleration $1 \cdot 10^{-4}$.

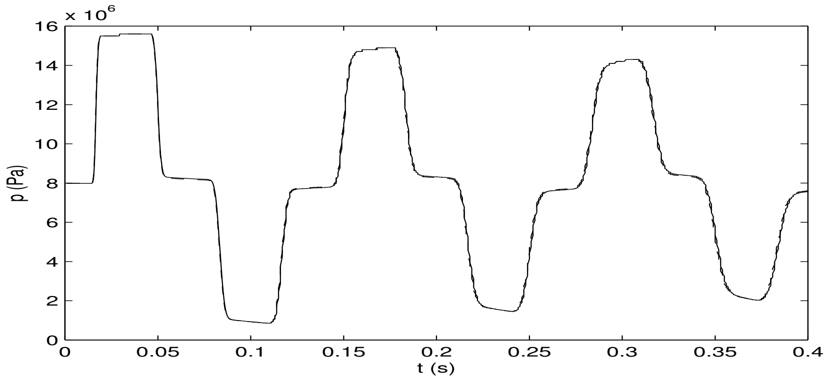

Figure 4.6: Water flow, $Re = 3{\cdot}10^6$. Pressure in the middle of the pipe versus time. Comparison between the exact Friction Relaxation Model (dashed line) and the approximated Friction Relaxation Model based on last time step (solid line). Relaxation time $\theta = 42$ms, k_T for acceleration $2 \cdot 10^{-4}$, k_T for deceleration $1 \cdot 10^{-4}$.

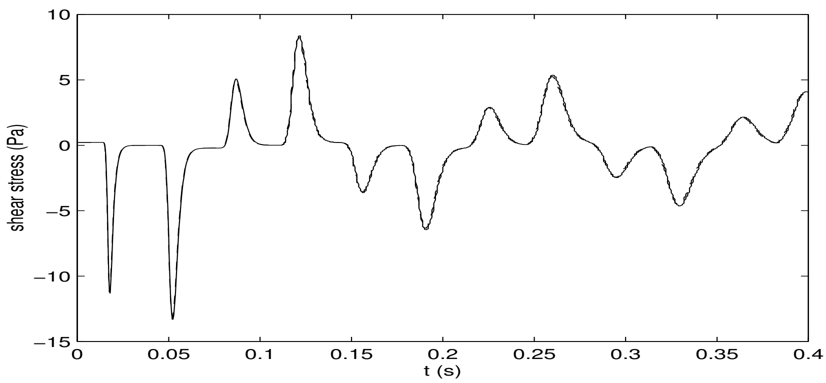

Figure 4.7: Water flow, Re=4000. Wall shear stress in the middle of the pipe versus time. Comparison between the exact Friction Relaxation Model (dashed line) and the approximated Friction Relaxation Model based on last time step (solid line). Relaxation time: $\theta = 1.4$ms, k_T for acceleration $2{\cdot}10^{-4}$, k_T for deceleration $1 \cdot 10^{-4}$.

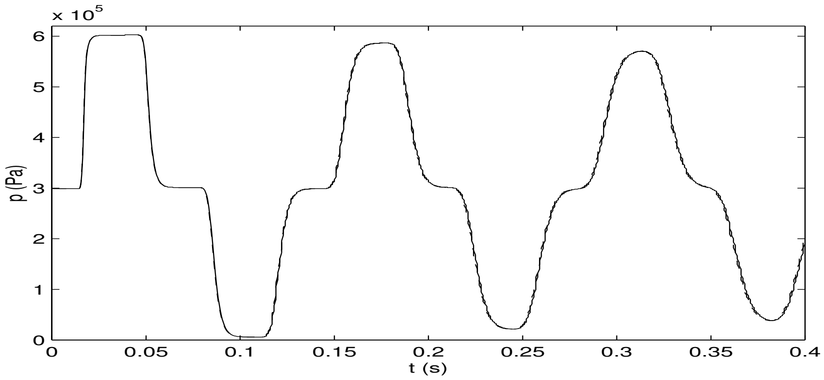

Figure 4.8: Water flow, Re=4000. Pressure in the middle of the pipe versus time. Comparison between the exact Friction Relaxation Model (dashed line) and the approximated Friction Relaxation Model based on last time step (solid line). Relaxation time $\theta = 1.4$ms, k_T for acceleration $2 \cdot 10^{-4}$, k_T for deceleration $1 \cdot 10^{-4}$.

4.4 Conclusions

Two 'algebraic versions' of the Friction Relaxation Model are proposed to programmers who would like to put a transient friction model in their codes without major modifications of these codes.

In order to include the relaxation process in the approximated models, the explicit information about the shear stress in the past was introduced into both models. The first model is based on the information recorded in the moment of a wave passage through a given point; the second one is based on the information from the last time step. Because the moment of a wave passage can often be difficult to detect, it is recommended to use the model based on the information from the last time step. This model gives the results which are very close to the results of the original Friction Relaxation Model for a very wide range of Reynolds numbers ($4000 < Re < 3000000$).

Chapter 5

Comparison between the Friction Relaxation Model and other transient friction models

The transient friction models for turbulent flows involving velocity derivatives (i.e. Brunone et al. [6, 7], Axworthy et al. [2]) give results which are close to the experimental results. Moreover there are some similarities between these models and the Friction Relaxation Model presented in this paper. In fact the Brunone equation has the form:

$$\tau = \tau_s + \frac{k}{4} D\rho \left(\frac{\partial w}{\partial t} - a\frac{\partial w}{\partial x} \right) \tag{5.1}$$

while the Friction Relaxation Model (Eq. 3.25) can be written in the following form:

$$\tau = \tau_s - \theta \frac{d\tau}{dt} - \theta k_T \rho \left| a \right| \frac{\partial w}{\partial t} \tag{5.2}$$

The term containing velocity derivative, responsible for the sudden shear stress jump during wave passage in the Friction Relaxation Model (Eq. 5.2) can be considered as an equivalent of the term between parentheses in the Brunone equation (Eq. 5.1). This term is responsible for the first step of the shear stress evolution *i.e.* the very fast change of the wall shear stress during the passage of the water hammer wave. However, the relaxation step is missing in the Brunone equation. If the wave already passed through a given point and the velocity derivatives are negligible, the transient shear stress is equal to the steady shear stress. The simplicity of the Brunone model is very attractive, but in order to predict the pressure history correctly, one is forced to significantly overpredict the shear-stress peak during the first step of the shear stress evolution as was shown by Brunone et al [8]. This simplification also has an influence on the predicted shape of the pressure peaks.

A similar observation can be made for the Axworthy equation [2]:

$$\tau = \tau_s + \frac{\rho D}{4} k_A (\frac{\partial w}{\partial t} + w \frac{\partial w}{\partial x}) \tag{5.3}$$

Here again, the transient shear stress differs from the steady-state shear stress only when the velocity derivatives are different from zero. Moreover, by comparison with experiments, the unsteady coefficient k_A is shown by these authors to be equal to zero for one of the characteristics (i.e. for acceleration or deceleration). Then the Axworthy equation is reduced to: $\tau = \tau_s$.

Many researchers have been tempted to find a transient friction model based on instantaneous conditions. However, it appears that 'instantaneous models' loose all information about the relaxation phase. The 1D models based on the sum of steady shear stress and the derivatives of velocity may have practical significance but they do not contain the whole physics of the phenomenon.

The problem with the description of the fast transient flows by the cross-section averaged variables is that what seems to be steady state is not always steady in reality. When the temporal derivatives of the independent variables are equal to zero, the system is supposed to be in steady state and this is what the shear stress models having the form similar to 5.1 and 5.3 describe. In fact, even during the absence of the derivatives, the system may be changing in time. During the relaxation step, even if the average velocity is constant, the profile of the velocity is being modified and tends to the steady-state profile. Indeed it is not in steady state, until it reaches the steady-state shape. If the water hammer wave is very fast and the pipe is sufficiently short, the steady state is never reached. This is the reason why the transient friction cannot be described properly only by the averaged velocity. It is possible that at two different points the independent variables averaged in cross-section are the same, but the values of the wall shear stress are different. The transient shear stress depends not only on instantaneous conditions but also whether the water hammer wave passed through this point and how long time ago this happened.

For laminar flows, Zielke [46] proved analytically that the transient shear stress depends on the flow history. Vardy et al. [40] developed an equivalent model for turbulent flows by representation of a turbulent flow as a laminar annulus surrounding a uniform core. They demonstrated that the dependance on the historical conditions decreases with the increase of the Reynolds number. They also proposed the approximated shear stress equation similar to Trikha's approximation [38] of Zielke's model. The weighting functions in Zielke's model were replaced by exponential series. Trikha argued that three terms in the series are sufficient to determine the shear stress in laminar flow. Vardy et al. [40] suggested two terms for turbulent flow at moderate Reynolds numbers:

$$\tau = \tau_s + \frac{4\mu}{D}(Y_1 + Y_2) \tag{5.4}$$

where

$$\text{For } t = 0 \qquad Y_i = 0 \tag{5.5}$$

$$\text{For } t > 0 \qquad Y_{i,t} = Y_{i,t-\Delta t}e^{-B_i\Psi} + A_i(w_t - w_{t-\Delta t}) \tag{5.6}$$

where $\Psi = \nu\Delta t/R^2$ is a non-dimensional time. The values of coefficients A_i, B_i for Holmboe and Rouleau experiment [20] (turbulent case) were evaluated as:

$$A_1 = 365; \quad B_1 = 120000 \tag{5.7}$$

$$A_2 = 35; \quad B_2 = 5000 \tag{5.8}$$

According to Vardy et al., these values are applicable for the particular case of $fRe = 69.5$ and $5 \cdot 10^{-7} \leq \Psi \leq 5 \cdot 10^{-5}$. Vardy et al. [40] compared the shear stress results obtained with their model with the results obtained using a five-region eddy viscosity model and found a good agreement between the two models.

Vardy's approximated equation is based on the unsteady shear stress resulting from the last time step and is quite similar to the approximated Friction Relaxation Model based on the last time step described in section 4.3. The main difference is that the approximated equation proposed here contains one exponential term instead of two:

$$\tau_{un}(t) = \tau_{un}(t - \Delta t)e^{\frac{-\Delta t}{\theta}} + k_T \rho \left| a \right| \Delta_t w$$

The good agreement between the results of the Friction Relaxation Model and the results obtained with FLUENT using the $k - \epsilon$ model of turbulence (Section 3.5) shows that one exponential term is likely to be sufficient. Another difference between the two models is that the coefficient k_T in the approximated Friction Relaxation Model is different for acceleration and deceleration, while the coefficients A_i in Vardy's model (1993) are identical for both acceleration and deceleration. The relaxation time in Vardy's equation corresponding to the coefficient $B1$ ($\theta_V = \frac{R^2}{B_1 \nu}$) is equal to $0.0016s$ while θ in Friction Relaxation Model is equal to $0.0014s$. The values are similar.

The coefficient A_2 in Vardy's model is 10 times smaller than the coefficient A_1. The coefficients A_i (like k_T in Friction Relaxation Model) which determine the first step of the transient shear stress are proportional to the amplitude of the jump $\Delta\tau$. The relaxation time corresponding to the coefficient B_2 is 24 times larger than the relaxation time corresponding to B_1. Therefore for the Holmboe and Rouleau experiment [20] the second exponential term in Vardy's model, in comparison with the first one, represents a small, very slowly decreasing function and its negligible character can be justified.

Vardy et al. found that coefficients A_i, B_i depend on the product fRe (where f is a steady friction coefficient) and they increase with the increase of fRe.

In their paper they suggested some values of A_i and B_i for different products fRe.

The exact Friction Relaxation Model expressed by a differential equation (Eq. 3.25) has a form similar to the transient wall-friction relation for laminar flows derived by Achard and Lespinard [1] for low-frequency cases. The non-dimensional form of their model is:

$$\frac{\partial \tau}{\partial t} = \frac{4w - \tau}{\sigma} + 6\frac{\partial w}{\partial t} \tag{5.9}$$

where σ is a relaxation coefficient. Achard and Lespinard postulated that the structure of their equation could be extended to turbulent cases. Such extension has been proposed in this thesis.

Chapter 6

The Friction Relaxation Model for Two-Phase Flows

6.1 Introduction

In this chapter, the Friction Relaxation Model is applied to two-phase models. Here, as a phase we mean the physical state of a matter. The calculations are made for steam and water mixtures.
Generally, two-phase models can be classified into two groups: mixture models and two-fluid models. In mixture models, the governing equations are written for the mixture variables, defined on the basis of the properties of each phase. In two-fluid models the governing equations are written for each phase separately.
The Friction Relaxation Model is applied to the models that take and those that do not take the non-equilibrium effects into account. In two-phase flows, we can distinguish up to four types of non-equilibrium:

1. Due to different phasic pressures.

2. Due to vapor temperature being different than saturation temperature.

3. Due to liquid temperature being different than saturation temperature.

4. Due to different phasic velocities (mechanical non-equilibrium).

The Friction Relaxation Model described in this thesis deals with another kind of non-equilibrium, which is due to the impact of a pressure wave on the velocity profile at the wall. The Friction Relaxation Model enables to model this non-equilibrium, which is lost in 1D modelling.

Calculations with three different two-phase models including transient wall friction have been performed. The calculations with the Homogenous Equilibrium Model and the Homogenous Relaxation Model have been done using the codes we developed. The Godunov scheme was used (the grid had 400 nodes, CFL=0.5). More details about the calculations are given in appendix A.
The calculations with the Two-Fluid Model have been performed using the WAHA code, which is described in details in the WAHA manual [37].

6.2 Homogenous Equilibrium Model

In the Homogenous Equilibrium Model (HEM), the fluid is considered as a homogenous mixture of a liquid phase and a gas phase. The phases are assumed to be in thermal and mechanical equilibrium *i.e.* to have the same temperature, pressure and velocity. The temperature in HEM is assumed to be equal to the saturation temperature corresponding to the given pressure. The mixture density is expressed as:

$$\rho_m(p,\alpha) = \alpha\rho_g(p) + (1-\alpha)\rho_f(p) \tag{6.1}$$

where ρ_g is the gas density, ρ_f is the liquid density and α is the void fraction defined as:

$$\alpha = \frac{A_g}{A} = \frac{1}{A}\int_A \alpha_A dA \tag{6.2}$$

where A_g is the fraction of the cross-section of a pipe occupied by the vapor and α_A is a local fraction of vapor.

The mixture internal energy is defined as:

$$\rho_m(p,\alpha)u_m(p,\alpha) = \alpha\rho_g(p)u_g(p) + (1-\alpha)\rho_f(p)u_f(p) \tag{6.3}$$

For a pipe with constant cross-section, the governing equations are:

$$\frac{\partial \rho_m}{\partial t} + \frac{\partial \rho_m w}{\partial x} = 0 \tag{6.4}$$

$$\rho_m \frac{\partial w}{\partial t} + \rho_m w \frac{\partial w}{\partial x} + \frac{\partial p}{\partial x} = -\frac{4}{D}\tau \tag{6.5}$$

$$\rho_m \frac{\partial u_m}{\partial t} + \rho_m w \frac{\partial u_m}{\partial x} + p\frac{\partial w}{\partial x} = \frac{4w}{D}\tau \tag{6.6}$$

One can notice that the governing equations of HEM have the same form as the governing equations for single - phase flow. Therefore, it is proposed that the closure law for the wall-shear stress has also the same form as in single-phase flows:

$$\frac{\partial \tau}{\partial t} + w\frac{\partial \tau}{\partial x} = \frac{\tau_s - \tau}{\theta} + k_T \rho_m \left|a\right| \frac{\partial w}{\partial t} \tag{6.7}$$

where:

$$\tau_s = \frac{f\rho_m w^2}{2} \tag{6.8}$$

f is a steady-state wall friction coefficient.

In order to show the impact of this new transient friction law on two-phase flows, some benchmark simulations were done. The calculations were made for a water hammer induced by the fast closure of a valve placed downstream of a pipe. The diameter of the pipe was 20 mm, its length: 50 m, the initial velocity: 5 m/s, the upstream pressure: 60 bars, and the temperature: 523 K. The chosen case is very similar to the benchmark case of the WAHA project. As there are no experimental data which can serve to evaluate the coefficients θ and k_T for this case, these coefficients were assumed to be equal to those in single-phase water flow analyzed in section 3.8. The results obtain with the Friction Relaxation Model are compared

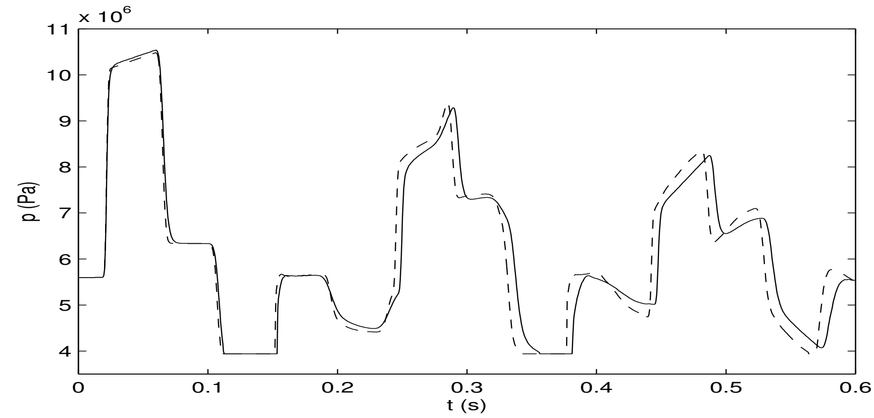

Figure 6.1: Two-phase flow, HEM. Pressure in the middle of the pipe versus time. Comparison between the Friction Relaxation Model (solid line) and steady-state friction results (dashed line). Relaxation time $\theta = 0.0014s$, k_T for acceleration $= 2 \cdot 10^{-4}$, k_T for deceleration $1 \cdot 10^{-4}$.

with steady-state friction results. For the values of coefficient k_T adjusted on the experiment of Holmboe and Rouleau [20] the results obtained with the Friction Relaxation Model presented in the Fig. 6.1 are almost the same as the steady-state results. However, the Reynolds number in this benchmark case (100 000) is much greater than the Reynolds number in the experiment of Holmboe and Rouleau (6200) and the coefficients k_T seem to be larger for fully turbulent flows than for slightly turbulent flows. In order to observe more clearly the impact of the transient friction on two-phase transients, the calculations have been made for k_T twice greater than those adjusted on the experiment of Holmboe and Rouleau.

For the chosen case, the Friction Relaxation Model does not have much influence on the quantity of vapor in the middle of the pipe (Fig. 6.2), but the evaporation starts a little bit later than for the computation made with the steady-state equation, especially for the second flashing. The quantity of vapor in the middle of the pipe for the presented case is rather small (order 10^{-4}), but there is much more vapor close to the valve. In the corresponding pressure history (Fig. 6.3), we can see that, at the beginning, there is not much difference between the amplitudes calculated with the steady and the transient models, but, after two periods, we can observe that the amplitude computed with the transient model is smaller. The significant effect of the transient model on the pressure is the positive phase shift in time. Similar observations concerning amplitude and phasing can be made for the velocity history (Fig. 6.4).

The transient shear stress is evidently much greater than the steady shear stress (Fig. 6.5). Due to the evaporation and additional waves which occur when vapor is produced in the system, the shear stress versus time has no longer the regular form (two negative followed by two positive peaks) as in the case of a single phase flow. After a certain time when the pressure is not low enough to cause evaporation, the transient shear stress recovers its regular form, characteristic of single-phase flow.

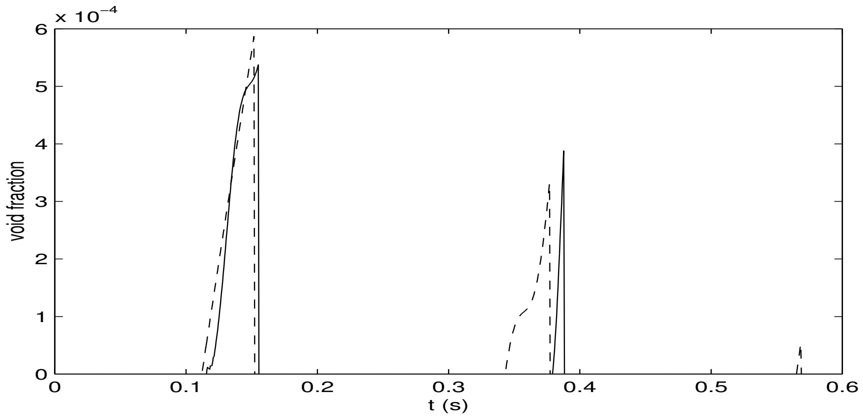

Figure 6.2: Two-phase flow, HEM. Void fraction in the middle of the pipe versus time. Comparison between the Friction Relaxation Model (solid line) and steady-state results (dashed line). Relaxation time $\theta = 0.0014s$, k_T for acceleration $= 4 \cdot 10^{-4}$, k_T for deceleration $2 \cdot 10^{-4}$.

In Fig. 6.6 we can see that there is much more void fraction at the valve

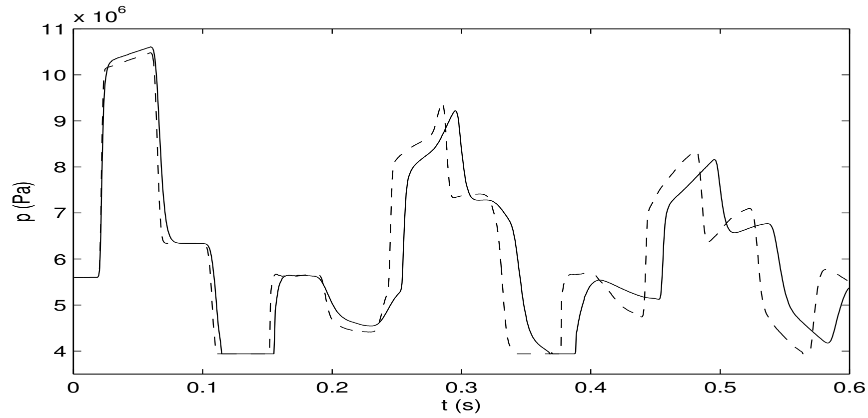

Figure 6.3: Two-phase flow, HEM. Pressure in the middle of the pipe versus time. Comparison between the Friction Relaxation Model (solid line) and steady-state results (dashed line). Relaxation time $\theta = 0.0014s$, k_T for acceleration $= 4 \cdot 10^{-4}$, k_T for deceleration $2 \cdot 10^{-4}$.

(about 5% of volume) than in the middle of the pipe. We can also observe that, at the valve, the transient model results in a smaller quantity of vapor than the steady model. The positive phase shift can be observed for both void fraction and pressure (Fig. 6.7).

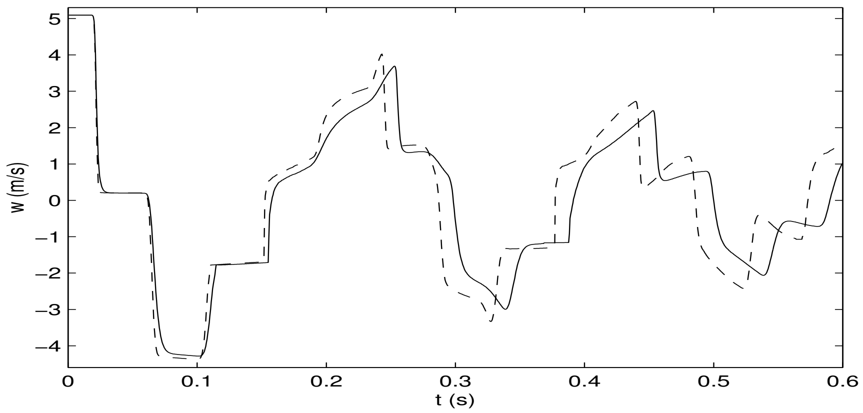

Figure 6.4: Two-phase flow, HEM. Velocity in the middle of the pipe versus time. Comparison between the Friction Relaxation Model (solid line) and steady-state results (dashed line). Relaxation time $\theta = 0.0014s$, k_T for acceleration $= 4 \cdot 10^{-4}$, k_T for deceleration $2 \cdot 10^{-4}$.

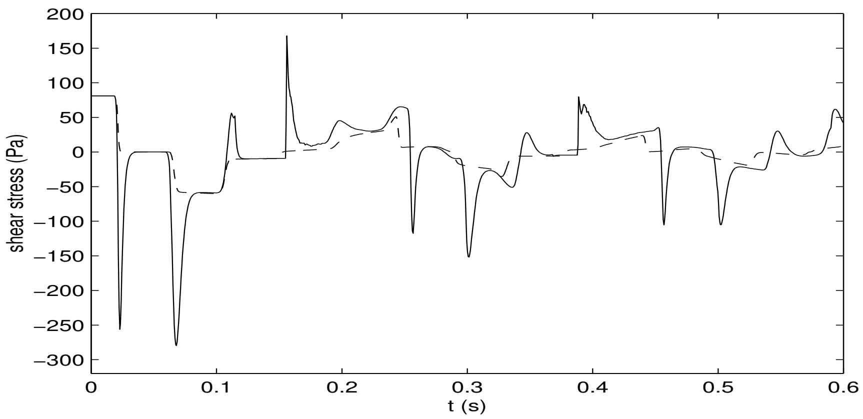

Figure 6.5: Two-phase flow, HEM. Shear stress in the middle of the pipe versus time. Comparison between the Friction Relaxation Model (solid line) and steady-state results (dashed line). Relaxation time $\theta = 0.0014s$, k_T for acceleration $= 4 \cdot 10^{-4}$, k_T for deceleration $2 \cdot 10^{-4}$.

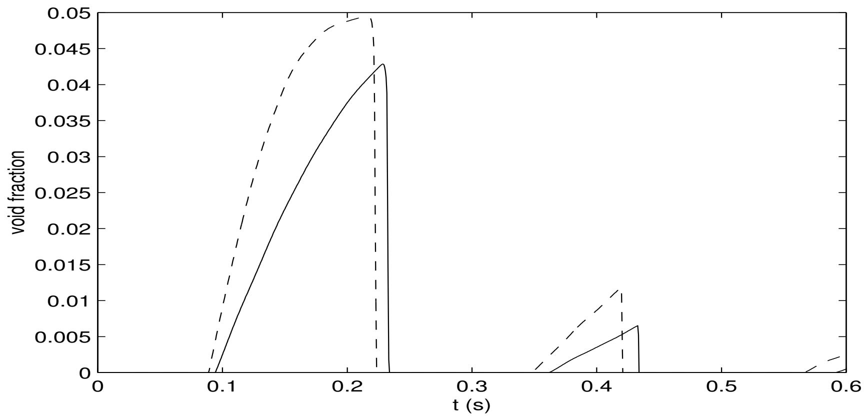

Figure 6.6: Two-phase flow, HEM. Void fraction at the valve versus time. Comparison between the Friction Relaxation Model (solid line) and steady-state results (dashed line). Relaxation time $\theta = 0.0014s$, k_T for acceleration $= 4 \cdot 10^{-4}$, k_T for deceleration $2 \cdot 10^{-4}$.

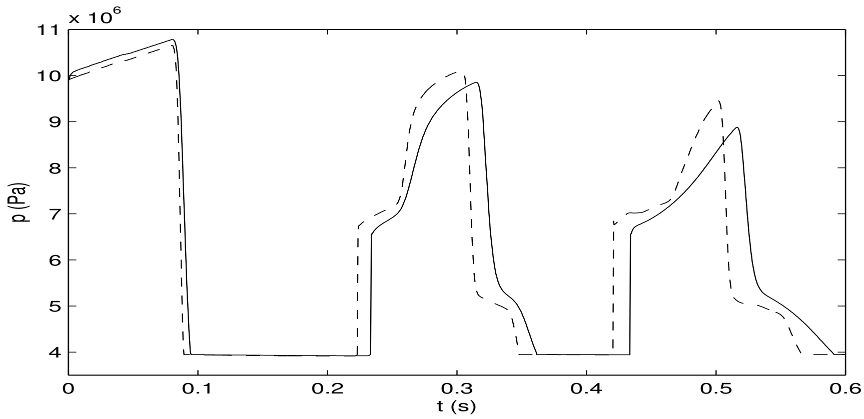

Figure 6.7: Two-phase flow, HEM. Pressure at the valve versus time. Comparison between the Friction Relaxation Model (solid line) and steady-state results (dashed line). Relaxation time $\theta = 0.0014s$, k_T for acceleration $= 4 \cdot 10^{-4}$, k_T for deceleration $2 \cdot 10^{-4}$.

6.3 Homogeneous Relaxation Model

In the Homogeneous Relaxation Model (HRM) the mechanical non-equilibrium is not taken into account *i.e.* both phases are considered to have the same velocity. The thermodynamic non-equilibrium is taken into account partially *i.e.* the gas phase is considered to be in a saturation state whereas the liquid phase may be in a metastable state or in a sub-cooled state. The thermal non-equilibrium of the liquid is relaxed towards equilibrium and this process of relaxation is described with a first order differential equation, similar to the Friction Relaxation Model. One can find the fundamentals of this model in the papers of Bilicki and Kestin [4] and Downar-Zapolski et al. [13]. The model was used and analysed by Lemonnier [23] in the frame of the WAHALoads project.

The closure law for transient wall shear stress expressed by the Friction Relaxation Model was included in HRM. Then the full system of the governing equations is:

$$\frac{\partial \rho_m}{\partial t} + \frac{\partial \rho_m w}{\partial z} = 0 \tag{6.9}$$

$$\rho_m \frac{\partial w}{\partial t} + \rho_m w \frac{\partial w}{\partial z} + \frac{\partial p}{\partial z} = -\frac{4}{D}\tau \tag{6.10}$$

$$\rho_m \frac{\partial u_m}{\partial t} + \rho_m w \frac{\partial u_m}{\partial z} + p\frac{\partial w}{\partial z} = \frac{4w}{D}\tau \tag{6.11}$$

$$\frac{\partial X}{\partial t} + w\frac{\partial X}{\partial z} = \frac{X_{eq} - X}{\theta_X} \tag{6.12}$$

$$\frac{\partial \tau}{\partial t} + w\frac{\partial \tau}{\partial z} = \frac{\tau_s - \tau}{\theta_\tau} + k_T \rho_m \left|a\right| \frac{\partial w}{\partial t} \tag{6.13}$$

where X is the mass fraction of a gas phase ($X = m_g/m$) also called quality.

In the above model, there are two relaxation equations. One of them describes the relaxation of the vapor quality, and the other expresses the relaxation of the wall shear stress. Therefore, we will refer to the above model as to the Double Relaxation Model.

Physically, the relaxation equation for X determines the rate of change of the quality, which tends to reach an equilibrium value. Therefore the relaxation equation for the quality influences the rate of phase change. It takes into account the fact that the liquid does not evaporate instantly at the point where the saturation temperature is reached. In certain situations (for example flashing phenomenon) this delay is not negligible. The water, the temperature of which, is above saturation and still remains in a liquid phase is called superheated water. Water whose temperature is below saturation and still remains in a gas phase is called subcooled steam. Both cases are referred to as metastable states.
If the vapour phase is saturated, the mixture density is defined as:

$$\rho_m(p, \alpha, T_f) = \alpha \rho_g(p) + (1 - \alpha)\rho_f(p, T_f) \tag{6.14}$$

where T_f is the liquid temperature. The mixture internal energy is defined as:

$$\rho_m(p, \alpha, T_f) u_m(p, \alpha) = \alpha \rho_g(p) u_g(p) + (1 - \alpha)\rho_f(p, T_f) u_f(p, T_f) \tag{6.15}$$

The relation between the quality and void fraction for homogeneous flow is:

$$X = \alpha \frac{\rho_g}{\rho_m} \tag{6.16}$$

To see the effect of thermal non-equilibrium, some calculations were done without transient friction ($k_T = 0, \theta_\tau = 0.0001s$; for these values the effect of transient friction is negligible). The relaxation time for the quality θ_X was chosen as $0.1s$. For this value, the difference between the non-equilibrium and the equilibrium void fractions is very clear (Fig. 6.8, 6.10). For smaller values of θ_X this difference is not significant. In Fig. 6.8, the history of the void fraction at the midpoint is presented. As was expected, the non-equilibrium void fraction is smaller than the equilibrium value during evaporation and greater during condensation. In fact, thanks to the relaxation equation, the instantaneous phase changes are avoided; on the contrary, these phase changes are rather smooth. The corresponding pressure history at the mid-point is shown in the Fig. 6.9. The effect of the thermal relaxation can be seen even more clearly at the valve (Fig. 6.10). During most of the time, the flow is two-phase because not all the vapor is condensed immediately when the pressure wave arrives. For the chosen $\theta_X = 0.1s$, vapor is not yet condensed completely when the second pressure wave arrives and produces flashing one more time. The corresponding pressure history at the valve is shown in Fig. 6.11.

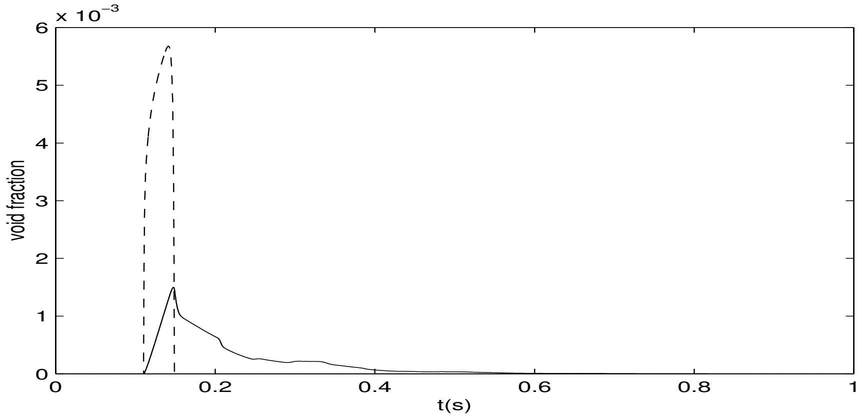

Figure 6.8: Two-phase flow, HRM with steady friction correlation. Void fraction at the middle of the pipe versus time. Solid line - non-equilibrium void fraction with $\theta_X = 0.1s$, dashed line - corresponding equilibrium void fraction.

Calculations with the Double Relaxation Model were made for $\theta_\tau = 0.0014s$, k_T for acceleration $4 \cdot 10^{-4}$, k_T for deceleration $2 \cdot 10^{-4}$. The values of k_T are two times greater than those adjusted against the experiment of Holmboe and Rouleau [20], similarly as in the calculations performed with the HEM. The values of k_T and θ_τ for this case may not be correct but the purpose of these calculations is to assess qualitatively the influence of the transient friction on the HRM. The quality relaxation time is chosen as

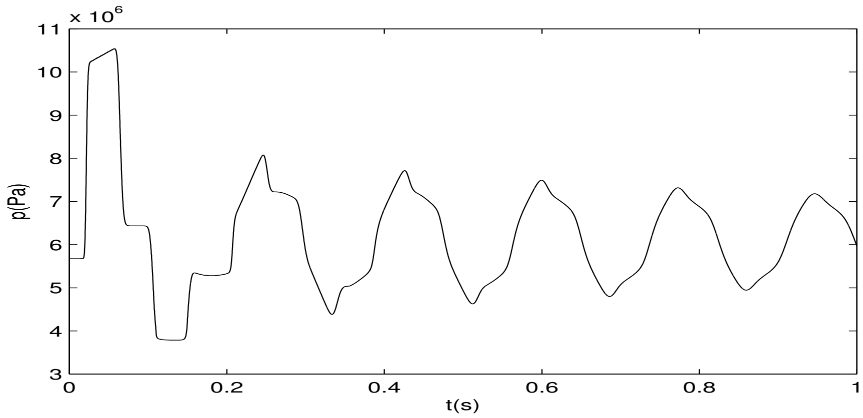

Figure 6.9: Two-phase flow, HRM with steady friction correlation. Pressure at the middle of the pipe versus time. $\theta_X = 0.1s$

$\theta_X = 0.1s$ as in previous calculations with the classical friction correlation (Fig. 6.8 - 6.11).

The transient wall shear stress results calculated with the Double Relaxation Model are shown in Fig. 6.12. It can be observed that, after one wave period, the regular shape typical of a transient shear stress (two negative peaks followed by two positive peaks) is deviated and the shear stress peaks can no more be easily observed. This is due to the dissipation of the water hammer wave which can be observed in the velocity (Fig. 6.13) and pressure histories (Fig. 6.14) in the middle of the pipe. After one period, the wave is no longer sharp, its shape becomes sinusoidal, the changes are no more dramatic, but rather smooth. This is not the case in equivalent computations with HEM (Fig. 6.3, 6.4). The wave computed with HRM and steady friction (Fig. 6.13, dashed line) is a little less dissipated than the wave computed with transient friction (Fig. 6.13, solid line), but still it is more dissipated than in HEM computations. This leads to the conclusion that the relaxation laws 'smooth' a water hammer wave.
The Friction Relaxation Model introduced to HRM gives an almost identical

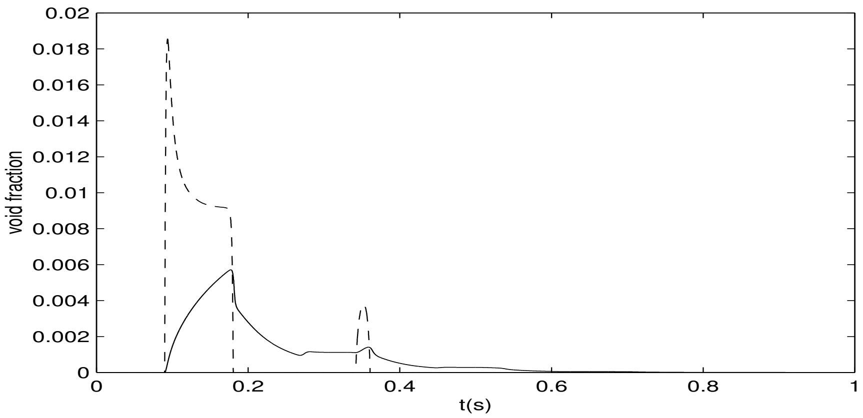

Figure 6.10: Two-phase flow, HRM, with steady friction correlation. Void fraction at the valve versus time. Solid line - non-equilibrium void fraction with $\theta_X = 0.1s$, dashed line - corresponding equilibrium void fraction.

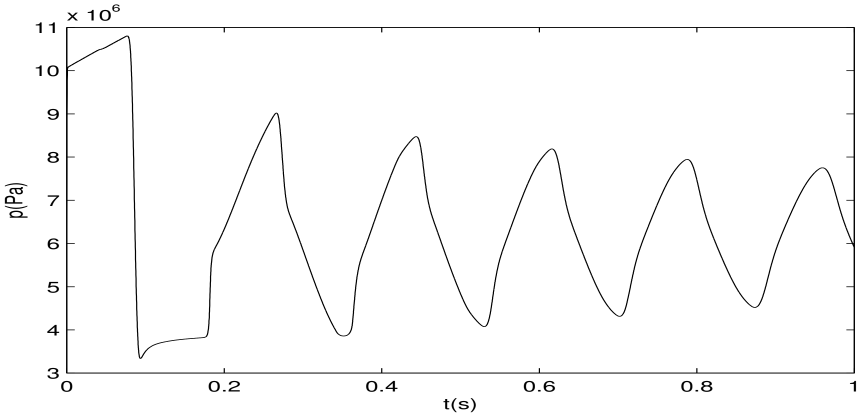

Figure 6.11: Two-phase flow, HRM, with steady friction correlation. Pressure at the valve versus time. $\theta_X = 0.1s$

amount of vapor as a steady friction (see Fig. 6.8, 6.10) for the proposed values of θ_τ and k_T. The history of pressure at the valve computed with the Double Relaxation Model is shown in Fig. 6.15. As expected, the Friction Relaxation Model produces positive phase shift and smaller amplitudes in comparison with the steady friction model. Both curves (obtained with steady and transient friction equations introduced to HRM) are smoother than the equivalent curves computed with HEM (Fig. 6.7).

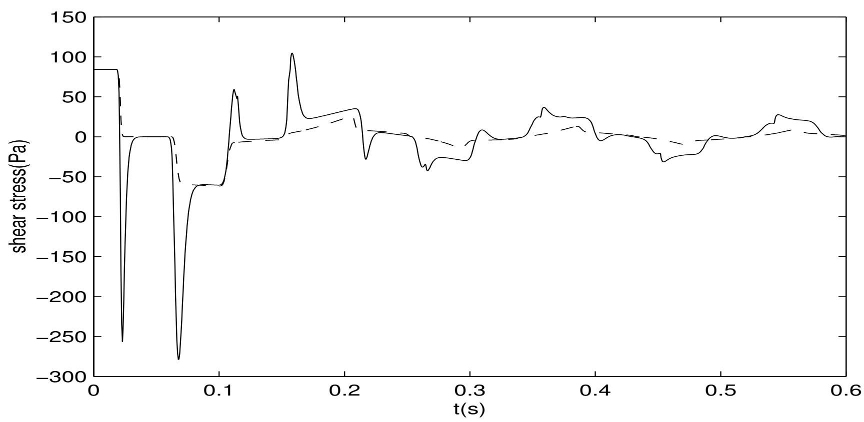

Figure 6.12: Two-phase flow, HRM. Shear stress at the middle of the pipe versus time. Solid line - transient friction, dashed line - steady friction. $\theta_X = 0.1$s, $\theta_\tau = 1.4$ms, k_T for acceleration $= 4 \cdot 10^{-4}$, k_T for deceleration $2 \cdot 10^{-4}$.

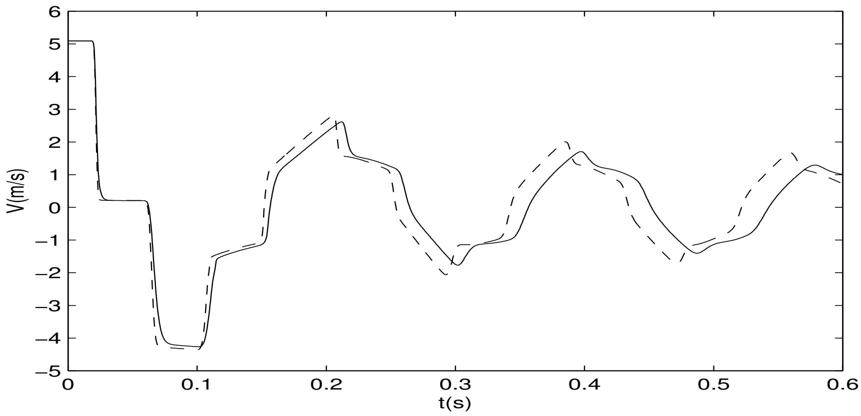

Figure 6.13: Two-phase flow, HRM. Velocity at the middle of the pipe versus time. Solid line - transient friction, dashed line - steady friction. $\theta_X = 0.1$s, $\theta_\tau = 1.4$ms, k_T for acceleration $= 4 \cdot 10^{-4}$, k_T for deceleration $2 \cdot 10^{-4}$.

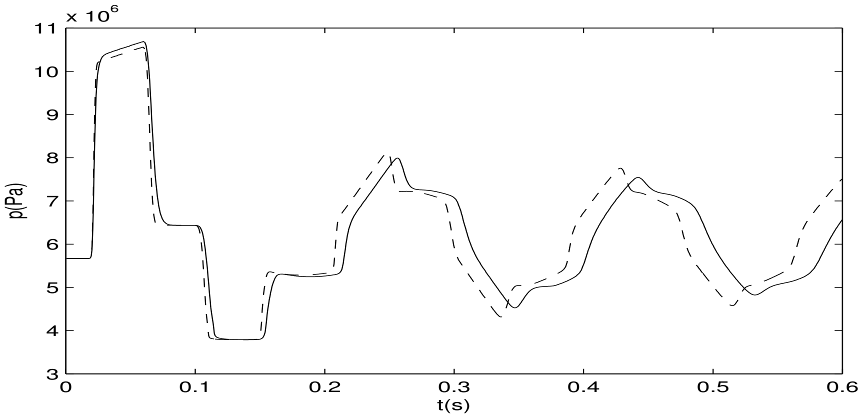

Figure 6.14: Two-phase flow, HRM. Pressure at the middle of the pipe versus time. Solid line - transient friction, dashed line - steady friction. $\theta_X = 0.1$s, $\theta_\tau = 1.4$ms, k_T for acceleration $= 4 \cdot 10^{-4}$, k_T for deceleration $2 \cdot 10^{-4}$.

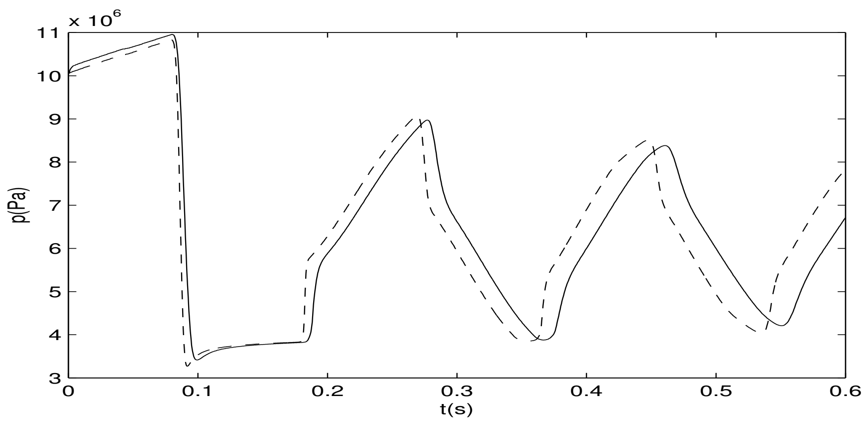

Figure 6.15: Two-phase flow, HRM. Pressure at the valve versus time. Solid line - transient friction, dashed line - steady friction. $\theta_X = 0.1$s, $\theta_\tau = 1.4$ms, k_T for acceleration $= 4 \cdot 10^{-4}$, k_T for deceleration $2 \cdot 10^{-4}$.

6.4 Two-Fluid Model

6.4.1 Basic Equations

A Two-Fluid Model takes into account both thermal and mechanical non-equilibrium. Every phase is treated as an independent fluid. The equations of mass, momentum and energy balance are written for each phase, therefore the basic two-fluid model has six equations. In this thesis, the calculations were made using the code WAHA3. Main features of the WAHA3 are:

- One - dimensional, six - equation, two - fluid model for two - phase flow of water. Some types of simulations are also possible for two - phase flow of water and ideal gas without inter - phase heat and mass transfer. Hyperbolicity is required.

- The code distinguishes two flow regimes: dispersed and horizontally stratified.

- The code contains correlations for mass, momentum and heat transfer between phases and for wall friction. The correlations are flow regime dependent.

- The pipe elasticity and variable pipe cross-section effects are included in the code.

- The WAHA code is using its own steam tables.

- Special models in WAHA3: two pipes can be connected with an abrupt-area change model, a tank (constant pressure boundary condition) and a pump (constant velocity boundary condition. A branch model is used to connect three pipes in a single point.

- Explicit numerical scheme based on the operator splitting: the characteristic upwind discretisation of convective and non-relaxation source terms is used in the first sub-step, while stiff relaxation source terms (inter-phase exchange terms) are treated in the second sub-step. Numerical diffusion can be suppressed with the second - order accurate treatment of the convective terms.

- Forces on the pipes are calculated
- The approximated unsteady Friction Relaxation Model is available. The transient friction coefficients in the present version of WAHA: $\theta = 1$ millisecond, $k_T = 0.0002$ for acceleration, $k_T = 0.0001$ for deceleration. They are coded at the end of the subroutine *main* and can be changed manually for the purpose of the numerical tests of transient friction.

The basic set of equations in the WAHA3 code is:

$$\frac{\partial A(1-\alpha)\rho_f}{\partial t} + \frac{\partial A(1-\alpha)\rho_f(w_f - w_p)}{\partial x} = -A\Gamma_g \tag{6.17}$$

$$\frac{\partial A\alpha\rho_g}{\partial t} + \frac{\partial A\alpha\rho_g(w_g - w_p)}{\partial x} = A\Gamma_g \tag{6.18}$$

$$\begin{aligned} &\frac{\partial A(1-\alpha)\rho_f w_f}{\partial t} + \frac{\partial A(1-\alpha)\rho_f w_f(w_f - w_p)}{\partial x} + A(1-\alpha)\frac{\partial p}{\partial x} - \\ &A\cdot CVM - Ap_i\frac{\partial \alpha}{\partial x} = AC_i\left|w_r\right|w_r - A\Gamma_g w_i + A(1-\alpha)\rho_f g cos\theta - AF_{wall,f} \end{aligned} \tag{6.19}$$

$$\begin{aligned} &\frac{\partial A\alpha\rho_g w_g}{\partial t} + \frac{\partial A\alpha\rho_g w_g(w_g - w_p)}{\partial x} + A\alpha\frac{\partial p}{\partial x} + A\cdot CVM + Ap_i\frac{\partial \alpha}{\partial x} = \\ &-AC_i\left|w_r\right|w_r + A\Gamma_g w_i + A\alpha\rho_g g cos\theta - AF_{wall,g} \end{aligned} \tag{6.20}$$

$$\begin{aligned} &\frac{\partial A(1-\alpha)\rho_f e_f}{\partial t} + \frac{\partial A(1-\alpha)\rho_f e_f(w_f - w_p)}{\partial x} + p\frac{\partial A(1-\alpha)}{\partial t} + \\ &\frac{\partial A(1-\alpha)p(w_f - w_p)}{\partial x} = AQ_{if} - A\Gamma_g(h_f^* + w_f^2/2) + A(1-\alpha)\rho_f g\cos\theta w_f \end{aligned} \tag{6.21}$$

$$\begin{aligned} &\frac{\partial A\alpha\rho_g e_g}{\partial t} + \frac{\partial A\alpha\rho_g e_g(w_g - w_p)}{\partial x} + p\frac{\partial A\alpha}{\partial t} + \frac{\partial A(\alpha p(w_g - w_p)}{\partial x} = \\ &AQ_{ig} - A\Gamma_g(h_g^* + w_g^2/2) + A\alpha\rho_g g\cos\theta w_g \end{aligned} \tag{6.22}$$

where A stands for the cross-section of a pipe, w_f and w_g for liquid and vapor velocities respectively, ρ_f and ρ_g for liquid and vapor densities respectively,

α for void-fraction, w_p for pipe velocity, Γ_g for vapor generation rate, p for pressure, CVM for the virtual mass term, p_i for the interfacial pressure, C_i for the interfacial friction coefficient, w_r for the relative velocity ($w_r = w_g - w_f$), w_i for the velocity of the interfacial area, g for the gravitational acceleration, θ for the pipe inclination, $F_{f,wall}$ and $F_{g,wall}$ for wall friction forces of liquid and gas respectively, e_f and e_g for specific total energies of liquid and gas ($e = u + w^2/2$), h_f and h_g for specific enthalpies of liquid and gas ($h = u + p/\rho$), Q_{if} and Q_{ig} for interface-liquid and interface-gas heat transfer rates per unit of volume.

One can find detailed information about the model, the numerical method and the code in the WAHA3 manual (Tiselj et al. [37]). Different transformations were performed on the balance equations to obtain the equations in the non-conservative form used in the WAHA code.
The model is similar to typical two-fluid models used in computer codes like RELAP5 (Carlson et al. [11]), TRAC (Mahaffy [25]) or Cathare (Bestion [3]). It takes into account pipe-elasticity and the eventual motion of the pipe with a velocity w_p. The diameter of a piping system can change due to the variable geometry and to the elasticity of the tubes:

$$A(x,t) = A(x) + A_e(p(x,t)) \tag{6.23}$$

The second term A_e is much smaller than the first one. The pressure pulse changes the pipe diameter D in accordance to a linear relation (Wylie and Streeter [45]):

$$\frac{dA_e}{A(x)} = \frac{D}{d}\frac{dp}{E} = K dp \tag{6.24}$$

where d represents the wall thickness, E stands for the elasticity modulus and K represents the constant of elasticity $\left(K = \frac{D}{dE}\right)$.

Two additional equations of state for each phase are needed. The equation of state for phase k is:

$$d\rho_k = \left(\frac{\partial \rho_k}{\partial p}\right)_{u_k} dp + \left(\frac{\partial \rho_k}{\partial u_k}\right)_p du_k \qquad k = f, g \tag{6.25}$$

The derivatives on the right hand side of Eq. 6.25 are determined by the water property subroutines described in section 5 of the WAHA code manual. Pressure and specific internal energies are used as input values.

Hyperbolicity of the equations is ensured with a virtual mass coefficient (CVM) and an interfacial pressure term (terms with p_i) in the momentum equations.

The virtual mass term (CVM) in the momentum equations is one of the virtual mass terms proposed by Drew et. al [14]:

$$CVM = C_{VM}\left(\frac{\partial w_g}{\partial t} + (w_f - w_p)\frac{\partial w_g}{\partial x} - \frac{\partial w_f}{\partial t} - (w_g - w_p)\frac{\partial w_f}{\partial x}\right) \tag{6.26}$$

where C_{VM} is the virtual mass coefficient (Tiselj and Petelin [36], Carlson et al. [11]), which ensures the hyperbolicity of the set of equations, if the relative velocity is not very high:

$$C_{VM} = (1-S)\rho_m\alpha(1-\alpha)\begin{cases} \frac{1}{2}\cdot\frac{1+2\alpha}{1-a} & \alpha \le 0.4 \\ 1.5 - 10(\alpha-0.4)(\alpha-0.6) & 0.4 < \alpha \le 0.6 \\ \sqrt{\left(\frac{3-2\alpha}{2\alpha}\right)^2 + \frac{(1-\alpha)(2\alpha-1)}{(1-\alpha+\alpha\rho_g/\rho_f)^2}} & \alpha > 0.6 \end{cases} \tag{6.27}$$

Only absolute velocities are taken into account in the derivatives in Eq. 6.26. The derivatives of the structure velocity w_p are neglected in the virtual mass term CVM. The factor S determines stratification of the flow. For $S = 0$, the flow is dispersed, while $S = 1$ means horizontally stratified flow and intermediate values mark transition (section 2.2.1 of the WAHA code manual).

The interfacial pressure term in the momentum equations contains the interfacial pressure p_i, which exists only in the stratified flow regime in the WAHA code (see Bestion [3], or Carlson et al. [11]):

$$p_i = S\alpha(1-\alpha)(\rho_f - \rho_g)gD \tag{6.28}$$

The closure relationship for the velocity of the interfacial area is simply defined as:

$$w_i = \begin{cases} w_f & \Gamma_g \ge 0 \\ w_g & \Gamma_g < 0 \end{cases} \tag{6.29}$$

The terms appearing at the right side of equations 6.17 to 6.22 describe inter-phase heat (Q_{if}, Q_{ig}), mass (Γ_g) and momentum transfer (terms with C_i), gravity forces and wall friction ($F_{wall,f}, F_{wall,g}$). The closure relationships for mass, momentum and heat transfer between both phases depend on the flow regime and are described in details in chapter 2.2 of the WAHA code manual.

6.4.2 Wall friction

The approximated wall shear stress model based on shear stress value from last time step (described in section 4.3) is applied to the two-fluid model. The total shear stress for each phase is the sum of the steady shear stress and the transient contribution:

$$\tau_k(t) = \tau_{st,k}(t) + \tau_{un,k}(t) \qquad k = f, g \tag{6.30}$$

Consequently the dissipative terms $F_{wall,f}, F_{wall,g}$ present in Eqns 6.19 and 6.20 can be written as:

$$F_{wall,f} = F_{st,f} + \frac{4}{D}\tau_{un,f} \tag{6.31}$$

$$F_{wall,g} = F_{st,g} + \frac{4}{D}\tau_{un,g} \tag{6.32}$$

It is explained below how both steady and unsteady contributions are evaluated for each phase in the WAHA code.

Steady wall shear stress contribution for the two-fluid model

The steady dissipative terms $F_{st,f}$ and $F_{st,g}$ are calculated according to Darcy equation:

$$F_{st,f} = f_f \frac{\rho_f w_f |w_f|}{2D} \frac{\rho_f}{\rho_m}(1-\alpha) \tag{6.33}$$

$$F_{st,g} = f_g \frac{\rho_g w_g |w_g|}{2D} \frac{\rho_g}{\rho_m}\alpha \tag{6.34}$$

where f_f and f_g are the steady friction coefficients for liquid and gas respectively and ρ_m is the mixture density. In order to take the influence of the inertia of each phase into account, the dissipative terms are multiplied respectively by the quotients of the liquid and gas densities to the mixture density.
The classical steady friction coefficient is based on the Reynolds number. For laminar flows the relation is:

$$f = \frac{64}{Re} \tag{6.35}$$

where Re is Reynolds number. For turbulent flow the equation of Colebrook and White is used:

$$\frac{1}{\sqrt{f}} = -2\log\left(\frac{2.51}{Re\sqrt{f}} + 0.27\frac{k}{D}\right) \tag{6.36}$$

where k is the roughness of the wall. For the transition region ($2000 < Re < 5000$) the interpolation between both values is used.

The calculation procedure for f_f and f_g depends on the flow regime. The WAHA code recognizes two basic flow regimes: dispersed and horizontally stratified two-phase flows, with a transition area between both regimes. The information about the flow regime in the WAHA code is transmitted by means of a parameter S called stratification factor.

- Dispersed flow

  If the stratification factor S is equal to zero, the flow is assumed to be dispersed. For $\alpha > 0.95$, a **droplet** flow is identified. We assume that the liquid friction coefficient is $f_f = 0$. The gas friction coefficient is based on the gas Reynolds number, calculated according to the equation:

$$Re_g = \frac{\rho_m \left|w_m\right| D}{\mu_g} \tag{6.37}$$

  where w_m is the mixture velocity and μ_g is the gas dynamic viscosity. The mixture momentum is expressed by: $\rho_m w_m = \alpha\rho_g w_g + (1-\alpha)\rho_f w_f$.

For $\alpha < 0.5$, a **bubbly** flow is identified. Here, the gas friction coefficient is assumed to be $f_g = 0$. The liquid friction coefficient f_f is based on the liquid Reynolds number:

$$Re_f = \frac{\rho_m |w_m| D}{\mu_f} \tag{6.38}$$

where μ_f is the liquid dynamic viscosity.

If $0.5 < \alpha < 0.95$, the friction factors are interpolated between the extreme values. The values of f_f and f_g are calculated at the limits $\alpha = 0.5$ and $\alpha = 0.95$ and these values are used to interpolate both friction factors for the given void fraction α:

$$f_g = \frac{\alpha - 0.5}{0.45} \cdot f_g(\alpha = 0.95) \tag{6.39}$$

$$f_f = \frac{0.95 - \alpha}{0.45} \cdot f_f(\alpha = 0.5) \tag{6.40}$$

- Horizontally stratified flow

If $S = 1$, the flow is identified as horizontally stratified. For horizontally stratified flows, first the friction factors are calculated from the Reynolds numbers of both phases:

$$f_g = f_g(Re_g) \quad \text{where} \quad Re_g = \frac{\rho_m |v_m| D}{\mu_g} \tag{6.41}$$

$$f_f = f_f(Re_f) \quad \text{where} \quad Re_f = \frac{\rho_m |v_m| D}{\mu_f} \tag{6.42}$$

Then these friction factors are multiplied by the fraction of the wall in contact with each phase. The fraction of wall in contact with the vapour is:

$$b = \frac{|\arccos(1 - 2\alpha)|}{\pi} \tag{6.43}$$

- Dispersed to horizontally stratified transition flow

If the stratification factor is $0 < S < 1$, the friction coefficients are interpolated between the values calculated for dispersed and stratified flows:

$$f_g = S \cdot f_{g,stratified} + (1 - S) \cdot f_{g,dispersed} \tag{6.44}$$

$$f_f = S \cdot f_{f,stratified} + (1 - S) \cdot f_{f,dispersed} \tag{6.45}$$

The dissipative effects due to the curvatures of the pipes are also taken into account in WAHA code. The friction coefficient responsible for the **minor losses** due to the curvatures is:

$$f_{ml} = \frac{\beta}{2\pi}\frac{D}{\Delta x} \tag{6.46}$$

where β is the angle between neighboring segments of the pipe and Δx is the numerical cell length. This friction factor multiplied with $(1 - \alpha)$ and α is added to f_f and f_g respectively.

Unsteady wall shear stress contribution for the two-fluid model

The unsteady shear stress contribution is first calculated for the mixture and then splitted between both phases. The unsteady term for the mixture is equivalent to Eq. 4.9 for single - phase flow:

$$\tau_{un,m}(0) = 0 \tag{6.47}$$

$$\tau_{un,m}(t) = \tau_{un,m}(t - \Delta t)e^{\frac{-\Delta t}{\theta}} + k_T \rho \, |a| \, \Delta_t w_m \tag{6.48}$$

where $\Delta_t w_m$ is the difference between the values of the mixture velocity for the last two time steps, θ is a relaxation time for mixture and k_T is a transient friction coefficient for mixture. These values must be evaluated on the basis of experimental data. They are probably close to the values of θ and k_T for single-phase liquid flow, as the transient friction effect seems to be much more significant in a liquid than in a gas. The challenge is to find the appropriate analytical expressions for these coefficients.

The splitting of the transient mixture shear stress into shear stresses for each phase in the WAHA code is the same for all flow regimes:

$$\tau_{un,f} = \tau_{un,m}\frac{\rho_f}{\rho_m}(1-\alpha) \quad (6.49)$$

$$\tau_{un,g} = \tau_{un,m}\frac{\rho_g}{\rho_m}\alpha \quad (6.50)$$

6.4.3 Results

In this section, some experimental and numerical results for two-phase flows are presented. The numerical results were obtained with the WAHA3 code including the Two-Fluid Model of flow (Eqs 6.17 - 6.22) and the approximated Friction Relaxation Model (Eqs 6.47 - 6.50).
The numerical scheme applied in the WAHA code is based on the Godunov methods *i.e.* high - resolution, shock - capturing methods, which are widely used in aerodynamics ([19], [24]). The scheme is non-conservative due to the choice of the basic variables. The source term vector is split into two parts: non-relaxation sources (wall friction, volumetric forces, sources due to the variable pipe cross-section and due to the pipe motion) and relaxation sources. The relaxation sources tend to establish thermal and mechanical equilibrium between both phases. They are often stiff, *i.e.* their characteristic times are much shorter than the characteristic times of other two - phase flow phenomena, even shorter than the characteristic times of the acoustic waves. Stiffness of the source terms is the reason for the use of the operator splitting in the numerical scheme of the WAHA code. Splitting means that the convection term with the non-relaxation sources in the basic set of equation are treated separately from the relaxation sources. Therefore a single time step includes two sub-steps:

1. Integration of the convection terms and the non-relaxation sources.

2. Integration of the relaxation sources with the initial conditions being the results of the integration in the first substep.

The numerical scheme is second order accurate. The problem of the oscillations, which appear in the vicinity of the non - smooth solutions, is solved by the use of the combination of the first and second - order accurate discretisation [24]. A part of the second - order discretisation is determined by the limiters, which 'measure' the smoothness of the solutions. If the solutions are smooth, a larger part of the second - order discretisation is used, otherwise a larger part of the first - order discretisation is used.
The numerical scheme used in the code is described in details in the WAHA3 manual (Tiselj et al. [37], Tiselj and Petelin [36]).

Simpson experiment

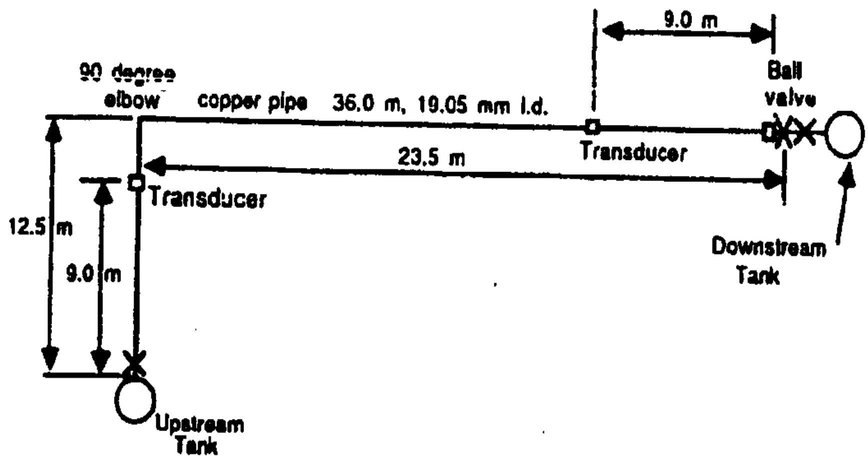

Figure 6.16: Simpson experimental loop. Plan view.

The Simpson apparatus [33] includes an upstream reservoir, a 36 meter long, 19 mm inside diameter copper pipe, a downstream one - quarter turn ball valve, and a downstream reservoir (Fig. 6.16, 6.17). The pipeline has a

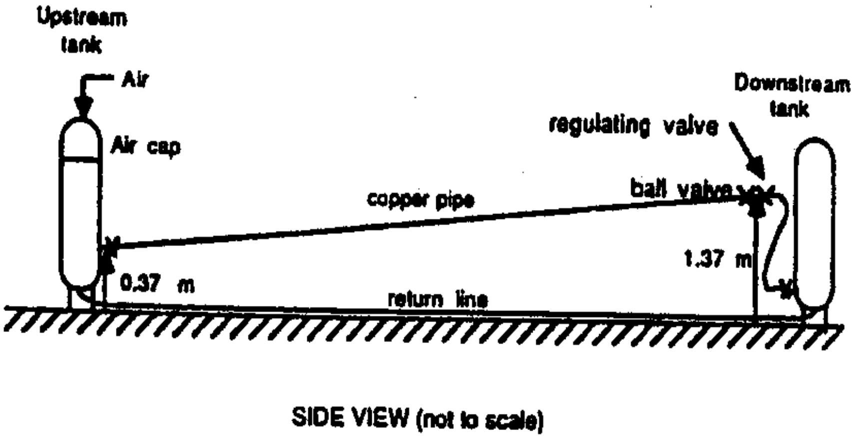

Figure 6.17: Simpson experimental loop. Side view.

right angle bend located 12.5 meters from the upstream end. The upstream and downstream reservoirs are 473 liter vertical standing Kargard ASME air receiver tanks. The overall height of the tank is 2.27 meters supported on a 30.5 cm base and the diameter of the tank is 61 cm. The tank has 11 orifices for connection of fittings and instrumentation. Each air tank may be pressurized with the G.G. Brown building air supply that has a minimum pressure of approximately 690 kilopascals. Air supply into the top of the tank is passed through a solids filter, a finer oil filter, and a pressure regulator. A pressure gage and air discharge valve are connected to the air supply line near the top of the tank. The tank is filled with water from the City of Ann Arbor supply through a hose connection at the top of the tank. Tank level is monitored using a sight glass at the side of the tank. A rubber hose return line extends from the bottom of the upstream tank to the bottom of the downstream tank. When water from the upstream tank has been emptied into the downstream tank, the water is returned to the upstream tank by

the return line. This configuration was used to minimize the amount of air content of the water.
Brackets affixed to the wall at approximately 2.5 meter intervals support the pipe. The copper pipeline is 36 meters long and is comprised of sections 6.1 meters in length connected by union fittings. These fittings enable the pipe sections to be disconnected for the establishment of a new pipe slope configuration.
Pipe slope may be adjusted by altering the vertical position of brackets. An elevation difference of 1 meter between the ends of the pipe has been selected for the experimental studies. Split ring hangers support the copper pipe on the brackets. These hangers can rotate in order to maintain a firm support, when adjusting the slope of the pipe.
Three pressure transducer mounting blocks, each machined from brass, are located at the downstream valve, at the upstream one-quarter point 9 m from the upstream end, and at the downstream one-quarter point 9 m from the downstream valve.
Four pressure transducers are used to measure the pressure variation in the pipeline. Three of the transducers are of the piezoelectric quartz type and the other transducer is a strain gage type. One of the piezoelectric transducers and the strain gage transducer are located at the downstream valve. The other piezoelectric transducers are located at the upstream and downstream one-quarter points.
The fast closing valve at the downstream end is a Marpac Petro B790 one-half inch, quarter-turn ball valve. The water hammer wave is caused by the fast closure of the valve, achieved by hand. A shutoff valve downstream of the ball valve is used to regulate the initial steady - state discharge in the system.
Velocity for steady - state flow conditions is obtained from the determination of the head loss along the pipe. The head drop from the reservoir to the upstream side of the ball valve is provided by a differential manometer containing red liquid 294 with a specific gravity of 2.94. A connection from the

bottom of the manometer to the return line is similar to that for the mercury manometer. The top of the red liquid or acetylene tetrabromide manometer is attached to the side of the brass transducer mounting block located at the downstream valve. A pressure gage is also located at the downstream end transducer mounting block. To compute the velocity from the head loss along the pipe, the friction factor is required and is obtained by a steady - state calibration analysis.
The steady - state friction coefficients calculated with the WAHA code are in agreement with the coefficients evaluated on the basis of the pressure drop measurements.
The effect of the gravity was not registered in the experimental results, therefore it was also ignored in the calculations.
The calculations were made for both single and two-phase cases. The results at the valve are presented.

Single-phase case

The initial thermodynamic state in the pipe is defined with constant parameters along the pipe: pressure p=3.419 bar, temperature T=296.3 K, velocity v=0.24 m/s and vapor volume fraction α=0. The experiment starts at time t=0 s when the valve is rapidly closed.
The second order scheme with MINMOD limiter was used to make the calculations. CFL = 0.8. Number of nodes = 100.
In Fig. 6.18 the steady friction results for pressure are compared with experimental results. The disagreement in the phase and amplitude is obvious. The corresponding wall shear stress calculated with a steady-state formula at the middle of the pipe is shown in the Fig. 6.19.
The calculations with the Friction Relaxation Model were performed with the same values of coefficients θ and k_T as adjusted against the experiment of Holmboe and Rouleau [20]). The diameter and the velocity were very similar in both experiments.
The effect of the elasticity of the pipe was taken into account in the calculations ($E = 1.2 \cdot 10^{11}$, d=1.6 mm).

In Fig. 6.20, transient friction results for pressure are compared with experimental results. The Friction Relaxation Model significantly improves the results but the amplitude is still not exactly the same as in the experiment. A certain discrepancy can be observed from the very beginning.
The evolution of the transient wall shear stress at the middle of the pipe is shown in the Fig. 6.21. The difference between steady and transient shear stresses is about two orders of magnitude.

In order to find the the results corresponding to the experimental data more calculations were done for larger k_T coefficients (k_T for acceleration $= 4 \cdot 10^{-4}$, k_T for deceleration $= 2 \cdot 10^{-4}$). The results are presented in Fig. 6.22. For these coefficients the damping appears to be better than in Fig. 6.20, but still the first pressure peak is not correctly predicted. As the diameter and the velocity in this experiment are very similar to those in Holmboe and Rouleau experiment [20] it is likely that the correct coefficients k_T are: $2 \cdot 10^{-4}$ for acceleration and $1 \cdot 10^{-4}$ for deceleration.

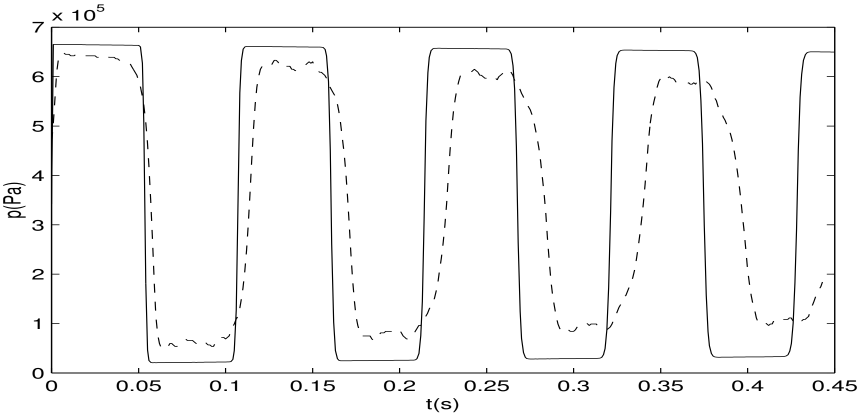

Figure 6.18: Simpson single-phase experiment. Pressure at the valve versus time. Solid line - steady friction, dashed line - experimental results.

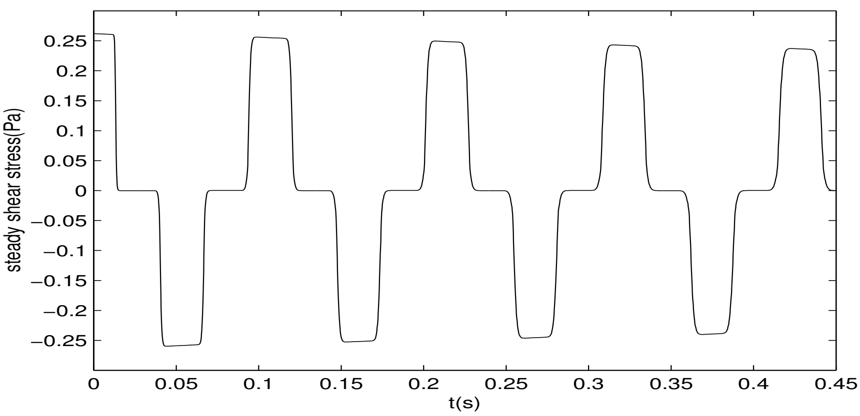

Figure 6.19: Simpson single-phase experiment. Steady shear stress at the midpoint versus time.

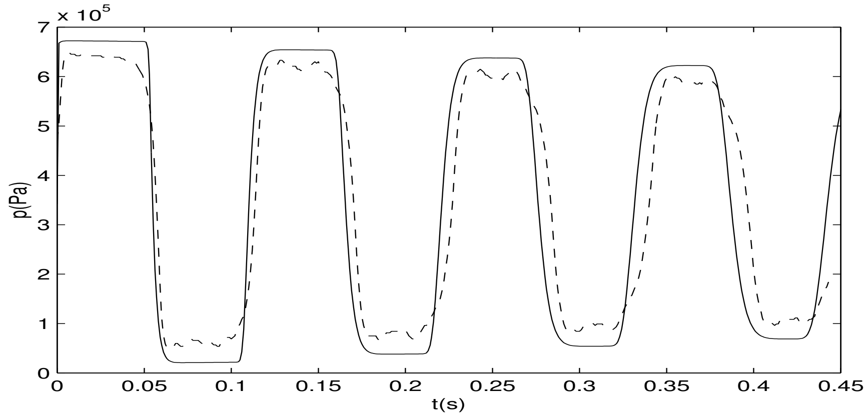

Figure 6.20: Simpson single-phase experiment. Pressure at the valve versus time. Solid line - transient friction, dashed line - experimental results; $\theta = 1.4$ms, k_T for acceleration $= 2 \cdot 10^{-4}$, k_T for deceleration $1 \cdot 10^{-4}$.

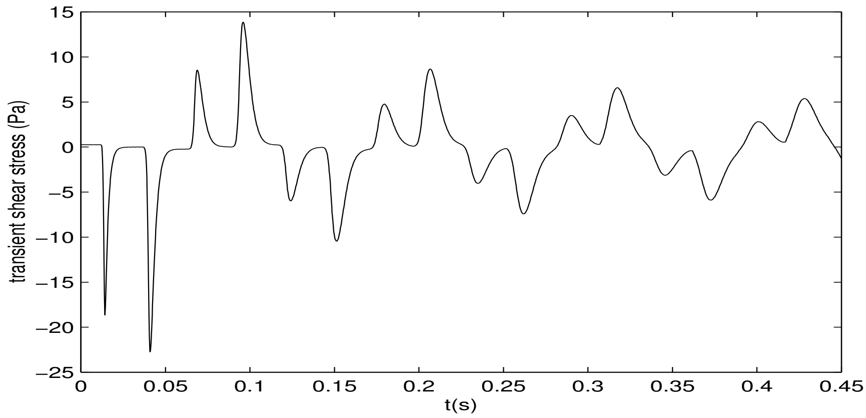

Figure 6.21: Simpson single-phase experiment. Transient shear stress at the midpoint versus time; $\theta = 1.4$ms, k_T for acceleration $= 2 \cdot 10^{-4}$, k_T for deceleration $1 \cdot 10^{-4}$.

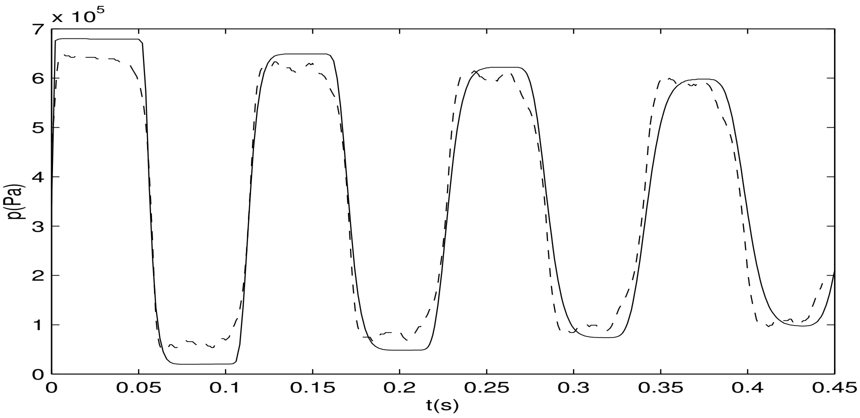

Figure 6.22: Simpson single-phase experiment. Pressure at the valve versus time. Solid line - transient friction, dashed line - experimental results; $\theta =$ 1.4ms, k_T for acceleration $= 4 \cdot 10^{-4}$, k_T for deceleration $2 \cdot 10^{-4}$.

Two-phase case

The two-phase flow was observed for the initial velocity 0.4m/s. The other data are the same as for the single-phase case. The numerical settings are also the same.

Inter - phase friction coefficient as well as inter - phase heat transfer coefficients are obtained from the WAHA correlations [37].

A comparison between pressure history obtained with the steady-state friction formula and the experimental results is shown in the Fig. 6.23. During the valve closure, the pressure increases suddenly and then the pressure wave travels to the tank. When the expansion wave reflected from the tank arrives at the valve, the pressure drops suddenly and the flashing phenomenon occurs. When the second wave reflected from the tank reaches the valve two reflections appear: one from the vapor and the other from the valve. The combination of both waves creates a pressure peak, which is higher than the initial pressure rise. The results in Fig. 6.23 show that the steady friction model overpredicts the amplitude of the pressure peaks and gives a small phase displacement, which is not in agreement with the experimental re-

sults.
The two-phase calculations with the Friction Relaxation Model were also performed with the same values of coefficients θ and k_T as those adjusted against the experiment of Holmboe and Rouleau [20]. The results are shown in Fig. 6.25. We can observe that the Friction Relaxation Model improves the results for the first pressure peak: it gives more damping and a small positive phase shift in comparison with the steady friction results presented in Fig. 6.23, and gives a better agreement with the experiment. Since the values of the coefficients k_T and θ are the same as those evaluated for the single-phase flow experiment by Holmboe and Rouleau, it seems that the adopted values of these coefficients for the specified fluid (water in this case) can be probably used for quite a wide range of initial conditions.
Both the steady and unsteady results are obtained with the assumption of elastic pipe, which also improves the results in comparison with those obtained for a stiff pipe.
The Friction Relaxation Model results in smaller amounts of vapour than the steady friction model for the Simpson data (Fig. 6.27). Unfortunately there are no experimental results for void fraction to make the comparison.

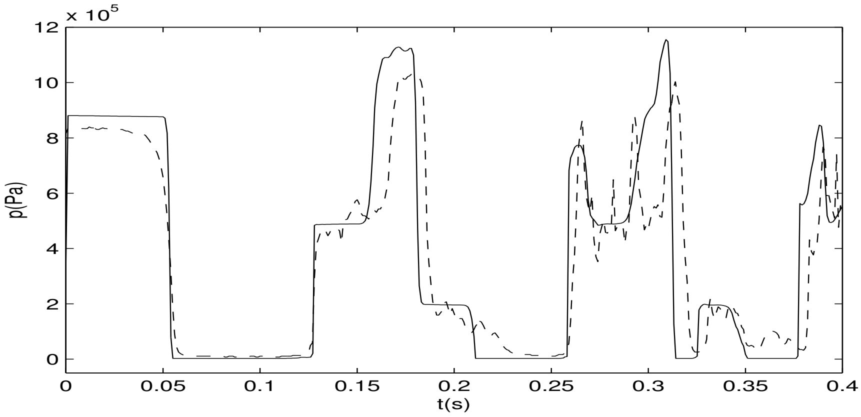

Figure 6.23: Simpson two-phase experiment. Pressure at the valve versus time. Solid line - steady friction, dashed line - experimental results.

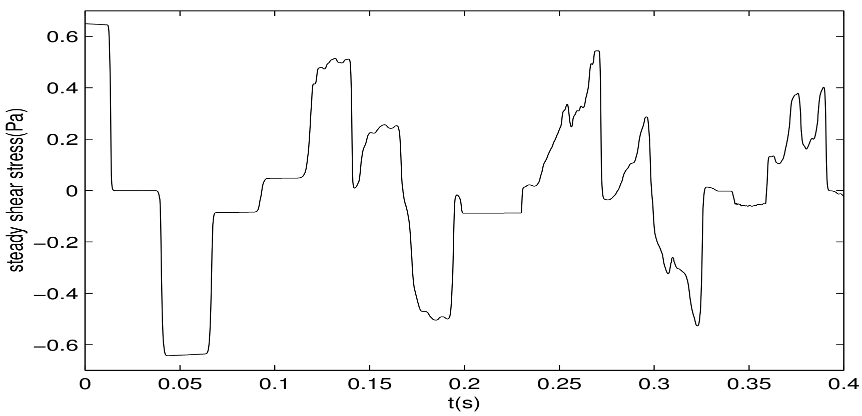

Figure 6.24: Simpson two-phase experiment. Steady shear stress at the midpoint versus time.

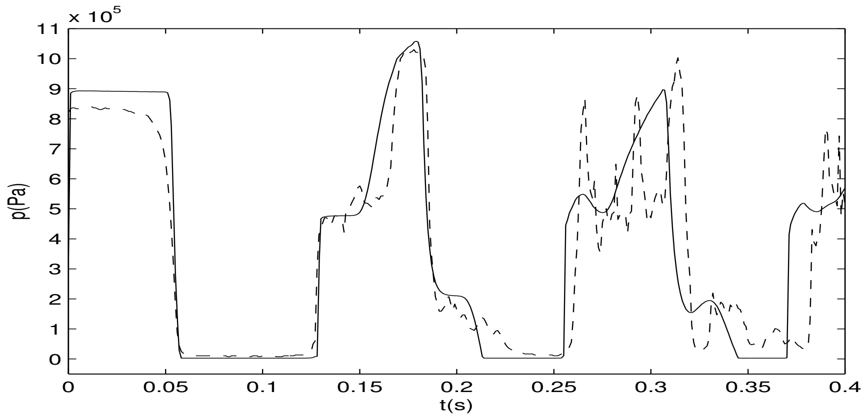

Figure 6.25: Simpson two-phase experiment. Pressure at the valve versus time. Solid line - transient friction, dashed line - experimental results; $\theta = 1.4\text{ms}$, k_T for acceleration $= 2 \cdot 10^{-4}$, k_T for deceleration $1 \cdot 10^{-4}$.

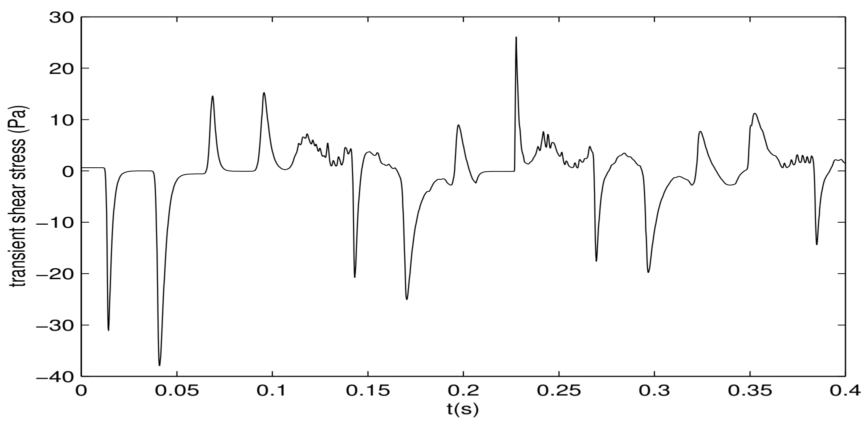

Figure 6.26: Simpson two-phase experiment. Transient shear stress at the midpoint versus time; $\theta = 1.4\text{ms}$, k_T for acceleration $= 2 \cdot 10^{-4}$, k_T for deceleration $1 \cdot 10^{-4}$.

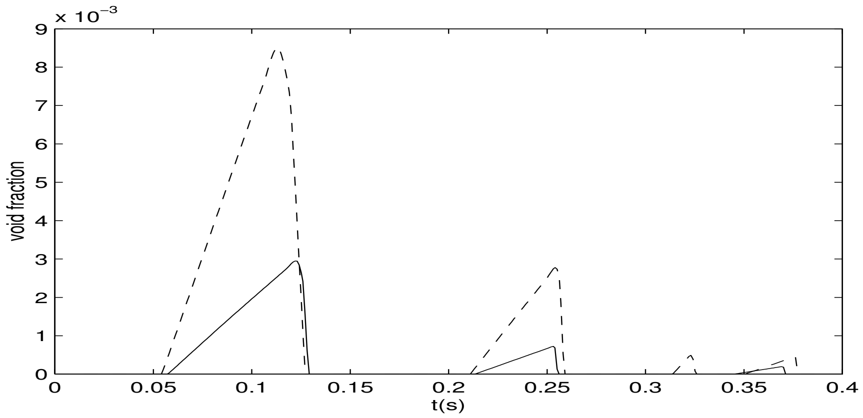

Figure 6.27: Void fraction at the valve versus time for Simpson two-phase transient. Dashed line - steady friction, solid line - transient friction; $\theta =$ 1.4ms, k_T for acceleration $= 2 \cdot 10^{-4}$, k_T for deceleration $1 \cdot 10^{-4}$.

UMSICHT Pilot Plant Pipework water-hammer experiment

A set of experiments was performed in the Fraunhofer UMSICHT test loop PPP (Pilot Plant Pipework) at Oberhausen (Germany) as part of the WAHA project. A photo of the experimental loop is shown in Fig. 6.28. The configuration of the PPP test loop is shown in Fig. 6.29. Demineralized tap water is pumped from the pressurized vessel B1 through the approximately 200 m long pipe and flows back to the vessel. At $t = 0$s, the valve at Pos.1 closes rapidly while the pump is still running. During the first phase of the transient, a rarefaction wave travels inside the pipe towards the downstream reservoir. As a consequence, cavitation occurs downstream of the valve and a vapour bubble is formed. The generated pressure wave oscillates between the vessel and the vapour bubble until the vapour condenses, inducing a cavitational hammer.
The locations of the pump, the valve, the fixed points (FP), where the force measuring devices are mounted, as well as the wire mesh sensor (GS) and the pressure sensors (P01 - P23) are shown in Fig. 6.29.

Figure 6.28: PPP experimental setup.

Fluid - Structure Interaction effects were expected in the newly constructed pipe bridge sections (see Fig. 6.30), where the pipe support is quite elastic to simulate typical pipe support conditions in power plants.
Wire-mesh sensors were used to perform a high-speed visualisation of gas-liquid two-phase flows (Fig. 6.31). They consist of two grids of thin parallel wires which span over the measuring cross-section. The wires of both planes cross at an angle of 90 deg. During the signal acquisition, one plane of electrode wires is used as transmitter, the other as receiver plane. The transmitter electrodes are activated by supplying them with voltage pulses in a successive order. The current at the receiver wire resulting from the acti-

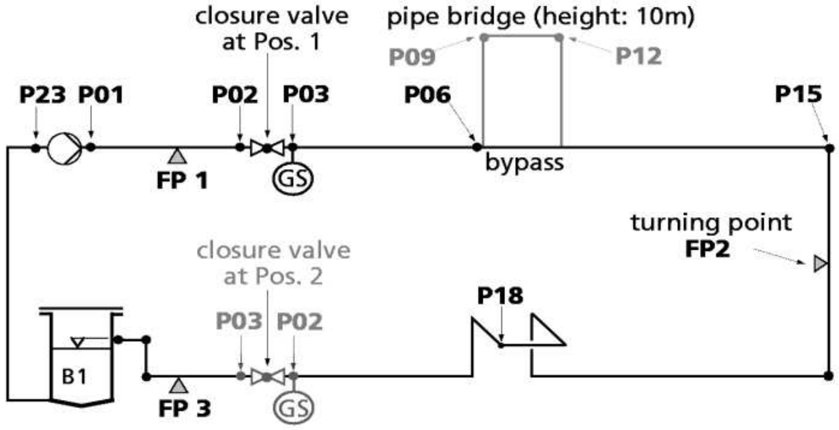

Figure 6.29: Configuration of the Fraunhofer UMSICHT test loop PPP.

vation of a given transmitter wire is a measure of the conductivity of the fluid in the corresponding control volume close to the crossing point of the two wires. The currents from all receiver wires are sampled simultaneously. This procedure is repeated for all transmitter electrodes. After activating the last transmitter wire, a complete matrix of measured values is filed in the computer. This matrix reflects the complete two - dimensional conductivity distribution in the sensor cross - section at the time of measurement. The conductivity values are transformed into local instantaneous volumetric gas fractions. The resulting data is the basis for the fast flow visualisation and for the calculation of void profiles, bubble size distribution as well as for the performance of a decomposition of radial gas fraction profiles according to bubble size classes.
Another new feature is the introduction of micro-thermocouples. The ends of these are placed in special openings cut into the transmitter electrodes. The thermocouples are put into channels milled into the transmitter rods. The thermocouples themselves are laid through capillaries which are soldered into these channels, so that they can be replaced without destroying the sensor.

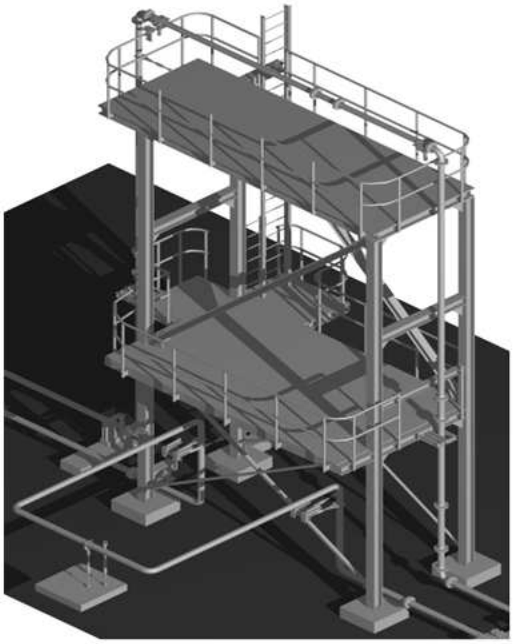

Figure 6.30: The pipe bridge

The construction of a mesh sensor with 2 x 16 electrodes is shown in Fig. 6.31. The lateral resolution given by the electrode pitch is 5.8 mm. The temperature measurement is carried out at the same frequency as the void distribution measurement. A framing rate of 500 Hz was used in the presented measurements. The sensor was installed 231 mm downstream the fast acting valve. It was arranged in the way shown in Fig. 6.31, *i.e.* the thermocouples were located along a vertical line in the centre of the measuring cross section. This arrangement was chosen to measure vertical temperature gradients which are likely to occur in the expected stratified flow.
The experimental setup and the test scenarios were described with details by

Dudlik [15].
The section of the pipe behind the valve shown in Fig. 6.32 was simulated with the WAHA code. The numbers in the squares in Fig. 6.32 represent the quantities of numerical volumes for each element of the pipeline. After the valve closure, the expansion wave travels towards the vessel and vapor is formed due to the pressure drop. The cavitation induced water hammer occurs after the flow direction is reversed, the vapor bubble condenses and the liquid water hits the closed valve.
A simulation was done for the run at the temperature of 392 K; the pressure in the vessel was 9.92 bars, and the velocity 4 m/s (test 307). The diameter of the pipeline is 108 mm. The elasticity of the pipe was taken into account. Inter - phase friction coefficient as well as inter - phase heat transfer coefficients are obtained from the WAHA correlations [37].
The numerical results for the pressure are compared with the experimental results in the Fig. 6.33. The parameters k_T and θ in the simulation with the Friction Relaxation Model are the same as those evaluated on the basis of the Holmboe and Rouleau experiment. It is clear from this figure that the Friction Relaxation Model with the suggested parameters k_T and θ does not predict sufficiently well the pressure amplitudes, especially after two wave periods. The possible reason for this is that the effect of transient friction is a short - timescale effect (it has the order of 1ms) while the period in the PPP experiment has the order of 1s, which is a thousand times larger. Therefore, it seems that the transient friction is a secondary effect in this experiment and is not the main reason for the pressure wave damping.
In order to see the effect of the transient friction in this simulation, the pressure results obtained with the Friction Relaxation Model are compared with the steady-state friction results in Fig. 6.34. At the beginning, there is no noticeable difference between steady and transient friction results. Only after several periods, some negative phase shift is observed in the results obtained with the Friction Relaxation Model.
Although the pressure results obtained with the WAHA code, including the

Friction Relaxation Model, are not very satisfactory, the void fraction is well predicted (Fig. 6.35). In Fig. 6.36, the comparison between transient and steady friction results is shown. The transient friction model gives almost the same amount of vapour as the steady model for the first flashing, and a slightly smaller amount of vapour afterwards. Again, this is due to the time scale of the phenomena with respect to the time scale of the unsteady friction.

It is likely that, in this experiment, there are other dissipative effects than transient friction, not taken into account in the code. Probably such a significant pressure damping is due to the singular head losses present in the pipeline, which are not modelled sufficiently well in the actual version of the WAHA code, used to make these computations.

As the diameter of the pipe in PPP experiment is large and the flow is highly turbulent (Re=432000) it is also possible that the values of θ and k_T for this experiment differ from those of Holmboe and Rouleau experiment.

More calculations have been done for significantly larger values of θ and k_T ($\theta = 7$ms and $k_T = 1 \cdot 10^{-3}$ for acceleration, $5 \cdot 10^{-4}$ for deceleration). For these values the difference between steady and transient friction results is significant (Fig. 6.37). The pressure peaks calculated with the transient friction are much smaller than those calculated with the steady formula. Curiously, for the two first pressure peaks, a positive phase shift is observed and afterwards the shift becomes negative.

The comparison between experimental results and transient friction results for larger values of θ and k_T is shown in Fig. 6.38. The pressure damping for this case is in better agreement with experimental results than for the smaller values of θ and k_T (Fig. 6.33) but the phase is not sufficiently well predicted. Also the quantity of vapor calculated with larger values of θ and k_T is too large at the beginning and too small afterwards.

In fact, in case of two-phase transient flows, also the effect of thermal non-equilibrium may have a large influence on pressure and void fraction and for this reason the evaluation of the correct values of the transient friction

coefficients is problematic.
The PPP experiment is rather complicated, the loop is complex and many effects have to be taken into account (singular head losses, air dissolved in water, thermal non-equilibrium), therefore it is not a good basis for the validation of the Friction Relaxation Model .
In order to validate the Friction Relaxation Model and model the coefficients k_T and θ, the database of simple experiments with water hammers in single pipes needs to be created.

6.5 Conclusions

In this chapter the Friction Relaxation Model was introduced into three different two-phase models: the Homogenous Equilibrium Model, the Homogenous Relaxation Model and the Two - Fluid Model. The results show that the pressure and void fraction histories depend on the choice of the two-phase model as well as on the choice of the friction model. However, it can be generally concluded that the transient friction damps more the pressure oscillations and produces smaller amounts of vapour than the steady friction model. For the fast closure of a downstream valve, there is also some positive phase shift; for the closure of the upstream valve the shift is negative.

The relaxation approach presented in this thesis can be useful for the modelling of other phenomena in fast transient two-phase flows like the interfacial shear stress or the heat transfer.
For the stratified flow it can be also useful to have the relaxation equation for the shear stress of each phase instead of one relaxation equation for the mixture and this may be the subject of the future research in this field.
Another suggestion is the possibility to adopt an approximated approach based on the last time step, as described in the Section 4.3, to the relaxation equation for the quality (in similar way as it was done for the wall shear stress). This would eliminate the differential equation for quality in the system 6.9 - 6.13.

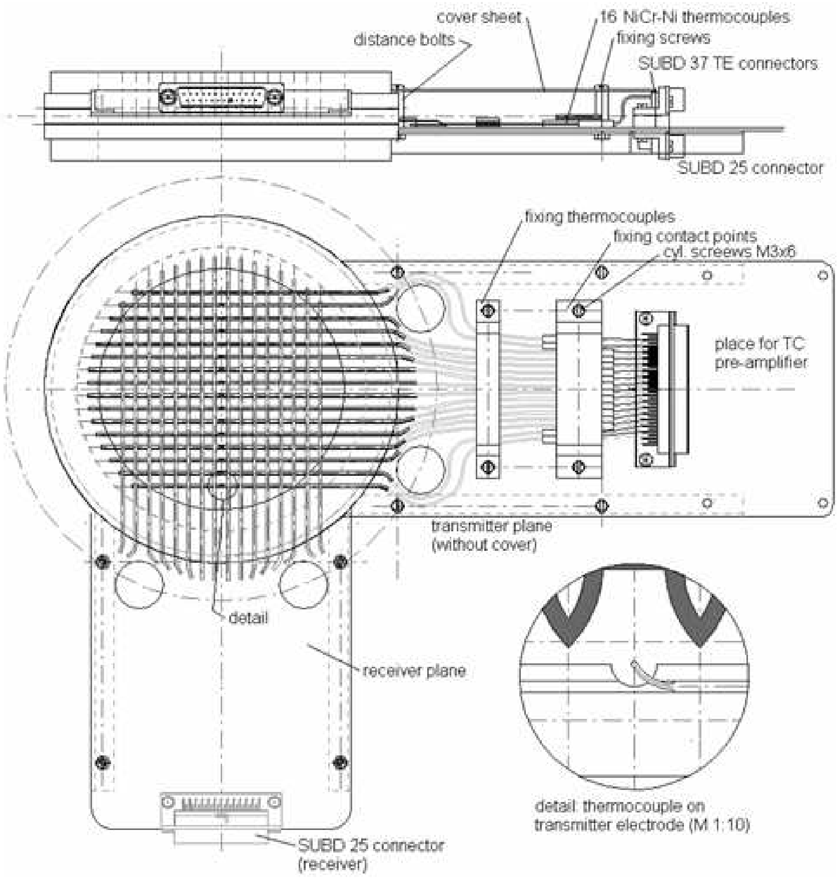

Figure 6.31: Mesh-sensor DN100 with 2x16 electrode rods and 16 micro-thermocouples.

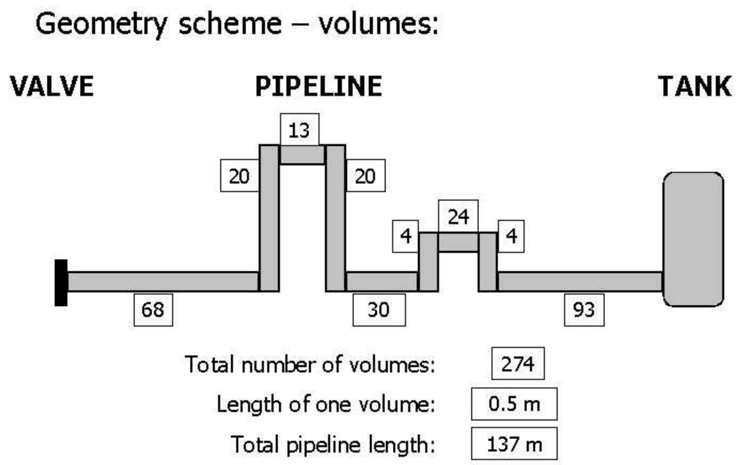

Figure 6.32: Scheme of the facility behind the valve.

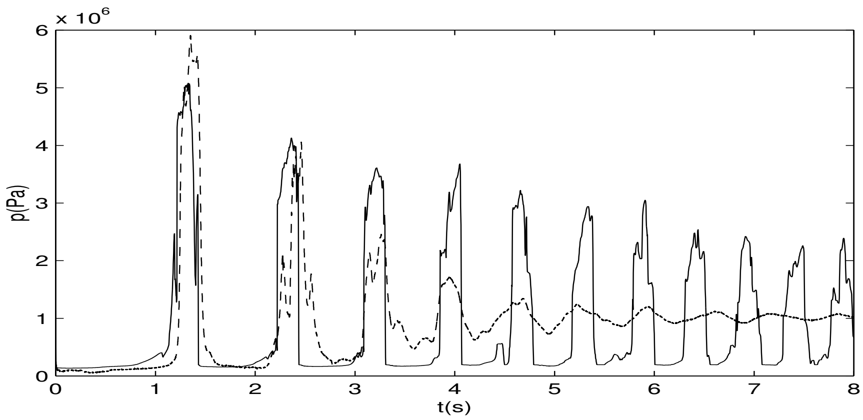

Figure 6.33: PPP two-phase experiment. Pressure at the valve versus time. Solid line - transient friction ($\theta = 1.4$ms, k_T for acceleration $= 2 \cdot 10^{-4}$, k_T for deceleration $1 \cdot 10^{-4}$), dashed line - experimental results.

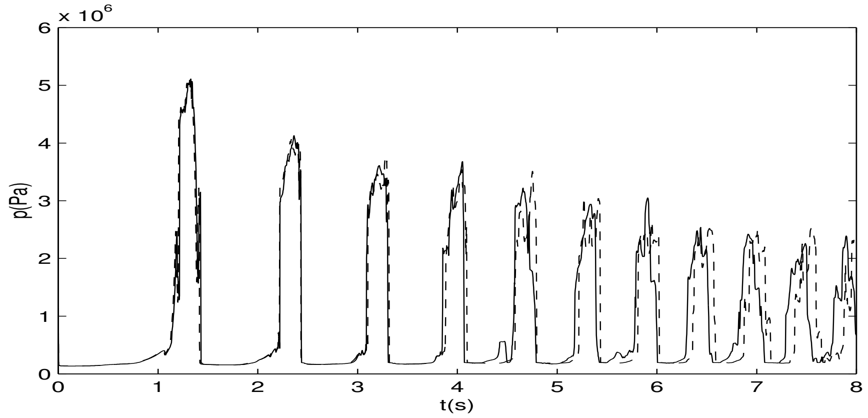

Figure 6.34: PPP two-phase experiment, comparison between numerical results for steady and transient friction. Pressure at the valve versus time. Solid line - transient friction ($\theta = 1.4$ms, k_T for acceleration $= 2 \cdot 10^{-4}$, k_T for deceleration $1 \cdot 10^{-4}$), dashed line - steady friction.

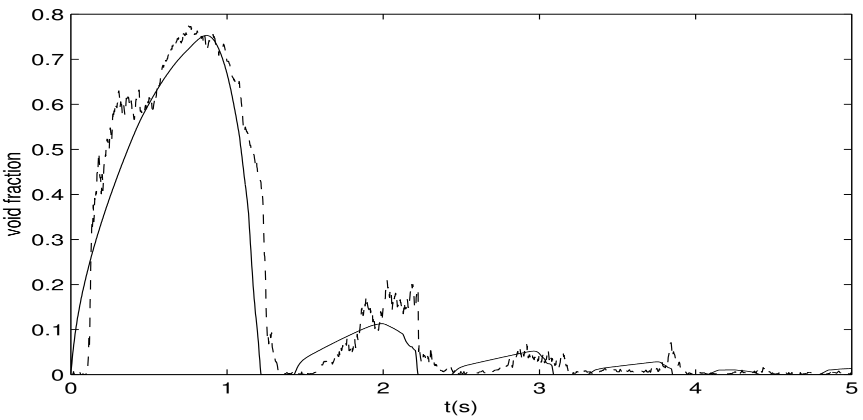

Figure 6.35: PPP two-phase experiment. Void fraction at the valve versus time. Solid line - transient friction ($\theta = 1.4$ms, $k_T = 2 \cdot 10^{-4}, 1 \cdot 10^{-4}$), dashed line - experimental results.

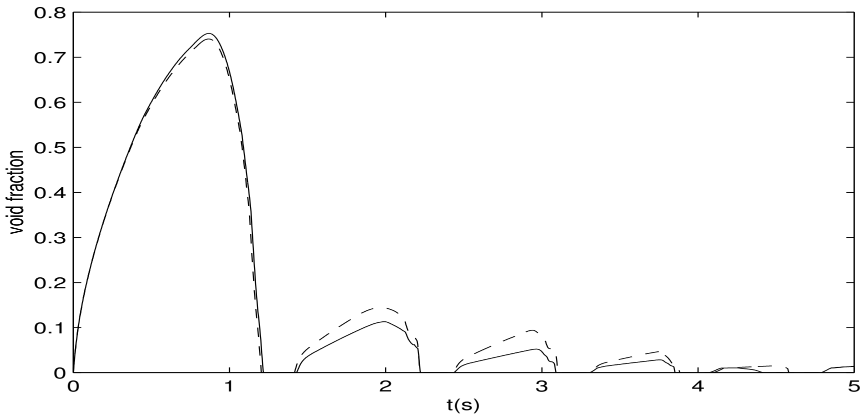

Figure 6.36: PPP two-phase experiment, comparison between numerical results for steady and transient friction. Void fraction at the valve versus time. Solid line - transient friction ($\theta = 1.4$ms,$k_T = 2 \cdot 10^{-4}, 1 \cdot 10^{-4}$), dashed line - steady friction.

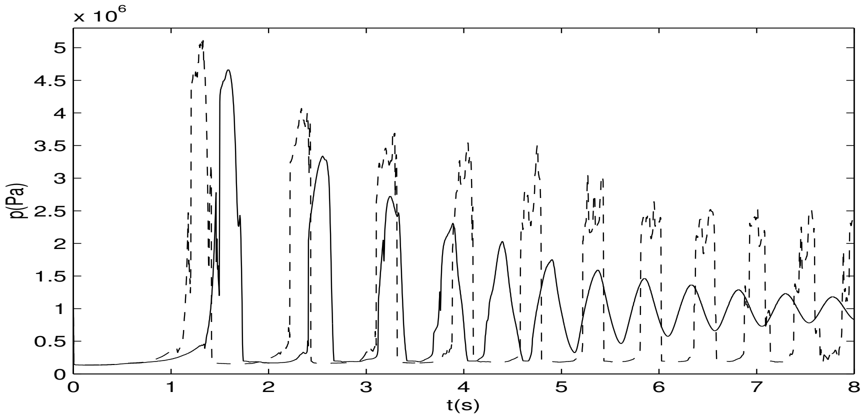

Figure 6.37: PPP two-phase experiment, comparison between numerical results for steady and transient friction. Pressure at the valve versus time. Solid line - transient friction ($\theta = 7$ms, k_T for acceleration $= 1 \cdot 10^{-3}$, k_T for deceleration $5 \cdot 10^{-4}$), dashed line - steady friction.

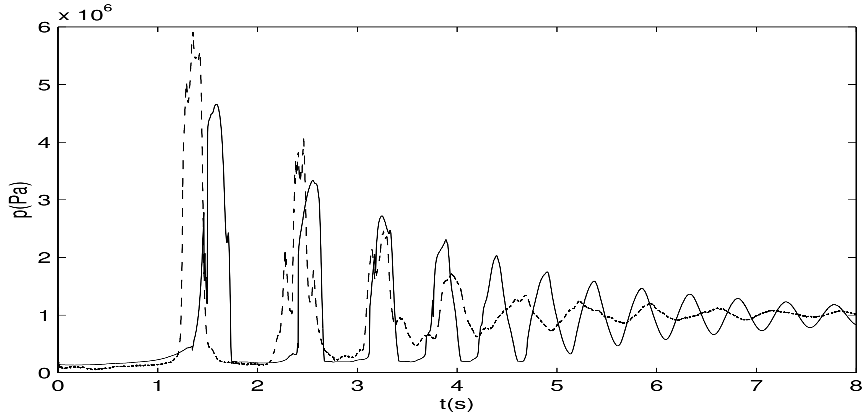

Figure 6.38: PPP two-phase experiment. Pressure at the valve versus time. Solid line - transient friction ($\theta = 7$ms, k_T for acceleration $= 1 \cdot 10^{-3}$, k_T for deceleration $5 \cdot 10^{-4}$), dashed line - experimental results.

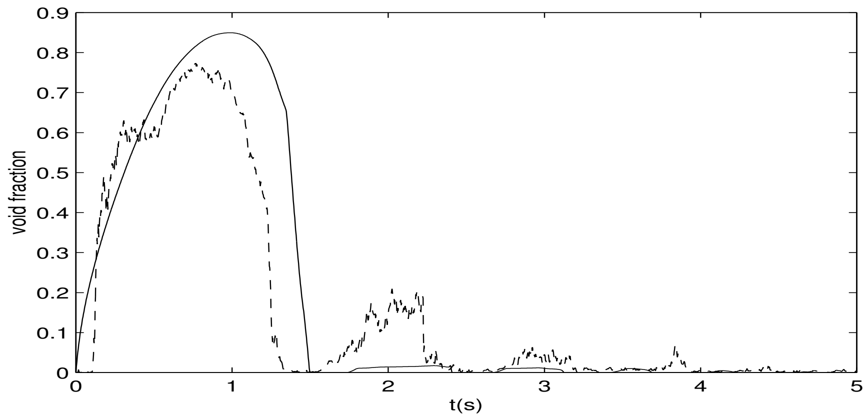

Figure 6.39: PPP two-phase experiment. Void fraction at the valve versus time. Solid line - transient friction ($\theta = 7$ms, $k_T = 1 \cdot 10^{-3}, 5 \cdot 10^{-4}$), dashed line - experimental results.

Chapter 7

Conclusions

This study was aimed at developing a 1D model of dissipative effects which occur during fast transient single- and two-phase flows. The evolution of the velocity profile in a boundary layer during transient flows has been studied by means of a 2D code (FLUENT) and it has been concluded that instantaneous values of variables averaged in the cross-section do not contain sufficient information to model transient friction effects. Therefore, steady friction models, which are based only on instantaneous, cross-section averaged velocities, are not appropriate for transient flows. This was confirmed experimentally by different researchers during the last 50 years.

A water hammer wave has a drastic effect on the velocity profile at the wall. It causes some kind of translation of the velocity profile in the whole pipe section and therefore produces a very large velocity gradient in the close neighborhood of the wall. After passage of the wave, the velocity profile at the wall tends to the steady-state profile, corresponding to the new value of the averaged velocity; in the meantime, the velocity gradient decreases. During time, when the transient profile is tending to the steady-state profile, the friction effects can be very significant even if the velocity averaged in the cross-section is equal to zero. The difference between the values of the steady and the transient shear stresses may reach two orders of magnitude.

In this thesis, it has been proposed to interpret the evolution of the shear stress in terms of two steps. The first step is a dramatic change of the shear stress during the wave passage. The second step is the tendency of the velocity profile to rebuild itself according to the steady-state profile after the wave passage. Each step is modelled separately. The shear stress jump, during the first step, is supposed to be proportional to the amplitude of the pressure wave. The modelling of the second step, called relaxation, is based on the theory of Extended Irreversible Thermodynamics.

Extended Irreversible Thermodynamics has already been used by other researchers to determine closure laws for the class of phenomena where the hypothesis of local equilibrium is questionable (e.g. Jou et al. [21], Bilicki et al [5]). Fast transient flows, described in terms of area averaged variables, belong to this class due to the strong gradients and fast changes. The derivation of the relaxation equation, which describes the second step of the shear stress evolution, is based on the introduction of the wall shear stress into the thermodynamic space. This introduction leads to a first order differential equation for the wall shear stress, which has an exponential function as a solution. The transient wall shear stress evolves exponentially in time, tending to the steady state value. This exponential evolution is in agreement with the evolution of the shear stress during the second step obtained with computations by FLUENT.

The Friction Relaxation Model proposed in this thesis integrates both steps of the shear stress evolution. It contains two coefficients that are needed to be evaluated on the basis of experimental data. One is the transient friction coefficient k_T responsible for the first step of the shear stress evolution, the other is the relaxation time θ responsible for the second step. By comparison with the transient shear stress results obtained with FLUENT for air flow, k_T was found to be different for acceleration and deceleration; the value for deceleration is about 75% of the value for acceleration. The value of k_T for water transient flows was evaluated on the basis of experimental data of Holmboe and Rouleau; here k_T for deceleration was about 50% of the value for acceleration. The value of θ was retained the same for water flow as for air flow and the results were satisfactory. It seems that the relaxation time has the order of milliseconds. Globally, the effect of the transient shear stress is much more important for a liquid flow than for a gas flow.

Two 'algebraic versions' of the Friction Relaxation Model are also proposed to programmers who would like to put a transient friction model in their codes without major modifications of these codes.
In order to include the relaxation process in the approximated models, which do not contain shear stress derivatives, the explicit information about the shear stress in the past was introduced into these models. The first model is based on the information recorded at the moment of a wave passage through a given point; the second one is based on the information from the last time step. Because the moment of a wave passage can often be difficult to detect, it is recommended to use the model based on the information from the last time step, which was proved to be more reliable to operate.

The Friction Relaxation Model can also be used for two-phase flow calculations. Evidently the pressure and void fraction history depend on the choice of the two-phase model as well as on the choice of the friction model. However, it can be generally concluded that transient friction damps pressure oscillations and produces smaller amounts of vapour than steady friction models. For the fast closure of a downstream valve, there is also some positive phase shift; for the closure of the upstream valve the shift is negative.

The Friction Relaxation Model can be treated as an alternative equation with respect to the wall friction models based on the sum of a steady term and a term containing velocity derivatives. These models have recently become very popular in the literature. They are easy to apply in the codes but, as they are based only on instantaneous conditions, they do not contain the information about relaxation. The exact Friction Relaxation Model, being a differential equation for the shear stress, can be problematic to introduce in the codes, as it implies increasing the number of differential equations in the system. However it has been shown that the approximated model based on the last time step gives almost identical results as the exact Friction Relaxation Model and is very easy to introduce in the codes. It has already been successfully introduced into the WAHA code developed for two-phase water hammer calculations and was found to improve the results obtained with this code for transient flows with short periods (up to two orders of magnitude greater than the relaxation time). In the case of a water hammer with very long period in comparison with the relaxation time (i.e. very long pipe), the effect of the transient friction has appeared to be negligible.

Interestingly, the exact Friction Relaxation Model has a similar form as the transient friction law derived analytically by Achard and Lespinard [1] for laminar flows and the approximated Friction Relaxation Model based on the last time step has a form similar to the approximate model of Vardy et al. [40] for turbulent flows at moderate Reynolds numbers. The three different approaches employed by different researchers appear to converge toward the same direction. This is proposed as an argument in favour of the correctness of the model developed in this thesis and also in favour of the use of the Extended Irreversible Thermodynamics, which is a rather new theory and still provokes controversies in the scientific world.

Future works on the Friction Relaxation Model should consist in the research of analytical expressions for the coefficients k_T and θ. In order to do this it is necessary to create a database of basic experimental results for fast transient flows with different fluids and with different initial conditions. The experiments analyzed in this thesis could serve to evaluate the order of magnitude of these coefficients and to propose their preliminary values, but a continuation of this research is needed in order to determine more reliable expressions for k_T and θ, verified against numerous experiments, and to determine the precise range of application of the model.
The relaxation approach presented in this thesis can also serve for the mod-

elling of other phenomena in fast transient two-phase flows like interfacial shear stress or heat transfer.

Through the presentation of the Friction Relaxation Model the author of this thesis would also like to encourage researchers working on the modelling of non-equilibrium phenomena to consider and use the theory of Extended Irreversible Thermodynamics as a physical basis and a mathematical tool for the development of new closure laws.

Appendix A

Description of the codes and numerical schemes used to perform the computations

The computations presented in this thesis were done with the codes developed by us and with the WAHA3 code developed by Dr Iztok Tiselj at the Jozef Stefan Institute at Ljubljana, Slovenia in the frame of the WAHALoads project described in the introduction.

The codes written by us were developed only for research purposes. They were used to verify the correctness of the proposed transient friction model during fast transient flows for the simple case of the fast closure of a valve in a single, horizontal pipe with a constant cross-section. More complicated water hammers studied with the WAHA code are described in details in the WAHA3 code manual [37].

There are three basic types of codes developed by the author of this thesis:

- A code for an adiabatic air flow
- A code for a water flow based on the Homogeneous Equilibrium Model
- A code for a water flow based on the Homogeneous Relaxation Model

A.1 Basic equations

The basic set of equations are the 1D balance equations for an adiabatic flow, averaged in the cross-section, written in the conservative form. The set of equations is closed with the Friction Relaxation Model for the wall shear stress. The set can be written:

$$\frac{\partial u}{\partial t} + \frac{\partial F(u)}{\partial x} = B(u) \tag{A.1}$$

where the vector of basic variables is defined as:

$$u = \begin{pmatrix} \rho \\ \rho w \\ \rho e \\ \rho \tau \end{pmatrix} \tag{A.2}$$

ρe is the total energy per volume:

$$\rho e = \rho(u + w^2/2) \tag{A.3}$$

The fluxes have the form:

$$F(u) = \begin{pmatrix} \rho w \\ p + \rho w^2 \\ w(\rho e + p) \\ \rho \tau w \end{pmatrix} \tag{A.4}$$

and the right hand side:

$$B(u) = \begin{pmatrix} 0 \\ -\frac{4}{D}\tau \\ 0 \\ \frac{\frac{f}{8}\rho^2 w|w| - \rho\tau}{\theta} + k_T \rho^2 \left|a\right| \frac{\Delta w}{\Delta t} \end{pmatrix} \tag{A.5}$$

where Δt is a time step and Δw is a difference between the values of the velocity from two last time steps.

One should take care about the value of the time step Δt with respect to θ during the calculations. In order to obtain correct results the condition:

$$\Delta t < \frac{\theta}{20} \tag{A.6}$$

has to be satisfied.
The Friction Relaxation Model does not influence the eigenvalues of the system.
The coefficient f is a steady-state friction coefficient. For the laminar flows it is calculated according to Darcy equation:

$$f = \frac{64}{Re} \tag{A.7}$$

For the turbulent flows it is calculated according to Colebrook and White formula:

$$\frac{1}{\sqrt{f}} = -2\log\left(\frac{\epsilon}{3.715D} + \frac{2.514}{Re\sqrt{f}}\right) \tag{A.8}$$

where ϵ is the roughness coefficient.

The initial conditions for the system represent the Riemann problem:

$$u(x,0) = \begin{matrix} u_l(x) & x < 0 \\ u_r(x) & x > 0 \end{matrix} \tag{A.9}$$

Physically these conditions can represent a discontinuity which is caused by a sudden change in the steady state of the flow. In this thesis, the case of the sudden closure of a valve was studied.

A.2 Numerical scheme

The method of solution is based on Godunov's approach. The continuous solution of the system A.1 is replaced, at any time, by a piecewise constant function (Seynhaeve et al. [31], Saurel and Abrall [30]). The computational domain is divided into intervals, the nodes j being the centers of the intervals. The solution at every time step is constant within every interval and

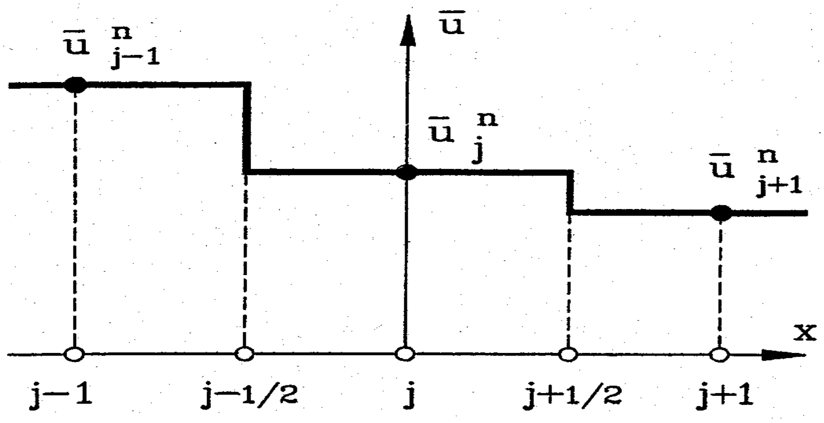

Figure A.1: The numerical solution at the time n

discontinuous at the boundaries of the intervals (Fig. A.1). u_j^n is the value of the function u in the interval centered at the point:

$$x_j = x_0 + j\Delta x \tag{A.10}$$

at time:

$$t^n = t^0 + n\Delta t \tag{A.11}$$

and it can be defined as:

$$u_j^n = \frac{1}{\Delta x}\int_{x_{j-1/2}}^{x_{j+1/2}} u(t^n)dx \tag{A.12}$$

We integrate Eq. A.1 on the computational cell P shown in Fig. A.2:

$$\int\int_P \left(\frac{\partial u}{\partial t} + \frac{\partial F(u)}{\partial x}\right) = \int\int_P B(u) \tag{A.13}$$

Using the Green theorem it can be written:

$$\int\int_P \left(\frac{\partial u}{\partial t} + \frac{\partial F(u)}{\partial x}\right) = \int_C (udx - F(u)dt) \tag{A.14}$$

where C is the contour limiting the computational cell P. From the definition of u_j^n one obtains:

$$\int_C udx = (u_j^n - u_j^{n+1})\Delta x \tag{A.15}$$

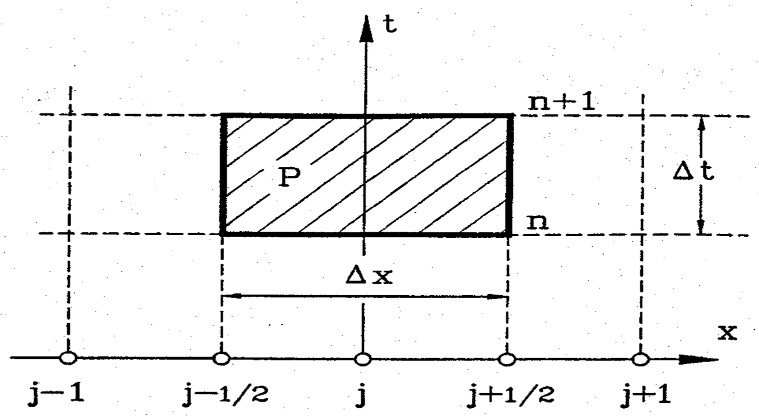

Figure A.2: The computational cell

The function u is not defined at the boundaries of the intervals, because it is discontinuous there, but a similar relation for the fluxes at the borders of the computational cell can be written:

$$\int_C F(u)dt = (F_{j+1/2} - F_{j-1/2})\Delta x \tag{A.16}$$

where $F_{j+1/2}$ and $F_{j-1/2}$ are the average values of fluxes between the cells. They can be determined by the local solution of the Riemann problem. Finally u_j^{n+1} is obtained as:

$$u_j^{n+1} = u_j^n - \frac{\Delta t}{\Delta x}\left(F_{j+1/2} - F_{j-1/2}\right) + B(u)\Delta t \tag{A.17}$$

The vector $B(u)$ at the right hand side is averaged in the computational cell.

The Godunov Method

According to the Godunov scheme (Tannehill et al. [35]) represented graphically in Fig. A.3 the values of the fluxes at the vertical borders of the computational cell are estimated as:

$$F_{j\pm1/2} = F(u_{j\pm1/2}^{n+1}) \tag{A.18}$$

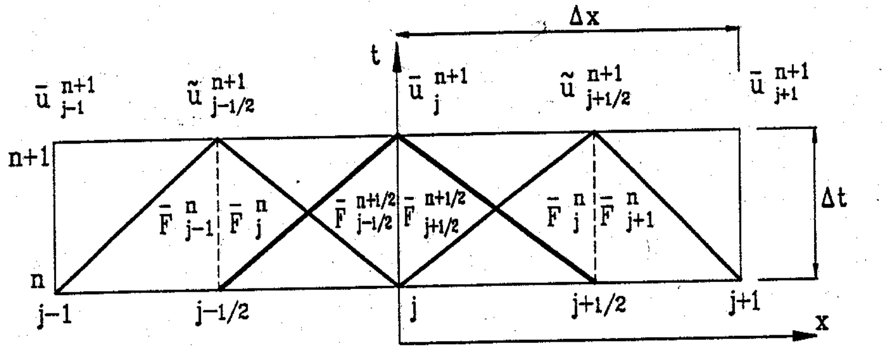

Figure A.3: Godunov scheme

where the intermediate values $u^{n+1}_{j\pm 1/2}$ between the cells are given by:

$$u^{n+1}_{j+1/2} = \frac{1}{2}(u^n_j + u^n_{j+1}) - \frac{\Delta t}{\Delta x}\left(F(u^n_{j+1}) - F(u^n_j)\right) + \frac{1}{2}\left(B(u^n_{j+1}) + B(u^n_j)\right)\Delta t \tag{A.19}$$

$$u^{n+1}_{j-1/2} = \frac{1}{2}(u^n_{j-1} + u^n_j) - \frac{\Delta t}{\Delta x}\left(F(u^n_j) - F(u^n_{j-1})\right) + \frac{1}{2}\left(B(u^n_j) + B(u^n_{j-1})\right)\Delta t \tag{A.20}$$

The averaged value of B is simply:

$$B(u) = B(u^n_j) \tag{A.21}$$

So the discretized form of Eq. A.1 according to Godunov's scheme is:

$$u^{n+1}_j = u^n_j - \frac{\Delta t}{\Delta x}\left(F(u^{n+1}_{j+1/2}) - F(u^{n+1}_{j-1/2})\right) + B(u^n_j)\Delta t \tag{A.22}$$

Most of the calculations were done using the Godunov scheme. This scheme does not produce numerical oscillations and is stable if the condition: $CFL \leq 0.5$ is satisfied, [35].

The Lax-Wendroff method

According to Lax-Wendroff scheme (Lax and Wendroff [22], Tannehill et al.

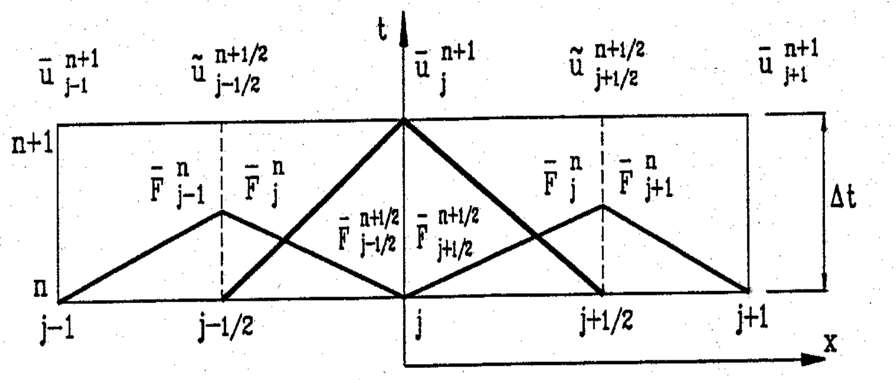

Figure A.4: Lax-Wendroff scheme

[35]) represented graphically in Fig. A.4 the fluxes at the vertical borders of the computational cell are evaluated as:

$$F_{j\pm1/2} = F(u^{n+1/2}_{j\pm1/2}) \tag{A.23}$$

where the values $u^{n+1/2}_{j\pm1/2}$ are given by:

$$u^{n+1/2}_{j+1/2} = \frac{1}{2}(u^n_j + u^n_{j+1}) - \frac{\Delta t}{2\Delta x}\left(F(u^n_{j+1}) - F(u^n_j)\right) + \frac{1}{4}\left(B(u^n_{j+1}) + B(u^n_j)\right)\Delta t \tag{A.24}$$

$$u^{n+1/2}_{j-1/2} = \frac{1}{2}(u^n_{j-1} + u^n_j) - \frac{\Delta t}{2\Delta x}\left(F(u^n_j) - F(u^n_{j-1})\right) + \frac{1}{4}\left(B(u^n_j) + B(u^n_{j-1})\right)\Delta t \tag{A.25}$$

So the discretized form of Eq. A.1 according to Lax-Wendroff's scheme is:

$$u^{n+1}_j = u^n_j - \frac{\Delta t}{\Delta x}\left(F(u^{n+1/2}_{j+1/2}) - F(u^{n+1/2}_{j-1/2})\right) + B(u^n_j)\Delta t \tag{A.26}$$

The Lax - Wendroff scheme has a small amount of numerical dissipation, but may produce oscillations trailing the shock wave. This scheme is stable if the condition: $CFL \leq 1$ is satisfied [34].

CFL condition

In order to avoid any loss of physical information, and to preserve the sta-

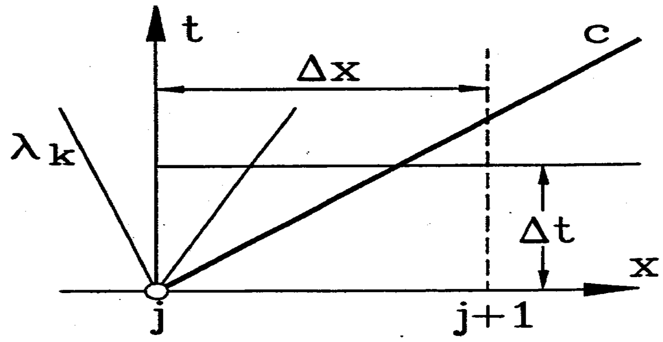

Figure A.5: Graphical interpretation of CFL condition.

bility of the scheme the condition concerning the value of the time step is imposed (Fig. A.5):

$$\Delta t \cdot c \leq \Delta x \tag{A.27}$$

where c is the largest characteristic of the flow. For the cases studied in this thesis c represents the speed of sound in the fluid.
This leads to the definition of the Courant number:

$$CFL = \frac{c\Delta t}{\Delta x} \tag{A.28}$$

Therefore the Courant-Friedrichs-Lewy condition may be written as:

$$CFL \leq 1 \tag{A.29}$$

For the Godunov scheme this condition is more restrictive in order to avoid the interaction of the waves from adjacent cells [35]:

$$CFL \leq 0.5 \tag{A.30}$$

Boundary conditions

The boundary conditions for the studied case of the fast closure of a valve are simple. At the tank (the first node) a constant pressure is imposed:

$$p(1) = p_{tank} \tag{A.31}$$

Other variables at the tank are:

$$\rho(1) = \rho(2) \tag{A.32}$$

$$w(1) = w(2) \tag{A.33}$$

$$e(1) = e(2) \tag{A.34}$$

$$\tau(1) = \tau(2) \tag{A.35}$$

At the valve (n-th node) the mirror condition for the velocity is suggested.

$$w(n) = -w(n-1) \tag{A.36}$$

According to this condition the valve is actually placed between the two last nodes. Other variables at the valve are:

$$\rho(n) = \rho(n-1) \tag{A.37}$$

$$p(n) = p(n-1) \tag{A.38}$$

$$e(n) = e(n-1) \tag{A.39}$$

$$\tau(n) = 0 \tag{A.40}$$

Appendix B

Analytical solution of the friction relaxation equation for short times

The equations 4.8 and 4.9 resemble the solution of the linear ordinary differential equation:

$$\frac{dy}{dt} = \frac{y_s - y}{\theta} + A\delta(t) \tag{B.1}$$

where y_s and A are some constants and $\delta(t)$ is the Dirac distribution.
If y_s and A are assumed to be constant for short times, by using $Y = y - y_s$, Eq. B.1 becomes:

$$\frac{dY}{dt} + \frac{Y}{\theta} = A\delta(t) \tag{B.2}$$

the solution of which is:

$$Y(t) = Y(0)exp(-t/\theta) + exp(-t/\theta)AH(t) \tag{B.3}$$

where $H(t)$ is the Heaviside function. Eq. B.3 is the approximation of Eq. 4.9 for short times.

Appendix C

Velocity profiles during wave passage calculated with FLUENT

Some 2D axisymmetric calculations with FLUENT have been done to observe the evolution of the velocity profiles in air flow during the passage of a pressure wave.

The analyzed case was the sudden closure of a downstream valve in a pipe of a length of 1 m and a diameter of 10 cm. The initial velocity was 6.95 m/s (mass flow rate = 0.0643 kg/s), the pressure was atmospheric.

The grid was refined at the wall (Fig. C.1). The valve was situated at the downstream (left) end of the pipe; y^+ for the steady - state calculations was about 1.8 (Fig. C.2). The increase of the value of y^+ at the right end of the pipe (position=1) is due to the condition of constant velocity imposed on this end for the whole cross - section.

The transient calculations were done using a second order explicit scheme (CFL=1). The two-layer model of turbulence was chosen to do the calculations, *i.e.* a $k - \epsilon$ model was applied in the fully turbulent region and the one-equation model of Wolfstein [44] in the viscosity-affected near-wall region. At the upstream end of the pipe a constant pressure was imposed, while at the downstream end the closed valve was simulated by the presence of the wall. The pipe wall was smooth.

After the closure of the valve the compression wave having an amplitude 2839 Pa travels towards the upstream end of the pipe and decelerates the flow. The location of the wave at the moment when the velocity profiles are calculated (t=1.85 ms after the closure of the valve) is shown in Fig. C.3. The velocity profiles during the sudden deceleration in the neighborhood of the wall (15 % of the radius of the pipe) are shown in Fig. C.4. The velocity is shown as a function of a non-dimensional variable which is the distance from the wall divided by the radius of the pipe. The locations where the profiles are calculated are also marked in Fig. C.4. The profile located at the point L=0.64 m is a typical steady - state profile, it is not yet disturbed by the pressure wave. The profile at the location L=0.58 m has already been disturbed by the passage of the wave; therefore a large pressure gradient at the wall can be observed. Other velocity profiles are located in the points where the wave is actually passing.

When the pressure wave reaches the tank it reflects and starts to travel towards the valve, accelerating the flow. The velocity profiles, which already had been perturbed by the compression wave, have not yet found their steady - state shape. The location of the wave at the moment when the velocity profiles are calculated (t=5.19 ms after the closure of the valve) is shown in Fig. C.5.
The velocity profiles during the sudden acceleration in the neighborhood of the wall are shown in the Fig. C.6. The profile at the point L=0.21 m is located downstream the pressure wave and has not yet been disturbed by the second wave passage. The profile at the point L=0.29 m has been already perturbed by the wave, which produced a large velocity gradient very close to the wall. Other velocity profiles are located at the points where the wave is actually passing, accelerating the flow.

When the wave reaches the valve, the pressure drops and the decompression wave starts to propagate towards the tank, decelerating the flow and disturbing the profiles in a similar way as shown in Fig. C.4. After reaching the tank the acceleration starts again. The wave will oscillate like this between the tank and the valve decelerating and accelerating the flow, and dissipating the kinetic energy. This dissipation is mostly due to the very large velocity gradients at the wall caused by the sudden translations of the velocity profiles during these wave passages.

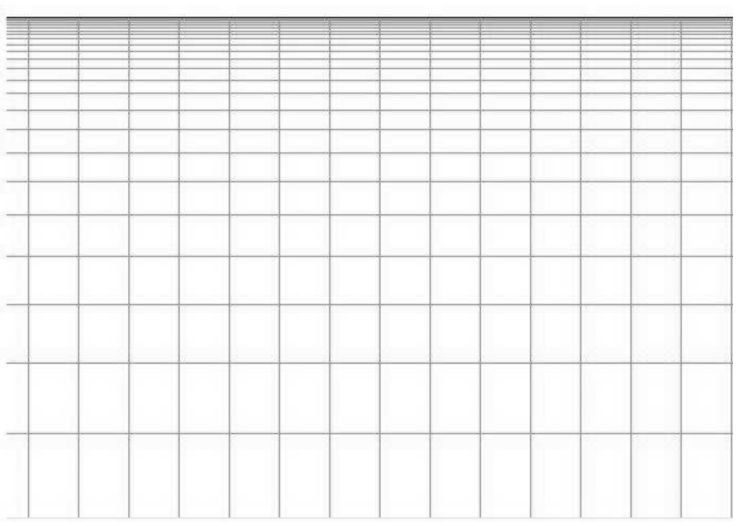

Figure C.1: The grid used for axisymmetric calculations. The upper half of the pipe is presented.

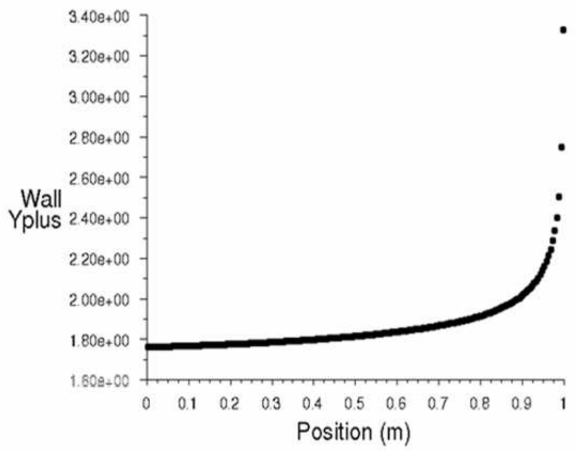

Figure C.2: Y plus.

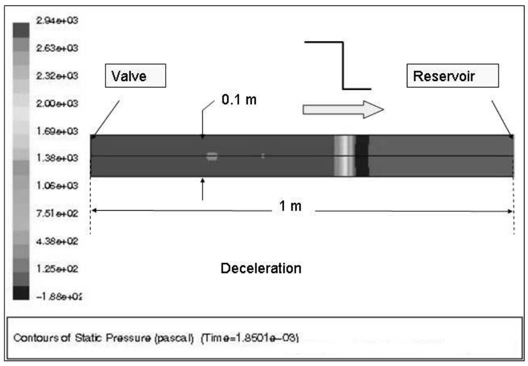

Figure C.3: A pressure wave during deceleration.

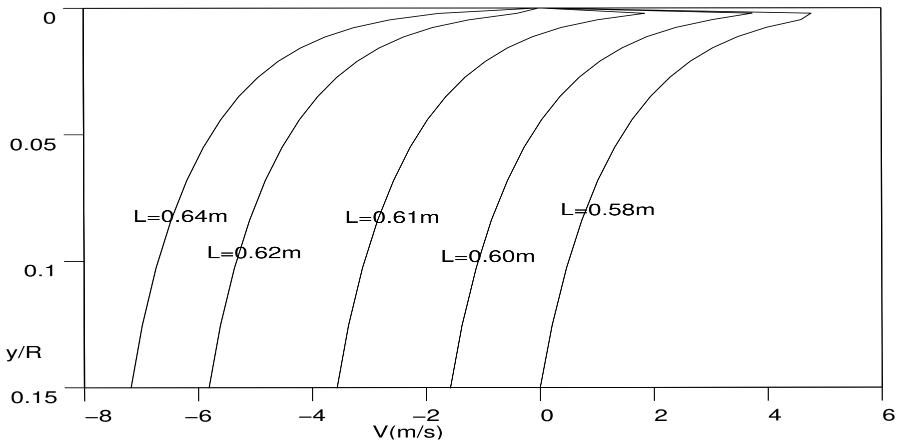

Figure C.4: Velocity profiles during deceleration at different pipe locations at the time 1.85 ms.

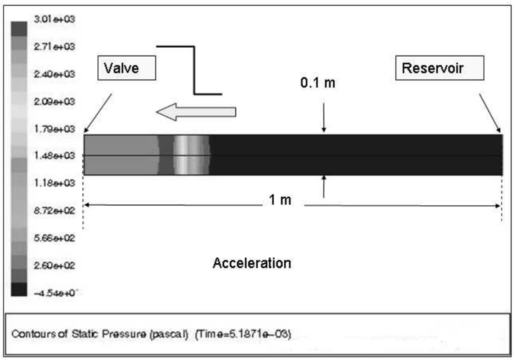

Figure C.5: A pressure wave during acceleration.

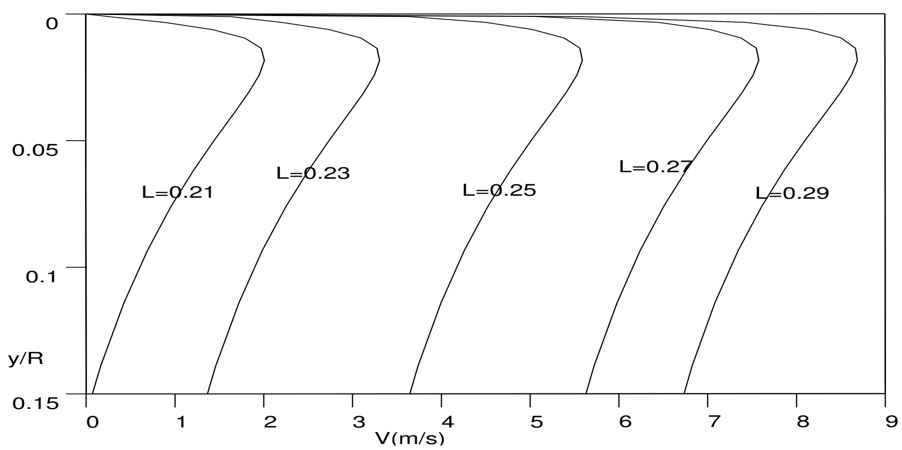

Figure C.6: Velocity profiles during acceleration at different pipe locations at the time 5.19 ms.

Appendix D

The comparison between original and approximated Friction Relaxation Model for refined grid

Some additional calculations were done in order to prove that the results of the approximated Friction Relaxation Model based on last time step (section 4.3) are in agreement with the original model, independently of the number of nodes.

The condition, which has to be satisfied concerns only the time step: $\Delta t < \theta/20$, where θ is the relaxation time in the Friction Relaxation Model .

The analyzed case was the water hammer event caused by a fast closure of a downstream valve in a pipe having a length 50 m and a diameter 20 mm. The initial velocity is 5 m/s and the temperature is 293 K. The upstream tank has a constant pressure: 8 MPa.

In the section 4.3 the calculations have been done for 400 nodes, $\Delta t = \theta/34$. The results presented in the Fig. D.1 and D.2 were obtained for 800 nodes, $\Delta t = \theta/68$. Both shear stress and pressure histories obtained with the approximated model are very close to the results obtained with original model,

the difference is almost invisible.
The results obtained on the grid having 800 nodes are almost the same as the results obtained on the grid having 400 nodes (section 4.3), therefore there is no need to use finer grid than 400 nodes.

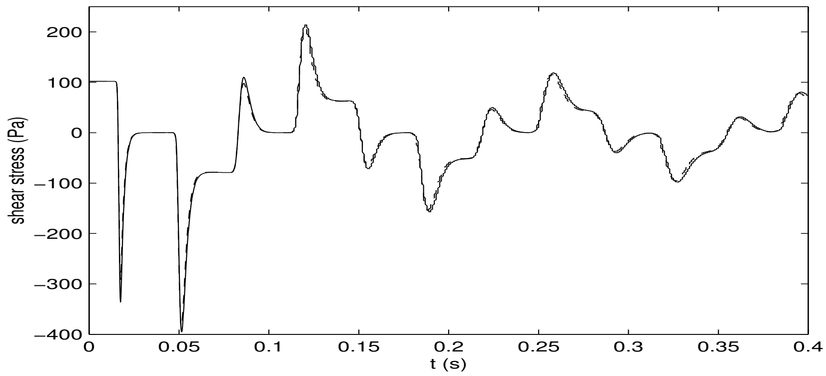

Figure D.1: Water flow, $Re = 10^5$. Wall shear stress in the middle of the pipe versus time. Comparison between original Friction Relaxation Model (dashed line) and approximated Friction Relaxation Model based on last time step (solid line). Relaxation time: $\theta = 1.4$ms, k_T for acceleration $2 \cdot 10^{-4}$, k_T for deceleration $1 \cdot 10^{-4}$.

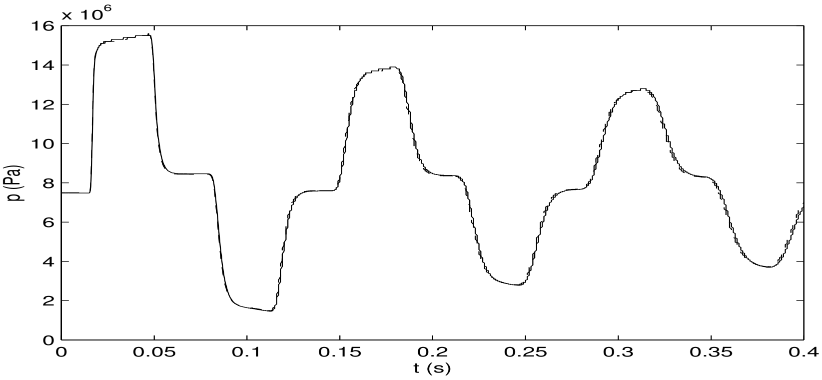

Figure D.2: Water flow, $Re = 10^5$. Pressure in the middle of the pipe versus time. Comparison between original Friction Relaxation Model (dashed line) and approximated Friction Relaxation Model based on last time step (solid line). Relaxation time $\theta = 1.4$ms, k_T for acceleration $2 \cdot 10^{-4}$, k_T for deceleration $1 \cdot 10^{-4}$.

Bibliography

[1] Achard, J.L., Lespinard, G.M., 1981. Structures of the transient wall-friction law in one-dimensional models of laminar pipe flow. Journ. of Fluid. Mech. 113, 283-298.

[2] Axworthy, D.H., Ghidaoui, M.S., McInnis, D.A., 2000. Extended thermodynamics derivation of energy dissipation in unsteady pipe flow. Journal of Hydraulic Engineering 126, 276-286.

[3] Bestion, D., 1990. The Physical closure laws in the CATHARE code. Nuclear Engineering and Design, 124, 229-245.

[4] Bilicki, Z., Kestin. J., 1990. Physical aspects of the relaxation model in two-phase flow. Proc. R. Soc. Lond. A 428, 379-397.

[5] Bilicki, Z., Giot, M., Kwidzynski, R., 2002. Fundamentals of two-phase flow by the method of irreversible thermodynamics. Int. J. Multiphase Flow 28, 1983-2005.

[6] Brunone, B., Golia, U.M., Greco, M., 1991a. Some remarks on the momentum equation for fast transients. Proc., Int. Conf. on Hydr. Transients with water Column Separation, IAHR, Delft, The Netherlands, 201-209.

[7] Brunone, B., Golia, U.M., Greco,M., 1991b. Modelling of fast transients by numerical methods. Proc. Int. Conf. on Hydr. Transients with water Column Separation, IAHR, Delft, The Netherlands, 273-280.

[8] Brunone, B., Golia, U.M., Greco, M., 1995. The effects of twodimensionality on pipe transient modelling. J. Hydr. Engrg. 121(12), 906-912.

[9] Brunone, B., Karney, B.W., Mecarelli, M., Ferrante, M., 2000. Velocity profiles and unsteady pipe friction in transient flow. Journal of Water Resources Planning and Management 126(4), 236-244.

[10] Bughazem, M.B, Anderson, A., 2000. Investigation of an unsteady friction model for waterhammer and column separation. BHR Group 2000 Pressure Surges, 471-482.

[11] Carlson K.E., Riemke, R.A., Rouhani, S.Z., Shumway, R.W, Weaver W.L., 1990. RELAP 5/ MOD3 Code Manual Vol 1-7, NUREG/CR-5535, EG&G Idaho, Idaho Falls.

[12] Carstens, M.R., Roller, J.E., 1959. Boundary-shear stress in unsteady turbulent pipe flow. J. Hyd. Div. 85, 67-81.

[13] Downar-Zapolski, P., Bilicki, Z., Bolle, L., Franco, J., 1996. The non-equilibrium relaxation model for one-dimensional flashing liquid flow. International Journal of Multiphase Flow, 22 (3), 473-483.

[14] Drew, D.A., Cheng L., Lahey Jr., R.T., 1979. The Analysis of Virtual Mass Effects in Two-Phase Flow. International Journal of Multiphase Flow 5, 232-242.

[15] Dudlik, A., June 2003. Data Evaluation Report on PPP water hammer tests, cavitation caused by rapid valve closing. WAHALOADS project, Deliverable D35.

[16] Eichinger,P., Lein,G., 1992. The influence of friction on unsteady pipe flow. Unsteady flow and fluid transients, R. Bettes and J.Watts, Eds., Balkema, Rotterdam, The Netherlands, 41-50.

[17] Fluent Incorporated. FLUENT 5 User's guide. 1998.

[18] Giot, M., Prasser, H.M., Dudlik, A., Ezsol, G., Habip, M., Lemmonier, H. Tiselj, I., Castrillo, M., van Hove, W., Perezagua, R., Potapov, S., 2001. Two-phase flow water hammer transients and induced loads on materials and structures of nuclear power plants (WAHALoads). Proc. FISA-2001, EU research in reactor safety, Luxembourg, 140-151.

[19] Hirsch, C., 1988. Numerical Computation of internal and external flow. Vol. 1 - 2, John Wiley and Sons.

[20] Holmboe, E.L., Rouleau, W.T, 1967. The effect of viscous shear on transients in liquid lines. Transactions of ASME, Journal of Basic Engineering, 174-180.

[21] Jou, D., Casas-Vazquez, J., Lebon, G., 2001. Extended Irreversible Thermodynamics. Springer-Verlag Berlin Heidelberg.

[22] Lax, P., Wendroff, B., 1960. System of Conservation Laws. Communications on pure and applied mathematics, vol. XIII, 217-237 (1960).

[23] Lemmonier, H., 2002. An attempt to apply the homogeneous relaxation model to the Wahaloads benchmark tests with interaction with the machanical structure, CEA-T3.3-D61-200302, WAHALoads project deliverable D61.

[24] LeVeque, R., J., 1992. Numerical Methods for Conservation Laws. Lectures in Mathematics, ETH, Zurich.

[25] Mahaffy, J.H., 1993. Numerics of Codes: Stability, Diffusion, and Convergence. Nuclear Engineering and Design 145.

[26] Pezzinga, G., Scandura, P., 1995. Unsteady flow in installations with polymeric additional pipe. J. Hydr. Engrg., ASCE, 121 (11), 802-811.

[27] Pezzinga, G., 1999. Quasi 2D Model for Unsteady Flow in pipe networks. Journal of Hydraulic Engineering 125(7), 676-685.

[28] Richardson, E.G., Tyler, E., 1929. The transverse velocity gradient near the mouths of pipes in which an alternating or continuous flow of air is established. Proc., The Physical Society, London, UK, 42(1), 1-15.

[29] Safwat, H.H., Polder, J., 1973. Friction-frequency dependence for oscillatory flows in circular pipe. J. Hyd. Div., Proc. ASCE, 99, 1933-1945.

[30] Saurel, R., Abgrall, R., 1999, A multiphase Godunov method for compressible multifluid and multiphase flows. Journal of Computational Physics 150, 425-467.

[31] Seynhaeve, J.M., Lombr, R., Ducrocq, J., Bolle, L., 1994. Physical modeling of rapid transients in long pipes in case of vaporization: an efficient tool for safety management. Process Safety Progress, Vol. 13, No.2.

[32] Silva-Araya, W.F., Chaudry, M.H, 1997. Computation of energy dissipation in transient flow. J. Hydr. Engrg. 123(2), 108-115.

[33] Simpson, A.R., 1986. Large water hammer pressures due to column separation in sloping pipes (transient cavitation), PhD thesis, The University of Michigan.

[34] Sod, G.A., 1985. Numerical Methods in Fluid Dynamics. Cambridge University Press.

[35] Tannehill, J.C., Anderson, D.A., Pletcher, R.H., 1997. Computational Fluid Mechanics and Heat Transfer. Taylor & Francis.

[36] Tiselj, I., Petelin, S., 1997. Modelling of two-phase flow with second order accurate scheme. Journal of Computational Physics, 136(2), 503-521.

[37] Tiselj, I., Horvat. A, Cerne, G., Gale, J., Parzer, I., Mavko, B., Giot., M., Seynhaeve, J.M., Kucienska, B., Lemonnier, H., March 2004, WAHA3 Code Manual. Jozef Stefan Institute, Ljubljana, Slovenia.

[38] Trikha, A.K., 1975. An efficient method for simulating frequency-dependent friction in Transient Liquid Flow. J. Fluids Engineering 97(1), 97-105.

[39] Vardy, A.E., Hwang, K., 1991. A characteristic model of transient friction in pipes. J. of Hydr. Res., IAHR, 29(5), 669-684.

[40] Vardy, A.E., Hwang, K., Brown J., 1993. A weighting function model of transient turbulent pipe friction. J. of Hydr. Res., IAHR, 31(4), 533-548.

[41] Vardy, A., Brown, J., 1995. Transient, turbulent, smooth pipe friction. J. of Hydr. Res., IAHR, 33(4), 435-456.

[42] Vardy, A., Brown, J., 1996. On turbulent, unsteady, smooth-pipe friction. Proc., 7th Int. Conf. on Pressure Surges and Fluid Transients in Pipelines and Open Channels, BHR Group Ltd., Harrogate, England, 289-311.

[43] Vitkovsky, J., Lambert, M., Simpson, A., 2000. Advances in unsteady friction modelling in transient pipe flow. BHR Group 2000 Pressure Surges, 471-482.

[44] Wolfstein, M., 1969. The velocity and temperature distribution of one-dimensional flow with turbulence augmentation and pressure gradient. Int. J. Heat Mass Transfer, 12, 301-318.

[45] Wylie, E.B., Streeter, V.L, 1978. Fluid Transients, McGraw-Hill, 1978.

[46] Zielke, W., 1968. Frequency-dependent friction in transient pipe flow. Journal of basic engineering 90, 109-115.